Fall 2019

The Development of Multi-functional System that Combine Patterned Hydrogels, Plasmin-Degradable Nanoparticles and Stem Cells for Applications in Tissue Engineering and Growth Factors Delivery

Safaa I. Kader

The Development of Multi-functional System that Combine Patterned Hydrogels, Plasmin-Degradable Nanoparticles and Stem Cells for Applications in Tissue Engineering and Growth Factors Delivery

By

Safaa I. Kader

Bachelor of Science
University of Al-Mustansiriyah, 1994

Master of Science
University of Al-Mustansiriyah, 1999

Submitted in Partial Fulfillment of the Requirements

For the Degree of Doctor of Philosophy in

Chemistry

College of Arts and Sciences

University of South Carolina

2019

Accepted by:

Esmaiel Jabbari, Major Professor

Thomas Makris, Major Professor

Maksymilian Chruszcz, Committee Member

John Lavigne, Committee Member

Cheryl L. Addy, Vice Provost and Dean of the Graduate School

DEDICATION

This dissertation is dedicated to the soul of my father, Ibrahim Kader, who passed away before I have done with my Ph.D., and to my lovely wife, Wafaa Jumaah, for her support, devotion, and supplications.

ACKNOWLEDGEMENTS

I would like to be especially thank my advisor, Prof. Esmaiel Jabbari for his guidance, and mentorship that has prepared me as an independent researcher. Also, I would like to be especially thank my co-advisor for his supporting, understanding, and encouraging during my study. I am highly appreciative of the members of my committee, Dr. Chruszcz Maksymilian, Dr. John Lavigne for their time, insights about my research projects, support, and encouragement throughout my Ph.D. studies.

I thank all my lab members (Dr. Moeinzadeh, Dr. Barati, and Mehri). I am heartily thankful to all my friends in the US and specifically Habeeb Al-Sudani and Ahmmed Abdul Shaheed who never left me alone during these years.

I should also like to thanks Perry Pellechia and Michael Walla at NMR and Mass Spectroscopy facility. I would also like to thank Dr. Leslie Lovelace and Dr. Amy Taylor for supporting me financially through the teaching assistantship. Thank also to Ms.Jennfier Merkel, Sarah Graham and Nanette Goodwin in Chemistry and Biochemistry Department. I should also like to thanks the Ministry of Higher Education and Scientific Research (MOHESR). Without your financial support, this dissertation wouldn't have been possible. Most importantly, none of this would have been possible without the love and patience of my family. My immediate family to whom this dissertation is dedicated to has been a constant source of love, concern, support, and strength all these years. I would like to express my heartfelt gratitude to my family. My extended family has aided and encouraged me throughout this endeavor.

ABSTRACT

This thesis spots the light on the development of a novel multi-functionalized system for application in tissue engineering and on-demand morphogens delivery. Three types of materials used in this study are synthetic polymer, biopolymer, and nanomaterials. Polyethylene glycol (PEG), a synthetic polymer was chosen in this study because of its high biocompatibility, non-immunogenicity, inert nature, ease of modification, and reduces protein denaturation to provide a wide range of physical and mechanical properties. Here, PEG is used one time as a hydrogel, linear polyethylene glycol-co-lactide (LPELA), and another time as peptide-PEG based nanoparticles (PxSPCP). Gelatin, a natural polymer has been widely used for several biomedical applications because of their suitable biocompatibility, tunable physical characteristics, closely mimic some essential properties of the native extracellular matrix (ECM) due to the presence of cell attaching and matrix metalloproteinase responsive peptide motifs. Meanwhile, the peptide-PEG based nanoparticles were included to provide hybrid hydrogel systems to form networks with desired combined properties and characteristics for specific biological applications. These properties could promote cell response to release certains growth factors that induce signaling pathways for cells differentiation. Hence, in this thesis, our goal was to integrate this multifunctional system to develop an ideal type of biomaterials that can letherage the tissue engineering and targeted morphogens delivery for various treatment applications.

TABLE OF CONTENTS

LIST OF TABLES

LIST OF FIGURES

LIST OF ABBREVIATIONS

BMPs..... Bone Morphogenic Proteins

BTE..... Bone Tissue Engineering

DSC..... Disuccinimidyl carbonate

ECFC..... Endothelial Colony Forming Cell

ECM..... Extra Cellular Matrix

FGF..... Fibroblast Growth Factor

GelMA..... Gelatin methacryloyl

HMSCs..... Human Mesenchymal Stem Cells

iPSCs..... Induced pluripotent stem cells

LPELA..... Linear polyethylene glycol -co-lactide acrylate

M-CSF..... Macrophage colony-stimulating factor

NG..... Nanogel

PDGF..... Platelet-derived growth factor

P0.5SPCP..... Polyethylene glycol (0.5k M.Wt) self-assembled cleavable peptide

P2SPCP..... Polyethylene glycol (2k M.Wt) self-assembled cleavable peptide

P5SPCP..... Polyethylene glycol (5k M.Wt) self-assembled cleavable peptide

P7.5SPCP..... Polyethylene glycol (7.5k M.Wt) self-assembled cleavable peptide

CB-MSCs..... Umbilical cord blood mesenchymal stem cells

VEGF..... Vascular Endothelial Growth Fact

CHAPTER 1: BACKGROUND INFORMATION

1.1 Bone Tissue Engineering (BTE)

In recent years, the spotlight increasingly focuses on tissue engineering (TE) as an alternative technique for bone defect repair and regeneration [1]. Tissue engineering combines biological elements such as stem cells and growth factors with engineering principles and synthetic materials in order to regenerate functional tissues [1, 2]. Like other tissues in the body, bone can repair minor small fractures and disease. However, it was estimated that more than half a million patients had received bone graft procedures yearly in the US to facilitate repair of a large bone defect [1, 3]. Current techniques for large bone defects include autologous or allograft bone transplantations. However, a secondary operation is required for the implementation of autografts and the risk of disease transfer, and rejection by the host is associated with allografts [4]. Therefore, there is a demand for better techniques for patients with large bone defects, and TE offers these bone graft alternatives.

Three critical features have been suggested to the materials that could substitute bone grafts and stimulate bone healing: osteogenicity, osteoconductivity, and osteoinductivity [5-8]. The osteogenic potential of the graft is determined by its cellular content, especially the number of osteogenic progenitor cells capable of differentiating into bone-forming cells. Osteoconduction is a physical attribute of a graft that permits it to act as a scaffold allowing vascular and cellular invasion and proliferation. This

osteoconductive graft, subsequently, resorbs over time and is replaced by new bone formation [5]. Osteoinduction is a molecular level process whereby specific growth factors stimulate the recruitment of undetermined mesenchymal cells and facilitate their differentiation into chondrogenic and osteogenic cells [8, 9].

1.2 Bone Structure and Formation

The macrostructure of bone is generally composed of two layers: the external dense, compact bone, and the internal spongy, trabecular bone. The compact, or cortical bone, provides mechanical strength and support to the structure. The spongy, or cancellous bone is highly porous to allow better penetration of the vasculature interwoven between calcified lattices [10]. The primary source of blood cells and vascular structures in bone is the marrow which is in the core of cortical bone and the spaces in cancellous bone [11]. There are two major types of skeletal elements, long and flat bones, formed by the processes of endochondral and intramembranous ossification, respectively [2]. During endochondral ossification, mesenchymal stem cells (MSCs) differentiate into so-called bone-forming cells, chondrocytes, osteoprogenitors, and osteoblasts [12]. The avascular cartilage is formed, serves as a template, and then the skeletal progenitors are formed from the invading vasculature and differentiate into osteoblasts, which eventually form new bone on the cartilage template [13]. Conversely, in intramembranous ossification, MSCs cluster and directly differentiate into cells of the osteoblast lineage. MSCs accumulate locally, create an ossification center and secrete an extracellular matrix (ECM) that promotes bone formation [2, 12]. A functional vasculature is thus vital within the bone regenerative process, supplying of oxygen, nutrients, and cells, and removing of waste [14]. In the

absence of a functioning and adequate vasculature network, tissue necrosis and failure of any implanted graft will eventually happen [15]. This suggests that there is a close correlation between vascularization and bone formation.

Several studies have shown that endochondral and intramembranous ossification of bone formation is closely tied to the process of the growth of blood vessels from existing vessels (angiogenesis) [13, 14, 16-18]. In the endosteum, endothelial progenitor cells form an osteoblast-vascular niche near osteoprogenitor cells within the bone marrow [19]. Bone cells secrete pro-angiogenic factors, such as vascular endothelial growth factor (VEGF), that can stimulate signaling responses in endothelial cells, chondrocytes, osteoblasts and osteoclasts populations that express VEGF receptors [20, 21]. By contrast, bone endothelial cells secrete factors that can stimulate chondrocytes and cells of the osteoblast lineage [22, 23]. It was shown that the expression of VEGF in the osteoblast lineage results in enhanced bone angiogenesis and osteogenesis [24]. VEGF, which is a master regulator of angiogenesis, plays a significant role in blood vessels' invasion into the hypertrophic cartilage where the endothelial cells in the invading vessels express factors that stimulate osteogenesis [4, 13, 18]. In the adult skeleton, bone morphogenetic proteins (BMPs) regulate the differentiation of periosteal skeletal progenitors during fracture healing and also mediates osteoblast formation in the bone marrow microenvironment [25]. BMPs stimulate angiogenesis by osteoblast-derived vascular endothelial growth factor A [26]. This suggests that osteogenesis and vascularization are coupled by spatiotemporal regulation of paracrine signaling in which the invading vascular endothelial cells secrete osteogenic factors to promote MSCs differentiation and bone formation [4].

1.3 Growth Factors in BTE

One of the approaches in tissue engineering includes delivery of growth factors to trigger cellular adhesion, proliferation, and differentiation thus accelerating bone and cartilage regeneration [27]. The type of growth factor and the target cell, cell density, receptor type, and other signaling events determine the ultimate biological response [28].

In vivo, bone regeneration involves the interplay between inflammatory cells, vascular cells, mesenchymal progenitor cells and osteocytes [29-32]. Their response is orchestrated by a certain set of GFs and cytokines that control cellular proliferation, migration, and differentiation during bone repair. In the first step of bone healing, inflammatory GFs and cytokines, including fibroblast growth factor (FGF), interleukin-1 (IL-1), and interleukin-6 (IL-6), macrophage colony-stimulating factor (M-CSF) and tumor necrosis factor-α (TNF-α), are involved in the recruitment of inflammatory cells. As the formation of the fracture callus occurs, high concentrations of pro-osteogenic factors, such as platelet-derived growth factor (PDGF), TGF-β, FGF-1, insulin-like growth factor (IGF), and bone morphogenic proteins (BMPs), stimulate the commitment of mesenchymal progenitor cells and their subsequent proliferation and differentiation. Simultaneously, proangiogenic factors, such as vascular endothelial growth factor (VEGF), FGF, BMPs and TGF-β, trigger the invasion of endothelial cells (ECs) into the newly formed soft callus re-establishing vascular network connection. Also, the intimate crosstalk between osteoblasts and ECs is mediated via the release of VEGF by osteoblasts that act on ECs to promote angiogenesis, and via the release of BMPs by ECs, which lead osteogenic differentiation [29, 33].

In vitro, several studies have reported that spatiotemporal and sequential growth factors release may lead to enhance tissue regeneration by providing release profiles and spatial gradients that emulate the natural healing response [34-36]. On the one hand, osteogenic growth factors of the transforming growth factor-β (TGF-β) superfamily, TGF-βs, activins, growth differentiation factors (GDF), bone morphogenic proteins (BMPs), play an essential role in embryonic development, tissue morphogenesis, cell proliferation and cell differentiation [37]. Several members of the TGF-β superfamily have been correlated to the biological processes of bone induction, including mesenchymal cell recruitment, proliferation, and extracellular matrix (ECM) production [38]. BMPs, particularly BMP-2, BMP-4, and BMP-7, are the most extensively utilized osteogenic factors for inducing *de novo* bone formation in ectopic and orthotopic sites, including critical size defects (CSD) [39]. Among BMPs, recombinant human BMP2 is currently FDA approved and available in a recombinant form for use as a potent osteogenic factor in specific medical applications such as spine fusion and alveolar ridge augmentation [40].

On the other hand, angiogenic growth factors that induce vascularization are essential for the formation and homeostasis of bone because of their role in the transport of oxygen, nutrients, growth and differentiation factors, and circulating cells [41]. The presence of a microvascular network supports the osteogenic, chondrogenic, and mesenchymal stem cells required for bone repair. Angiogenesis is regulated by growth factors such as vascular endothelial growth factor (VEGF), platelet-derived growth factor (PDGF), fibroblast growth factor (FGF) and insulin-like growth factor (IGF) [42]. Recent studies have shown that the delivery of VEGF was found to increase blood vessel density and stimulate bone regeneration in rabbit and rat critical-size bone defects [43].

Additionally, it has been shown that the combined delivery of VEGF with osteoinductive growth factors synergistically enhances osteogenesis [44]. Dual delivery of osteogenic and angiogenic factors is a novel strategy in bone regeneration engineering [45]. VEGF and BMP2 have been widely used in the fields of tissue engineering and regenerative medicine to stimulate angiogenesis and bone formation [46]. These two growth factors have additive effects and synergistically enhance bone regeneration [46]. VEGF and BMP-2 stimulated the chemotaxis of BMSCs. *In vivo*, these two growth factors also have been confirmed to induce the homing of tail vein injected BMSCs to the site of scaffold subcutaneous implantation in nude mice.

However, concerns about these bioactive strategies remain, such as the uncontrollable release and types of the delivered growth factors, and a high degradation rate resulting from a high in vivo instability of the angiogenic factors [47]. For the clinical therapy, BMP-2 in a high dosage needs to be used which associated with a high cost as well as a side effect, such as excessive bone resorption and promotion of tumor angiogenesis [4]. Additionally, it has been reported that the extent of bone formation in vivo depends on the exposure duration of osteoprogenitor cells and endothelial progenitor cells to BMP2 and VEGF [4, 47].

1.3.1 Carriers for Controlled Growth Factor Delivery. Direct administration of growth factors is not recommended in vivo. Injecting high doses of potent growth factors into the body may lead to severe side effects because of the extremely high initial concentration, and short half-lives due to the rapid degradation and cleaving. Since growth factors undergo rapid degradation, encapsulation within a material carrier can provide protection from enzymes and enhanced growth factor retention at the target site [35]. Additionally,

controlled release prevents unwanted cytotoxic and inflammatory effects as well as ectopic bone formation. A variety of natural, synthetic and inorganic materials have been used as controlled delivery systems [48]. Synthetic polymers including poly(α-hydroxy acids), poly(orthoesters), poly(anhydrides), poly(amino acids) and copolymers of lactic and glycolic acid have been investigated for encapsulated delivery for their controllable physicochemical properties [35]. For instance, PLG-based nano- or microcapsules encapsulating growth factors formed by a double emulsion–solvent evaporation method are widely used. Sustained delivery of encapsulated VEGF in PLG microspheres may upregulate angiogenesis [34]. The degree and mechanism of growth factor encapsulation are dependent on hydrophobic–hydrophobic or hydrophilic–hydrophilic interactions between the molecules and polymers [34]. Several studies have revealed that the release profile of recombinant human BMP-2 from PLGA microparticles is controlled by the molecular weight, lactic to glycolic ratio, end-group functionalization, and amount of incorporated growth factor [35, 49, 50].

Several studies have shown that PLGA microparticles sustain retention and release of rhBMP-2 and rhBMP-7 to adequately bridge rat and ovine critical-size cranial defects, respectively [49, 50]. However, the release profiles were affected higher by the functionalization of acidic moieties to PLGA end groups, which increased the degradation of the vehicle, resulting in the early release of encapsulated growth factor and sub-optimal bone formation [49, 50].

Natural materials including silk, keratin, collagen, gelatin, fibrinogen, elastin, chitosan, hyaluronic acid, cellulose, and alginate have also investigated as growth factor carriers [34]. For example, gelatin microspheres and gelatin combined with glycidyl

methacrylated dextran have been used to deliver certain growth factors such as BMP-2 and IGF-1 [27, 34]. For immobilization and timed-release of BMP2 and VEGF, PLGA micro- and nanoparticles are used due to their wide range of degradation times. However, protein denaturation because of surface adsorption and acidic degradation products of PLGA can significantly reduce protein bioactivity [4]. Another example of classical sustain release of GFs is the colloidal micro/nanoparticles where the GFs formulated in poly(lactic acid)/poly(D,L-lactic-co-glycolic acid) (PLA/ PLGA) particles for delivery. Drawbacks of these particles include low encapsulation efficiency and burst initial release, as well as the complex formulations to retain GF stability [51]. These biopolymers can be formulated into a variety of physical structures relevant to growth factor-delivery using several methods but common major issues are the maintenance of the bioactivity of the encapsulated growth factors and degradation rate [34, 52]. The development of new vehicles for bone regeneration focuses on promoting local growth factor retention and sustained release for augmenting osteoinductivity in vivo [48]. The release profiles of a GF of particulate carrier systems are eventually determined by the rate of vehicle degradation, loaded amount of growth factor, growth factor diffusion, and particulate size [35]. Therefore, there is a need for delivery strategies that respond to local signals or externally applied signals to control the release, so-called ‘the on-demand release’ [34, 53]. The on-demand release by external triggering signal can be engineered by the incorporation of stimuli-responsive components within the delivery systems. The most commonly used triggering mechanisms involve proteins such as enzymes that cleave a cross-linker used to immobilize a growth factor [34, 53].

The engineering of multi-functional nanomaterials that enable the simultaneous, spatially-controlled, and sequential release strategies of dual growth factors are necessary to recapitulate the early expression factors for bone regeneration.

1.4 Scaffolds in BTE

One key feature of TE is to develop biomimetic scaffolding materials that can harmonize the proliferation, self-renewal, and differentiation of multipotent stem cells into different lineages [54]. The interactions between cells and materials guide many cellular activities. These interactions of cell-material can direct the cell shape and the cytoskeletal organization that in turn regulate the biological processes, such as cell adhesion, growth, differentiation, and apoptosis [55]. Mammalian cells can sense and interact with the extracellular microenvironment at the nanometer scale despite their micrometer dimensions [54]. Bone tissue engineers have suggested that scaffolds have to be mimic the structure and properties of natural bone ECM [56]. Thus, the ideal scaffold for BTE should satisfy basic scaffold requirements such as porosity to allow vascularization, biocompatibility, and biodegradability with a controllable rate to accommodate the growth and maturation of cells, and appropriate surface characteristics for cell proliferation, migration, and differentiation [57-59].

Typically, these specific properties for an ideal scaffold are found in hydrogels. Hydrogels are three-dimensional polymeric networks that can retain a large volume of water and swell in a physiological environment without dissolving [60]. The hydrogel affords efficient cell delivery into the bone defect site, cell niche establishment, and enhancement of mineralization [4]. Their unique properties, including similarities with the ECM, hydrophilicity, high permeability to oxygen and nutrients, and inherent cellular

interaction capabilities, make them leading candidates for engineered tissue scaffolds [1, 61], Figure 2.

1.4.1 Physical Versus Chemical Crosslinking Hydrogels. The hydrogel 3D network can be formed via physical or chemical crosslinking methods. An increased interest in physically cross-linked hydrogels is due to the absence of cross-linkers reagents used for formation. The formation of physical bonds achieves the physical crosslinking through hydrogen bonds or van der Waals interactions between the constitutive polymer chains. For instance, Polyacrylic acid (PAA) and polymethacrylic acid (PMAA) make complexes with polyethylene glycol (PEG). These complexes have hydrogen bonding between the oxygen of the PEG and the carboxylic group of PAA/PMAA[62]. These physical crosslinks may not be irreversible in nature, but they are adequate to form hydrogels insoluble in aqueous biological solutions. So, these physical crosslinking can absorb the water but network defects may happen due to free chain ends or chain loops [29].

On the other hand, an increased interest in chemically cross-linked hydrogels is due to the excellent mechanical strength of chemically cross-linked hydrogels [62]. The chemical crosslinking is achieved by the formation of stable covalent bonds, mediated by crosslinking agents, between the polymer chains [63, 64]. Hydrophilic polymers have certain functional groups such as NH_2, COOH, OH that may be used for the formation of hydrogels. The reactions such as an amine-carboxylic acid or an isocyanate-OH/NH_2 reaction or Schiff base formation may be used to form covalent linkages between polymer chains [62, 64]. The chemically cross-linked method is highly versatile to improve the mechanical property of the hydrogels. Although, cross-linking agents are often toxic compounds. The harmful effects of chemical cross-linking can be avoided by the process

of using radiation or electron beam method. Radiation cross-linking is more advantageous as the degree of cross-linking can be managed by the amount of dose used and is an energy-efficient and cleaner process with no harmful residuals in the products [62, 64].

1.4.2 Natural Versus Synthetic Hydrogels. Hydrogels are categorized according to their source (natural or synthetic). Hydrogels can be made of wide range of natural biodegradable polymers such alginate, chitosan, hyaluronic acids, collagen, gelatin, and keratin or synthetic polymers such as polyethylene glycol (PEG), polyvinyl alcohol (PVA), poly(ε-caprolactone) (PCL), poly glutamic acid (PGA), and poly methacrylic acid [61].

Natural hydrogels are recognized as a nature-inspired biomaterial with similarity with the extracellular matrix (ECM), attractive biocompatibility and biodegradability traits. Because of their similarity to ECM, the natural hydrogels may avoid the stimulus of inflammation or immunological response and toxicity [52]. Also, these biomaterials may potentially incorporate peptide sequences within their backbone, such as arginine–glycine–aspartate (RGD) or matrix metalloproteinases (MMPs) sensitive domains that allow modulating the cells attachment, as well as their migration and proliferation within the hydrogel along with its controlled degradation [52, 64, 65]. Natural hydrogels provide a conductive matrix for cell adhesion and migration. However, they lack sufficient mechanical strength to prevent soft tissue compression [64]. On the other hand, synthetic hydrogels provide tremendous flexibility in the design of polymers with defined physical and mechanical properties. Nevertheless, they lack bioactive recognition ligands to support cell-matrix interactions required for adhesion, proliferation, differentiation, and maturation of the seeded cells. This limitation had been overcome by conjugating bioactive ligands or peptide sequences of the extracellular matrix (ECM) proteins to the synthetic matrix. For

instance, the focal adhesion RGD sequence that interacts with integrin binding receptors on the cell surface is the most widely used peptide. Hydrogels have been used as BTE-matrices capable of mimicking ECM topography and delivering bioactive proteins [1]. For example, osteogenic differentiation of MSCs requires a supporting matrix with high modulus and slow degradation, whereas vasculogenic differentiation of progenitor ECs requires a low modulus and relatively fast-degradation of the matrix. For matrices with high modulus and slow degradation rate, many research groups have demonstrated that hydrolytically degradable PEG-based hydrogels, such as linear polyethylene glycol-co-lactide acrylate (LPELA), are potentially useful as a delivery matrix for stem cells in regenerative medicine, (Table 1). They have also implicated gelatin methacrylate (GelMA) as a delivery matrix with low modulus and fast-degradation which afford cell-responsive properties [66].

1.5 Cells Sources for BTE

Selecting the appropriate cell type as part of a TE approach to produce a functional bone graft substitute is vital for the success of the implant. The choice of cells is determined by several criteria in order to achieve effective, successful repair of defected tissues [67]. A sufficient number of cells have to be introduced to fill the defect, cells have the capacity to differentiate into desired phenotypes, cells have to adopt appropriate 3D structural scaffold and produce tissue-like ECM as well as signaling molecules, cells must be structurally and mechanically adaptable with the host cells, cells have to successfully be able to integrate with the host cells and overcome the risk of immunological rejection [59, 67, 68]. The source of the selected cells can be from the patient (autologous), from a human donor but not immunologically identical (allogenic), or from a different species donor

(xenogenic) [69]. Autologous cells consider an excellent source for use in TE due to the low association with immune complications. However, these cells are not cost-effective and batch controlled for universal clinical use [70]. Conversely, allogenic cells provide advantages in terms of uniformity, standardization of procedure, quality control and cost-effectiveness [70]. Furthermore, the source of cells can be categorized into non-stem cells (mature), or stem cells (adult and embryonic stem cells), and zygotes (totipotent stem cells). The use of mature cells is constrained due to its low potential in proliferation and differentiating [70].

Stem cells are undifferentiated cells that can self-renew and commit to specific cell lineages in response to stimuli that provide excellent regenerative potential which will most likely lead to the functionality of the engineered tissue [71]. Because of their capacity for expansion and potential to differentiate into BTE, pluripotent stem cells, and multipotent stem cells have become the cell types of choice. Pluripotent stem cells encompass embryonic stem cells (ESCs) and induced pluripotent stem cells (iPSCs) whereas multipotent stem cells include mesenchymal stem cells (MSCs) and other tissue-specific adult stem cells along with hematopoietic stem cells (HSCs) [72]. Embryonic stem cells (ESCs), umbilical cord blood mesenchymal stem cells (CB-MSCs), induced pluripotent stem cells (iPSCs), and adult stem cells, are among the major candidates for BTE applications [73, 74]. Additionally, an adipose-derived stromal vascular fraction (SVF) is a useful and inexhaustible source for vascularization applications, where regenerating vascularized bone tissues is required [73, 74].

ESCs are isolated from the inner cell mass of the blastocyst during embryological development. ESCs have a high multilineage differentiation capacity and able to self-renew

over long periods, which make them promise for use in regenerative medicine. However, there are ethical considerations, regulatory constraints, and teratomas production when transplanted *in vivo* associated with ESCs [75]. Due to limited and controversial regulations associated with ESCs, cord blood has been found to be an excellent source of fetal MSCs and is safer than ESCs for clinical applications [76].

Umbilical cord blood mesenchymal stem cells (CB-MSCs) are known by their high availability due to the existence of cord blood banks, broad differentiation and proliferation potential, and higher in vivo safety since CB-MSCs have not been reported as teratomas producer when implanted in vivo [73, 77]. The umbilical cord contains 60–80 cm^3 of cord blood that contains ESCs and MSCs, as well as hematopoietic stem cells and endothelial progenitor cells (EPCs). However, more studies are needed to confirm the potential of CB-MSCs for TE applications [73, 77].

Induced pluripotent stem cells (iPSCs) are other attractive stem cell sources for TE due to their ability to be reprogramed, enabling the generation of multiple cell types from a single cell [78]. Human iPSCs have been demonstrated for tissue repair and regeneration, enabling researchers to overcome the ethical and immunological limitations associated with the use of ESCs. Furthermore, iPSCs can be derived from a patient's own cells; as a result, they can be used to model diseases and for screening drugs in human *in vitro* [79]. Taking these into account, implantation of iPSCs in critical-sized defect of immune-deficient mice has been reported to promote new bone formation and partial repair of the defect [43]. In Japan, depending on recent clinical trials involving patients who had debilitating eye diseases, iPSCs are being represented as promising cell sources in clinical settings [44].

Adult stem cells are located in many types of adult tissue including bone marrow, peripheral blood, adipose tissues, nervous tissues, and muscles [80]. For example, mesenchymal stem cells (MSCs) which reside in the bone marrow can differentiate into osteoblasts (bone), chondrocytes cells (cartilage), myoblasts (muscle), and adipocytes (fat), while neural stem cells (NSCs) either differentiate to astrocytes in order to support cells in the nervous system of vertebrates or oligodendrocytes (neurons), respectively [81]. *In vivo*, self-renewal and differentiation of stem cells are determined by signals from their surrounding microenvironment or "niche" [82]. This niche is composed of several other cell types as well as numerous chemicals, mechanical and topographical cues at the micro- and nano-scales, which are believed to serve as signaling mechanisms to determine cell-specific recruitment, migration, proliferation, differentiation as well as the production of numerous proteins required for hierarchical tissue organization [83].

Among cells with therapeutic potential, mesenchymal stem cells (MSCs) have had more attention because they are capable of self-renewal and can differentiate into several types of mesenchymal tissues, including cartilage, bone, and adipose tissue [84]. Additionally, MSCs are very promising for TE applications because of their high ex vivo proliferation capacity and the low donor-site morbidity of the harvesting procedure [85, 86]. It has been demonstrated in various animal models that ex vivo-expanded MSCs are capable of stimulating the regeneration of skeletal defects after implantation [87, 88].

1.6 Cells Sources for Vascularization

Since bone is particularly a highly vascularized tissue, the synergistic development of vasculature and mineralized matrix needs a synchronal interaction between osteogenic and endothelial progenitors [89]. In TE, successful engineered grafts will need a

microvascular network to supply oxygen and nutrients to the cells as well as removing wastes [90]. One of TE approaches for creating a microvascular network is through stimulating pre-vasculogenesis in situ by seeding vascular progenitor cells into a biodegradable scaffold engineered with the appropriate mechanical properties and then promoting cell growth and differentiation in vitro [91]. Capillaries and vessels are generated *de novo* (vasculogenesis) in vitro culture systems by endothelial or endothelial progenitor cells (EPC) instead of existing vasculature (angiogenesis) [92], figure 3. The generation of vasculature within a TE tissue will depend on several factors: progenitor EC type, the microarchitecture of the scaffold material, the biochemical environment, and mechanical signals [89]. Vascularization supported by cell-based therapies has gained more attention using differentiated macrovascular endothelial cells (ECs) or endothelial progenitor cells (EPCs) [92, 93]. Mature ECs have been well-established to stimulate angiogenesis. Among them, human umbilical vein endothelial cells (HUVECs), microvascular endothelial cells (MVECs) and human aortic endothelial cells (HAECs) are well-known applied primary endothelial sources for TE vascular graft (TEVG) construction [92]. HUVECs, MVECs, and HAECs are derived from vessel walls, considered to be differentiated, mature endothelial cells (ECs), and are employed as "controls" for EPC studies [94]. Although human MVECs have been reported to reseed decellularized vasculature in vitro successfully, the graft stimulates hematoma formation after transplantation and occlusions within capillaries after implantation for one week [95]. While HUVECs, which represent one of the most commonly employed cells in vascularized BTE. These cells naturally generate vessel-like structures when cultured in hydrogels [15, 89, 96].

Contrarily with mature ECs, EPCs have been found to be ten times more proliferative than HUVECs and have a higher capacity to contribute to angiogenesis [97]. EPCs are heterogeneous ECs in different stages of differentiation, from hematopoietic bone marrow progenitors to mature endothelial cells that have a role in adult vascular repair [98]. EPCs are mostly unipotent stem/progenitor cells with the implicit in differentiating into mature ECs. Accumulated data suggest the significance of EPCs for neovascularization, vascular remodeling, curing vascular diseases, enhancing the reconstruction of ischemic regions, and promoting angiogenesis in regenerative medicine [99-102].

EPCs types have been described based on isolations from various sources as well as for sharing similar phenotypic characteristics into Haematopoietic EPCs, Non-haematopoietic EPCs, and Tissue-resident EPCs [103]. EPCs that are isolating and culturing endothelial cells from the peripheral blood have gained most of the attention and been categorized into two different types according to their morphologies, appearance time, and protein expression [97, 103]. According to their surface morphology, EPCs showed different types of cells, spindle-shaped and cobblestone-shaped cells. The “spindle-shaped” ECs were later termed early EPCs (eEPCs) while ECs with a “cobblestone” morphology are referred to as late EPCs (lEPCs), or endothelial colony-forming cells (ECFCs)[97, 103].

ECFCs have attracted significant attention because ECFCs are the only population that has all the characteristics of a real EPCs [94]. ECFCs are a subset of progenitor cells that circulate in peripheral blood and contribute to the formation of new vasculature [104, 105]. ECFCs exhibit clonal proliferative ability, present endothelial cell surface markers, and possess prominent postnatal vascularization potential in vitro and in vivo [105]. The

identification of ECFCs in humans opened a promising avenue to noninvasively isolate large quantities of autologous ECs for clinical application [104, 106]. Several preclinical studies have demonstrated the inherent and robust vasculogenic properties of ECFCs and their therapeutic potential to endothelialize cardiovascular grafts in vivo [105-107]. Furthermore, ECFCs can self-assemble into long-lasting microvascular networks that integrate with the host vasculature after post-transplantation into immunodeficient mice [108].

In several studies, ECFCs have been used for the generation of prevascularized TE constructs in combination with other cells and biocompatible scaffolds [109]. Natural or synthetic scaffold mimic structural and functional properties of the natural ECM and can be regulated by physicochemical processes to optimize the biomechanical properties of the scaffold to maintain the cell function, the progression of the vascular network, and tissue regeneration [108, 109]. This approach provides better control of the microenvironmental components that govern blood vessel assembly [110]. It also provides the potential to coculture other cell types that either promote angiogenesis or give rise toward tissue-specific cell lineage [109]. Additionally, it allows regulating the biological activity of ECFCs by changes in the structure of biocompatible scaffold or by introducing of trophic mediators that assist neovascularization and regeneration [110]. Previous studies with ECFCs encapsulated in Matrigel reported that these cells generated functionally long-lasting and host-interconnected vascular networks in vivo particularly in coculturing with MSCs or ADSCs [33, 110-112]. ECFCs can also employ as paracrine mediators before the initiation of blood perfusion, regulating the regenerative potential of MSCs [104]. It has shown that MSCs are highly dependable on PDGF-BB and that ECFCs provide essential

angiocrine factors required to preserve MSCs as viable [4, 104]. This early angiocrine ultimately supports extensive engraftment and long-term differentiation of transplanted MSCs [104].

1.7 Challenges to BTE Approaches

Despite the wealth progress that has been made in the field of TE, critical obstacles must be overcome in order to generate functional tissues. The first challenge is the demand to use massive doses of growth factors to differentiate cells to compensate their degradation, poor retention time as well as control of the sustained delivery of growth factors to the progenitor cells [4, 113, 114] effectively. The second challenge is the lack of sufficient scaffold vascularization.

Regarding growth factors, since they undergo rapid degradation, encapsulation within a material carrier can provide protection from enzymes, enhanced growth factor retention at the target site, and sustained growth factor release [35]. Furthermore, it has been reported that the extent of bone formation in vivo depends on the exposure time of osteoprogenitor cells and endothelial progenitor cells to BMP2 and VEGF, respectively. Therefore, the controlled delivery system of growth factors becomes increasingly necessary and vital [4].

Hence, to address the first challenge a set of self-assembled, plasmin-cleavable NPs for on-demand release of BMP2 in response to enzymes secreted by hMSCs and ECFCs encapsulated in a micropatterned composite hydrogel for induction of vascularized osteogenesis. To do this, polyethylene glycol (PEG) chain-extended with self-assembling peptide glycine-(phenylalanine)3 (GFFF) and the plasmin-cleavable GGKFKTGG peptide were used to form self-assembled NPs and facilitate a wide range of timed release for

rhBMP2. Regarding VEGF delivery, nanogel (NG) was engineered to control the release rate of VEGF in the patterned hydrogel. To do this, polyethylene glycol (PEG) chain-extended with short lactide (L) and glycolide (G) segments were used to form self-assembled NGs and facilitate a wide range of timed release of VEGF.

Regarding lack of sufficient vascularization, TE encounters a mass transfer challenge that limits scaffold construct size in vivo regardless of tissue-specific goals. The majority of progenitor cells are encapsulated within 100-200 microns of capillaries where sufficient oxygen and nutrition is provided, and metabolic waste can be transported [113, 115]. Therefore, successful regeneration of large bone defects needs early induction of vascularization in the scaffold [4, 115].

As it is mentioned earlier, one of TE approaches for creating a microvascular network is through stimulating pre-vasculogenesis in situ by seeding vascular progenitor cells into a biodegradable scaffold engineered with the appropriate mechanical and patterning properties and differentiating them using vascular endothelial growth factor (VEGF). The second approach is to induce prevascularization in vitro by using a co-culture system of vascular progenitors' cells and osteoprogenitor cells. Cells that are cultured in conjunction with ECs may have either a direct or indirect effect on the development of vascular networks in tissue-engineered constructs [92]. Mesenchymal stem cells (MSC) have been reported to provide structural support for neovessel formation. The co-culture of MSCs with endothelial progenitor cells such as EPC and HUVEC cells has been reported to induce MSC to differentiate into mural [92, 116]. It is remarkable that the ultimate effective bone regeneration and vessel formation in a critical-sized defect is also related to the close association and interaction between angiogenesis and osteogenesis.

Hence, to address the second challenge, micropattern channels loaded with a suspension of hMSCs + ECFCs and NG-VEGF in a crosslinked gelatin methacryloyl (GelMA) hydrogel. While hMSCs and NP-BMP2 were encapsulated in a patterned matrix based on acrylate-functionalized lactide-chain-extended linear polyethylene glycol (LPELA) hydrogel. This system will be designed to form an osteoblastic-vascular niche in the structure of the engineered scaffold.

It should be also emphasized that osteogenesis and vascularization processes are coupled during the bone formation and regeneration as the maximum extent of osteogenesis follows the maximum level of vascularization and vice-versa. Therefore, in this work, a patterned hydrogel was designed to facilitate controlling both osteogenesis and vasculogenesis processes in the scaffold and consequently increase the extent of bone formation.

Accordingly, the following aims are considered for testing the hypothesis toward the objectives.

Aim 1. To evaluate the temporal expression of proteases by the encapsulated hMSCs and ECFCs.

Aim 2. To synthesize biodegradable, self-assembled, polyethylene glycol-based nanoparticles and evaluate with respect to size, degradation rate and the release kinetics of BMP2- grafted nanogels.

Ami 3. To evaluate the extent of vasculogenesis and osteogenesis of human mesenchymal stem cells (hMSCs) and human colony-forming endothelial cells (ECFCs) encapsulated in a patterned hydrogel with the spatiotemporal release of BMP2 and VEGF.

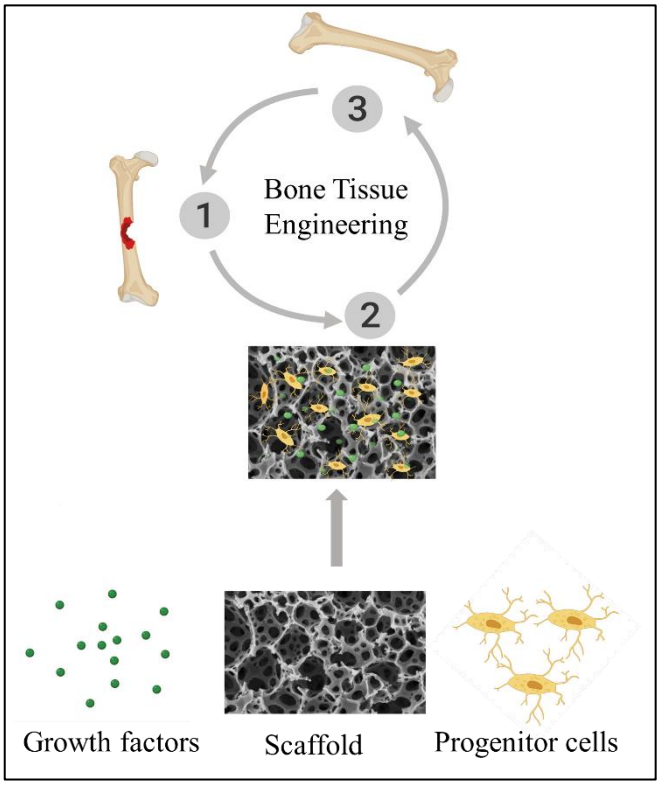

Figure 1.1 TE approach for reconstruction of large bone defects

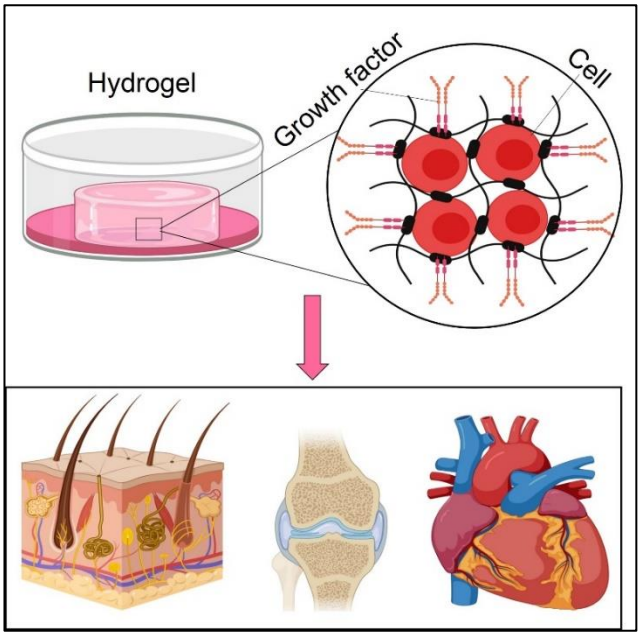

Figure 1.2: Applications of hydrogels in TE

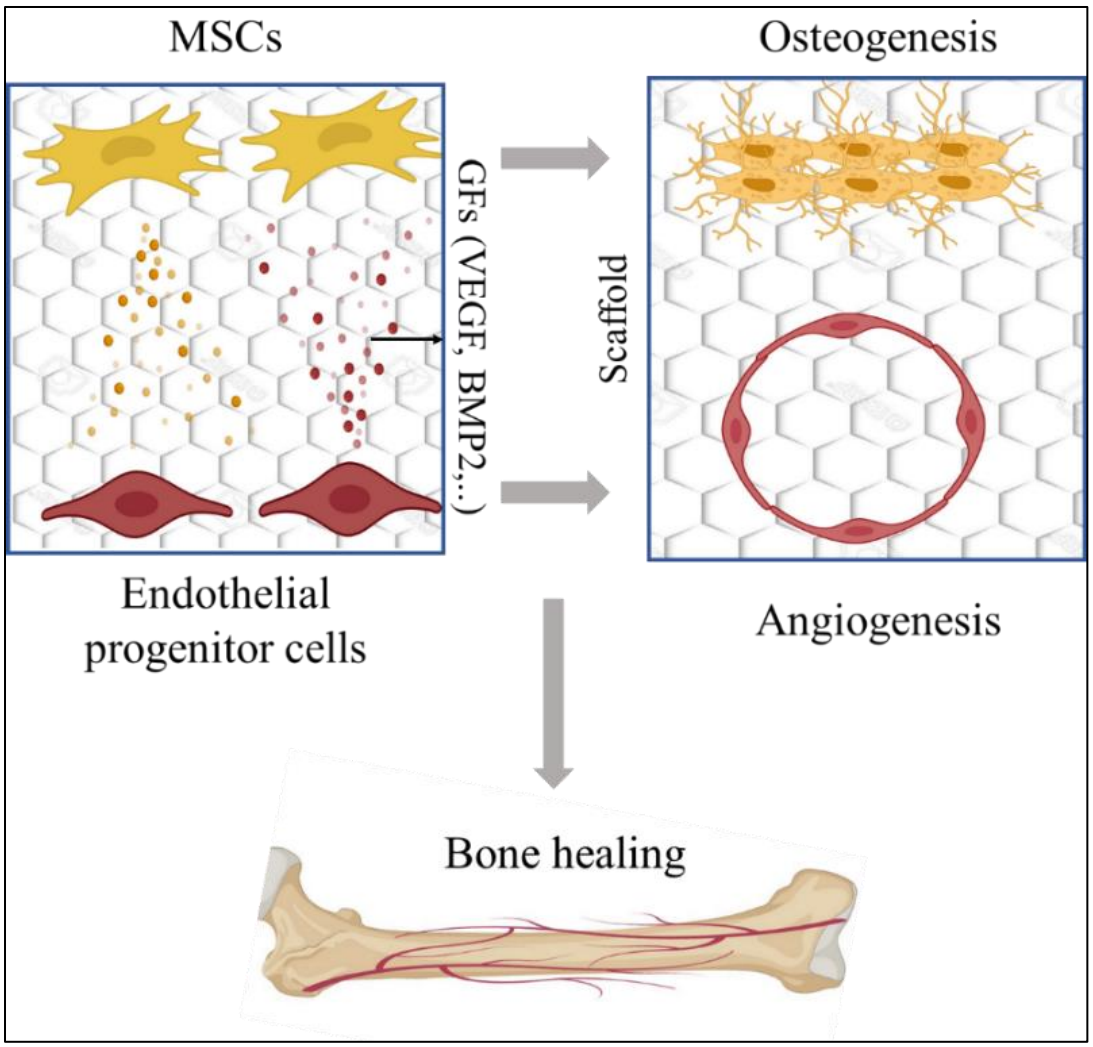

Figure 1.3: Synchronize vasculogenesis and osteogenesis in BTE

CHAPTER 2: PLASMIN-CLEAVABLE NANOPARTICLES FOR ON-DEMAND RELEASE OF MORPHOGENS IN VASCULARIZED OSTEOGENESIS[1]

2.1 Introduction

A major obstacle to the use of tissue engineered (TE) constructs for the reconstruction of skeletal defects is insufficient vascularization and slow rate of bone regeneration [117]. Bone morphogenetic proteins (BMPs) are used as potent osteogenic factors in certain clinical applications like spinal fusion to accelerate bone formation [118]. In addition to BMPs, rate of bone formation can be regulated by angiogenic factors like vascular endothelial growth factor (VEGF) via the crosstalk between the differentiating mesenchymal stem cells (MSCs) and endothelial colony-forming cells (ECFCs) [119]. VEGF is predominantly expressed during the early phase of bone formation to vascularize the regenerating volume whereas BMPs are continuously expressed during mineralization, callus formation and remodeling [120]. Several studies by us and others have shown that sustained delivery of bone morphogenetic protein-2 (BMP2) enhances osteogenic differentiation of MSCs [121-123]. In a previous study, we demonstrated that sustained release of VEGF from nanogels (NGs) in the first five days within the microchannels of a patterned construct and sustained release of BMP2 from NGs over three weeks within the matrix of the construct considerably increased the extent of vasculogenesis and

[1] Safaa Kader, Mehri Monavarian, Danial Barati, Seyedsina Moeinzadeh, Thomas M. Makris, Esmaiel Jabbari. Biomacromolecules 2019, 20, 8, 2973-2988. Reprinted here with permission of publisher.

osteogenesis by the encapsulated MSCs and ECFCs [4, 124]. Further, the timed-release of EGF and BMP2 from the NGs significantly increased the expression of basic fibroblast growth factor (bFGF) which was attributed to the coupling of paracrine signaling between the MSCs and ECFCs [4]. Cell-mediated delivery systems are reported to improve temporal bioavailability of growth factors [125, 126]. We hypothesized that on-demand release of osteogenic and vasculogenic morphogens in response to enzymes secreted by human MSCs (hMSCs) and ECFCs could further enhance the exchange of paracrine factors between the two cell types, leading to robust bone formation. Further, the on-demand release could potentially mitigate the adverse effects of BMP2 in spinal fusion and other clinical orthopedic applications [127].

An exciting approach to the on-demand release of morphogens in tissue regeneration is the use of enzymatically-responsive systems that release the morphogen in response to proteases secreted by stem cells and their progenies [128, 129]. In particular, MSCs and ECFCs express proteases to degrade the extracellular matrix (ECM) as they migrate to the site of injury [130, 131]. MSCs invade the ECM during angiogenesis via different protease families including the plasmin axis of serine proteases and the plasmin-independent matrix metalloproteinases (MMPs) [132]. Human MSCs have a strong fibrinolytic activity by expressing key elements of the fibrinolytic cascade including urokinase plasminogen activator (uPA) and its receptor (uPAR), tissue plasminogen activator (tPA) and plasminogen inhibitor PAI [133]. Further, it has been shown that the expression level of fibrinolytic enzymes tPA and uPA in hMSCs is dependent on factors that mediate vascularization and bone formation like basic fibroblast growth factor (bFGF), transforming growth factor-β (TGF-β) and interleukin-1β (IL-1β) [134]. Studies on

fibrinolytic capacity of MSCs in a fibrin clot indicate that the activity of plasmin and the extent of fibrin degradation during wound healing is controlled by MSCs [134-136]. Therefore in this work, the plasmin-specific lysine-phenylalanine-threonine-lysine (KFTK) peptide was used for enzymatic degradation of PEG-based nanoparticles (NPs) in response to plasmin-related proteases secreted by hMSCs and ECFCs [137].

Peptides due to their sequence diversity, specificity, and tunable configuration have been used extensively as building blocks for self-assembled nanostructures in drug delivery and tissue engineering [138-140]. Among these the oligopeptides diphenylalanine (FF), triphenylalanine (FFF), tetraphenylalanine (FFFF) and their derivatives assemble into a variety of micro- and nano-structures by aromatic interaction between the phenyl side chains [138, 141-143]. For example, the oligopeptide FF assembles into highly ordered nanotubes and nanowires in response to changes in temperature or ionic strength [138, 144] and the structure can be changed from tubular to fibrillar or spherical by FF modification with Fmoc-protecting or thiol groups [144]. Similarly, oligopeptide FFF and its derivatives assemble into a wide range of nanostructures from spheres to plates, rods, doughnuts, and needles [130, 143]. Conjugation of polyethylene glycol (PEG) to these peptides enhances water solubility and biological stability and reduces immunogenicity of the peptides [145]. In this regard, conjugation of oligopeptide FFKLVFF to PEG produced a fibrillar nanostructure with FFKLVFF and PEG as the core and corona, respectively [145]. In another study, PEG-FFFF conjugates self-assembled into nanotubes, fibers, and wormlike micelles as the length of the PEG macromer was increased [146]. Due to the structural diversity of phenylalanine oligopeptides, we used the short peptide FFF in this work to generate self-assembling and enzymatically-cleavable PEG-peptide NPs.

The objective of this work was to synthesize self-assembled, plasmin-cleavable NPs for on-demand release of BMP2 in response to enzymes secreted by hMSCs and ECFCs encapsulated in a micropatterned composite hydrogel for induction of vascularized osteogenesis. The following approach was used to achieve the objective. The sequence triphenylalanine (FFF) was used for self-assembly; [130, 140, 143] the sequence lysine-phenylalanine-threonine-lysine (KFTK) was used as a plasmin-cleavable peptide ;[132, 147] and short glycine (G) sequences were used as spacers in synthesizing the PEG-peptide conjugate. The difunctional cysteine-terminated (C) peptide CGGK(GFFF-acetyl)GGKFKTGG was synthesized in the solid phase using doubly-protected α-Fmoc and ε-MTT lysine (Figure 2.1a). The peptide was conjugated to polyethylene glycol diacrylate (PEGDA) by the reaction between cysteine and acrylate groups (Figure 2.1b). Next, the chain-ends of the PEG-peptide conjugate were functionalized with succinimide (suc) groups (Figure 2.1c) and the suc-peptide-PEG-peptide-suc macromer was self-assembled in aqueous solution to form NPs, hereafter referred to as PxSPCP NPs (Figure 2.1d). Then, BMP2 was grafted to the NPs by the reaction between succinimide and amine groups to form BMP2-PxSPCP NPs (Figure 2.1e). The vasculogenic protein VEGF was conjugated to the self-assembled hydrolytically-degradable NGs based on PEG with short lactide and glycolide segments as previously described [4]. The BMP2-PxSPCP NPs were characterized with respect to size, particle stability, grafting efficiency, protein stability and release, and osteogenic differentiation of hMSCs. The synthesized BMP2-PxSPCP NPs were tested in a patterned, cellular, composite hydrogel encapsulating hMSCs and ECFCs with respect to osteogenesis and vasculogenesis. A hydrogel construct patterned with microchannels was generated using a cylindrical mold inserted with needles through

two end-caps as we previously described (Figure 2.2a) [4]. The needle-inserted mold was filled with a suspension of hMSCs and BMP2-PxSPCP NPs in acrylate-functionalized poly(ethylene glycol-co-lactide) (LPELA) hydrogel (Figure 2.2b) and crosslinked. After removing the needles, a suspension of ECFCs+hMSCs and VEGF-NGs in gelatin methacryloyl (GelMA) was injected in the microchannels and crosslinked (Figure 2.2c). The constructs with spatiotemporal patterns of cells and growth factors were cultured in vasculogenic/osteogenic medium (without VEGF or BMP2) and characterized with respect to cellularity, expression of osteogenic and vasculogenic markers, mineralization, and vasculogenesis.

2.2 Materials and Methods

Lactide (L) monomer with >99.5% purity (Ortec, Easley, SC) was dried as described.[4] PEG with molecular weights (MW) of 2.0, 5.0 and 7.5 kDa, PEGDA with 575 Da MW, porcine skin gelatin (type A, 300 bloom), tin (II) 2- ethylhexanoate (TOC), dimethyl sulfoxide (DMSO), methacrylic anhydride (MA), Alizarin red, and 4,6 diamidino-2-phenylindole (DAPI) were received from Sigma-Aldrich (St. Louis, MO). Dichloromethane (DCM, Acros Organics, Pittsburg, PA) was dried by distillation over calcium hydride. Diethyl ether, dimethylformamide (DMF) and hexane were received from VWR (Bristol, CT) and used as received. Dialysis tubing with 0.1-0.5 kDa and 3.5 kDa cutoff MW was received from Spectrum Laboratories (Rancho Dominquez, CA). N,N′-disuccinimidyl carbonate (DSC) and bovine serum albumin (BSA) were received from Novabiochem (San Diego, CA) and Jackson ImmunoResearch (West Grove, PA), respectively. EBM2 medium, EGM-2 BulletKit medium, human basic fibroblast growth factor (bFGF), R3-insulin-like growth factor-1 (IGF-1), human epidermal growth factor

(EGF), ascorbic acid (AA), β-sodium glycerophosphate (βGP), dexamethasone (DEX), hydrocortisone, gentamycin sulfate (GS), penicillin (PN), streptomycin (SP), and amphotericin-B were received from Lonza (Hopkinton, MA). PECAM-1 (CD31) and bovine anti-rabbit IgG-FITC (secondary antibody) were received from Santa Cruz Biotechnology (Dallas, TX). Human VEGF, rhBMP-2 (hereafter referred to as BMP2), their Enzyme-Linked Immunosorbent Assay (ELISA) kits, and bFGF (FGF2) ELISA kit were received from MyBioSource (San Diego, CA). Human plasminogen and MMP-2 ELISA kits were received form Innovative Research (Court Novi, MI) and Boster (Pleasanton, CA), respectively. Acetomethoxy derivative of calcein (cAM) and ethidium homodimer (EthD) were received from Life Technologies (Grand Island, NY), and MTS cell viability assay was received from ThermoFisher (Waltham, MA). Quant-it PicoGreen dsDNA reagent kit was received from Invitrogen (Carlsbad, CA). The kits for QuantiChrom calcium and alkaline phosphatase (ALP) assays were received from Bioassay Systems (Hayward, CA).

2.2.1 Material Synthesis. A two-step procedure was used to synthesize linear LPELA macromonomer as we previously described [66, 148, 149]. Acrylamide-terminated glycine-arginine-glycine-aspartic acid (Ac-GRGD) cell-adhesive peptide was synthesized and purified as we previously described [150]. GelMA was synthesized by the reaction of gelatin with methacrylic anhydride as we previously described [124, 151]. PEG with PEG MW of 12 kDa was chain-extended with short lactide (L) and glycolide (G) blocks (LG/PEG molar ratio of 24 and L:G ratio of 60:40), the chain-ends were terminated with succinimide groups, the macromers were assembled into NGs by dialysis, and VEGF was grafted to the NGs to generate VEGF-NGs as we previously described [4]. The grafting

efficiency of VEGF to the NGs was 92±1%. VEGF was released steadily from VEGF-NGs in 7 days, as we previously measured by ELISA [4].

2.2.2 Synthesis of Plasmin-Cleavable NPs. The following approach was used to synthesize the PEG-SPCP conjugate as illustrated in Figure 2.1. The sequence cysteine-glycine-glycine-lysine with doubly-protected lysine residue [CGGK(α-Fmoc)(ϵ-MTT)] was synthesized in the solid phase on Wang resin as described [126, 152]. The acetyl-terminated triphenylalanine with a glycine spacer (GFFF-ac) was synthesized separately in the solid phase on Wang resin and coupled to the MTT terminus of CGGK to yield the CGGK(GFFF-ac)(α-Fmoc) sequence. After MTT deprotection, the sequence plasmin-cleavable KFKT with two glycine spacers on each side (GGKFKTGG) was coupled by EDC chemistry to the Fmoc terminus of CGGK(GFFF-ac)(α-Fmoc) to yield the CGGK(GFFF-ac)GGKFKTGG peptide (SPCP) (Figure 2.1a). After cleaving from the resin, the SPCP peptide was purified by high-performance liquid chromatography (HPLC) and characterized by electrospray ionization spectrometry as we previously described [150]. The peptide CGGK(GFFF-ac)GGG without the KFKT sequence (SP) was synthesized to produce NPs that did not undergo cleavage in response to plasmin.

PEG with MW of 2, 5, and 7 kDa was reacted with acryloyl chloride to produce PEGDA as described [153]. Next, PEGDA in PBS was added dropwise to the solution of SPCP peptide (PEGDA:SPCP molar ratio of 1:2.5) in acetonitrile/PBS (pH 7.4, 1 mM TCEP) in a reaction flask with stirring and nitrogen flow. The reaction between the cysteine groups of SPCP and acrylate groups of PEGDA was allowed to proceed for 6 h under ambient condition. After the reaction, the PEG-SPCP conjugate was purified by dialysis (500 Da MW cutoff membrane) against PBS and lyophilized (Figure 2.1b). Then, the

carboxyl end-groups of PEG-SPCP conjugate were succinimide functionalized by reaction with DSC as we previously described (Figure 2.1c) [126]. The chemical structure of the lyophilized PEG-SPCP conjugate was characterized by ^{1}H-NMR (Varian Mercury-300, Palo Alto, CA) and FTIR (Perkin Elmer Spectrum 100, Waltham, MA) as described [126]. The functionalized conjugates with and without the plasmin-cleavable peptide are hereafter referred to as PxSPCP and PxSP, respectively, where the letter "x" is the PEG MW in kDa, "SP" is for the self-assembled peptide FFF, and "CP" is for the plasmin-cleavable peptide KFKT.

To form NPs, the functionalized PxSPCP conjugates were dissolved in DMSO and self-assembled by dialysis against PBS. The NP suspension was freeze-dried to produce a free-flowing powder (Figure 2.1d). The average particle size, size distribution, and zeta potential of PxSPCP NPs were measured with a Zetasizer dynamic light scattering (Nano ZS, Malvern Instruments, Malvern, UK) at 25°C in Nano-pure water (Millipore, Billerica, MA) as described.[4] To observe particle shape, 20 μL of the suspension was deposited onto a 300-mesh carbon-coated copper grid and imaged with a transmission electron microscope (Hitachi H8000, Schaumburg, IL).

2.2.3 Cell Culture. Human MSCs (Lonza, Allendale, NJ) were cultured in basal MSC medium (high-glucose DMEM supplemented with 10% FBS, 100 units/mL penicillin and 100 μg/mL streptomycin) at a seeding density of 5000 cells/cm^2 as we previously described [137]. Human ECFCs (Boston Children Hospital) were cultured on 1% gelatin-coated flasks in basal ECFC medium (Bluekit EBM-2 medium supplemented with 20% FBS) at a density of 6500 cells/cm^2 as described [147].

2.2.4 Cell Encapsulation in LPELA and GelMA Hydrogels. The LPELA precursor solution was prepared by mixing 200 mg LPELA, 4 mg Ac-GRGD cell-adhesive peptide (2% by weight of LPELA) and 1.5 mg photo-initiator (0.75 wt%) in 1 mL PBS. After sterilization by filtration, hMSCs at a density of 2×10^6 cells/mL were added to the sterile LPELA solution, the suspension was injected between two sterile glass slides separated by a spacer and crosslinked by UV irradiation as we described previously [4, 149]. The GelMA precursor solution was prepared by mixing 50 mg GelMA and 0.375 mg photo-initiator (0.75 wt%) in 1 mL PBS. After sterilization by filtration, a 50:50 mixture of hMSCs+ECFCs at a total density of 2×10^6 cells/mL were added to the sterile GelMA solution, injected between two sterile glass slides separated by a spacer and crosslinked by UV irradiation as we previously described [4]. After washing with PBS, the cell-encapsulated LEPLA or GelMA hydrogels were cultured in the appropriate medium for osteogenic or vasculogenic differentiation, respectively.

2.2.5 Grafting BMP2 to PxSPCP NPs and Protein Release. BSA was grafted to PxSPCP NPs for particle size analysis, grafting efficiency and protein stability studies whereas BMP2 was grafted for protein release and cell culture experiments. For grafting, 10 mg PxSPCP NPs were dispersed in PBS by sonication for 5 min. Next, 0.5 mL of BMP2 (400 ng/mL) or BSA (20 mg/mL) were added to the NP suspension and the grafting reaction between the free amine groups of BMP2 or BSA and the succinimide groups of the NPs was allowed to proceed overnight under ambient condition as we previously described to produce BMP2-PxSPCP NPs (Figure 2.1e) [4]. After the reaction, the suspension was centrifuged at 15000 rpm for 10 min and the amount of free (not grafted) BMP2 or BSA in

the supernatant was quantified by ELISA or BCA protein assay, respectively, as we previously described [126].

For release studies, plasmin (0.2 U/mL) was added to the suspension of 10 mg BMP2-PxSPCP NPs in 1 mL PBS and incubated at 37°C with shaking at 50 rpm. At each time point, the suspension was centrifuged at 10,000 rpm for 5 min, the supernatant containing the free BMP2 was collected and replaced with fresh plasmin solution. BMP2 content of the supernatant solution was measured with a BMP2 ELISA kit as we previously described [4]. BMP2 added directly to the plasmin solution and BMP2-PxSP NPs were used as control groups.

2.2.6 Bioactivity and Cell Compatibility of BMP2-PxSPCP NPs. Circular dichroism (CD) was used to determine the effect of grafting on the secondary structure of the model BSA protein. CD spectra of free or grafted BSA in PBS were collected with a spectropolarimeter (JASCO J815, Essex, UK) at 20°C with a cuvette of 0.1 cm path length as we previously described [154] For evaluation of cell compatibility, hMSCs (1×10^6 cells/mL) and PxSPCP NPs (10 mg) were encapsulated in LPELA hydrogel as described in section 2.5 and cultured in basal medium. At each time point, the hydrogels were stained with cAM/EthD live/dead assay (1 μg/mL) and the stained cells were imaged with an inverted fluorescent microscope (Nikon Eclipse Ti-ε, Nikon, Melville, NY) as described [149]. To quantify cell viability, the medium was replaced with fresh medium containing 10% MTS and incubated for 6 h at 37^{o}C and the sample absorbance was measured with a microplate reader (Molecular Devices, San Jose, CA) at a wavelength of 490 nm.

The bioactivity of BMP2 released from the NPs was determined by measuring the expression of osteogenic markers for hMSCs encapsulated in LPELA hydrogel and

incubated in the osteogenic medium (without BMP2 or DEX) supplemented with BMP2 released from the NPs. The measured markers of osteogenic differentiation included Runx2 (early marker) and calcium (late marker). Control groups included hMSCs encapsulated in LPELA hydrogel and incubated in osteogenic medium with or without BMP2 directly added to the medium.

2.2.7 Measurement of Protease Expression of Encapsulated hMSCs and ECFCs. hMSCs at a density of 2×10^6 cells/mL were encapsulated in LPELA hydrogel whereas ECFCs or a 50:50 mixture of hMSCs+ECFCs at a total density of 2×10^6 cells/mL were encapsulated in GelMA hydrogel as described in section 2.5. After gelation, disk-shape samples were cut from the gels and incubated in the appropriate medium for up to 7 days. hMSCs encapsulated in LPELA was cultured in osteogenic medium whereas ECFCs or hMSCs+ECFCs in GelMA were cultured in vasculogenic medium. At each time point, samples were divided into two parts for analysis. One part was used for measurement of differential RNA expression of plasminogen, uPA, tPA, matrix metalloproteinase-2 (MMP2), and membrane-type matrix metalloproteinase-1 (MT-MMP1) by real-time polymerase chain reaction (RT-qPCR) as we previously described [150, 155]. The gene-specific primers for RT-qPCR were designed and selected using the Primer3 web-based software as described [155]. The forward and reverse primers, synthesized by Integrated DNA Technologies (Coralville, IA), are listed in Table 1. The expression of GAPDH house-keeping gene was used as a reference and the model of Pfaffl was used to determine the expression ratio of the genes as described [156]. The other part was used to quantify protein expression of the total plasmin and MMP-2 in the intracellular and extracellular compartments as well as the extracellular expression of bFGF. To quantify the extracellular

expressions, the medium of the hydrogel cultures was centrifuged at 15000 rpm for 10 min to separate the insoluble residue, the supernatant was concentrated 5-fold using a 10 kDa cutoff membrane, and the protein concentration was measured by ELISA as we previously described [4]. To quantify the intracellular expressions, the hydrogel sample was washed, digested in RIPA buffer, centrifuged at 15000 rpm for 15 min, and the concentration of proteins in the supernatant was measured by ELISA as described [4].

2.2.8 Encapsulation of hMSCs and ECFCs in Patterned Constructs. Patterned hydrogel constructs with GelMA micro-channels in LPELA matrix were generated for co-culture experiments as we previously described (Figure 2.2) [4]. Needles with a diameter of 400 μm and inter-needle separation of 500 μm were inserted through the end-caps of a cylindrical Teflon mold with a diameter and height of 5 and 3 mm, respectively (Figure 2.2a). Next, the sterile LPELA precursor suspension composed of 200 mg LPELA, 4 mg Ac-GRGD cell-adhesive peptide, 1.5 mg photo-initiator, 20 mg plasmin-cleavable PxSPCP NPs, and $2x10^6$ hMSCs in 1 mL PBS was injected in the cylindrical mold and crosslinked by UV irradiation as we previously described (Figure 2.2b) [66]. Then, the needles were removed from the LPELA matrix and the sterile GelMA precursor suspension composed of 50 mg GelMA, 0.375 mg photo-initiator, 2 mg VEGF-NGs, 2×10^6 of 50:50 hMSCs+ECFCs was injected in the channels and crosslinked by UV irradiation as described (Figure 2.2c) [4]. After gelation, the patterned hydrogel constructs were washed with warm PBS, cultured in basal medium for one day followed by cultivation in vasculogenic medium (without VEGF) for days 2-7, 50:50 mixture of vasculogenic and osteogenic medium (without VEGF, BMP2 or DEX) for days 8-10, and finally in osteogenic medium (without DEX or BMP2) for days 11-21.

2.2.9 Biochemical, mRNA and Protein Analysis, and Immunofluorescent Staining. At each time point after washing the hydrogel constructs to remove serum proteins and sonicating to lyse the encapsulated cells [157], the samples were divided into four groups for biochemical, mRNA and protein analysis, and immunofluorescent staining. For biochemical analysis, the double-stranded DNA content, ALP activity and calcium content of the homogenized samples were measured as we previously described [157]. For mRNA expression, the RNA of the homogenized samples was extracted and used for measurement of mRNA expression of osteogenic markers (Runx2, Col I and ALP) and vasculogenic markers (vWF, VEGFR, VE-cadherin, and CD31) as we previously described [4]. The designed primer sequences for mRNA marker expression are listed in reference [4]. To compare expression between the groups, mRNA fold difference for expression of the gene of interest was normalized to that of GAPDH followed by normalization against day one expression as described [157]. The expression of CD31 vasculogenic marker of the homogenized samples at the protein level was quantified by western blot as we previously described [4] Alizarin red and immunofluorescent staining were used to image the intensity of mineralization and CD31 expression as we previously described [158, 159]. The stained samples were imaged with a Nikon Eclipse Ti-ε inverted fluorescent microscope.

2.2.10 Statistical Analysis. All experiments were done in triplicate. Significant differences between experimental groups were evaluated using a two-way ANOVA with replication test, followed by a two-tailed Student's *t* test. A value of $p < 0.05$ was considered statistically significant.

2.3. Results

2.3.1 Temporal Expression of Proteases by the Encapsulated hMSCs and ECFCs. The mRNA expressions of uPA, tPA, and plasminogen in the fibrinolytic cascade for the LPELA encapsulated MSCs, GelMA encapsulated ECFCs, and GelMA encapsulated MSCs+ECFCs with incubation time are shown in Figures 2.3a, 2.3b and 2.3c, respectively; the mRNA expressions of MMP2 and MT-MMP1 for the encapsulated MSCs, ECFCs, and MSCs+ECFCs are shown in Figures 2.3d, 2.3e and 2.3f, respectively. The encapsulated hMSCs expressed significant levels of uPA, tPA, plasminogen, MMP2 and MT-MMP1 in osteogenic medium (days 1, 4 and 7) as shown in figures 2.3a and 2.3d. The expression of uPA by MSCs did not change with differentiation in osteogenic medium whereas that of tPA decreased, those of plasminogen and MMP2 increased, and that of MT-MMP1 peaked on day 4. The encapsulated ECFCs did not express significant levels of proteases of the fibrinolytic cascade and the expressions did not change with differentiation in vasculogenic medium (Figures 2.3b and 2.3e). The encapsulated hMSCs+ECFCs expressed significant levels of tPA and plasminogen with differentiation in vasculogenic medium but did not express uPA, MMP2 and MT-MMP1. The expression of tPA of hMSCs+ECFCs peaked on day 4 whereas that of plasminogen increased slightly with differentiation in the vasculogenic medium.

Based on mRNA results, the extra- and intra-cellular expressions of plasmin and MMP2, as well as extracellular expression of bFGF for the encapsulated hMSCs, ECFCs, and hMSCs+ECFCs, were measured at the protein level and the expressions are shown in Figure 2.4. For all cell types, the expressions of plasmin, MMP2 and bFGF increased with cell differentiation. For all cell types, the extracellular expression of MMP2 was higher

than the intracellular (Figures 2.4a and 2.4b) whereas the difference was not significant for plasmin (Figures 2.4c and 2.4d). After 7 days of culture, the extracellular expression of bFGF by the encapsulated hMSCs in osteogenic medium was higher than the ECFCs or hMSCs+ECFCs in vasculogenic medium with hMSCs+ECFCs showing the lowest bFGF expression (Figure 2.4e). Based on the results in Figures 2.3 and 2.4, the encapsulated hMSCs showed higher expression of proteases with differentiation in osteogenic medium as compared to ECFCs or hMSCs+ECFCs in vasculogenic medium. Therefore, BMP2 was conjugated to plasmin-cleavable PxSPCP NPs and co-encapsulated with hMSCs in LPELA hydrogel of the patterned matrix for on-demand release of BMP2 in response to plasmin expression by hMSCs. As plasmin and MMP2 expression by the encapsulated hMSCs+ECFCs was relatively low, VEGF was conjugated to hydrolytically-degradable NGs and co-encapsulated with hMSCs+ECFCs in GelMA hydrogel of the patterned matrix for release in the first 7 days to stimulate vasculogenic differentiation of the encapsulated ECFCs in the channels.

2.3.2 Characterization of PxSPCP macromer. The mass spectra of CGGK(GFFF-ac)GGKFKTGG (SPCP, MW=1638.9 Da) and CGGK(GFFF-ac)GGG (SP, MW=1018.2 Da) peptides are shown in figure 2.6. In the SPCP spectrum (Figure 2S1a), m/z values of 820 and 1638 Da corresponded to the divalent $[(M+2H)]^{2+}$ and monovalent $[(M+H)]^{+}$ hydrogen cations of the peptide, respectively. In the SP spectrum (Figure 2.6c), m/z value of 1018 Da corresponded to the monovalent $[(M+H)]^{+}$ hydrogen cation of the peptide. The HPLC chromatographs of SPCP and SP peptides are shown in the inset b and d of Figure 2S1, respectively. The retention times of SPCP and SP peptides were 10.1 (Figure 2.6b)

11.0 (Figure 2,6d) min, respectively. The ^{1}H-NMR spectra of PEGDA and PEG-SPCP-NHS (PxSPCP) are shown in Supplementary Figure 2.7a.

Two chemical shifts with peak positions at 3.6 and 4.2 ppm in the spectrum of PEGDA were attributed to the methylene hydrogens of PEG attached to ether and ester groups, respectively; three chemical shifts with peak positions between 5.85-6.55 ppm were attributed to vinyl hydrogens of the acrylate groups at chain ends as described [153] The disappearance of chemical shifts for methylene protons (5.85-6.55 ppm) of the acrylate groups in the spectrum of PxSPCP confirmed conjugation of the peptide to PEGDA. Further, the appearance of a shift due to methylene hydrogens with a peak position at 2.77 ppm confirmed succinimide functionalization of PxSPCP. The FTIR spectra of PEGDA, PEG-SPCP, and PEG-SPCP-NHS are shown in Supplementary Figure 2S2b. The appearance of characteristic absorption bands in the spectra of PEG-SPCP and PEG-SPCP-NHS with peak positions at 1630 and 3330 cm^{-1} due to vibrations of amides and secondary amines, respectively, confirmed the conjugation of peptide to PEGDA. The appearance of a characteristic band with peak position at 1779 cm^{-1} due to vibrations of NHS group confirmed succinimide functionalization of PEG-SPCP-NHS.

2.3.3 Characterization of PxSPCP NPs. The number-average size distribution of PxSPCP NPs with or without BSA protein grafting for PEG MW of 0.5, 2, 5 and 7.5 kDa are shown in Figures 2.5a to 2.5d, respectively. The corresponding TEM images of the NPs are shown in the inset of Figures 2.5a-d. The average particle size, polydispersity index (PDI), and zeta potential of PxSPCP NPs as a function of PEG MW are listed in Table 1. The average size of the NPs increased from 145±15 nm to 225±10, 265±20 and 325±25 nm as the PEG MW was increased from 0.5 kDa to 2, 5 and 7.5 kDa, respectively. The size

distribution of the NPs was relatively narrow and increased with PEG MW. The average size of P0.5SPCP NPs increased slightly after BSA grafting and the size increase with BSA grafting increased with PEG MW.

The effect of incubation time in basal culture medium on the average size and size distribution for different PEG MW of PxSPCP NPs is shown in Figures 2.6a and 2.6b, respectively. For P0.5SPCP NPs, the hydrodynamic size increased significantly from 200 nm on day 1 to 500 nm on day 7 and PDI increased from 0.13 on day 1 to 0.38 on day 7 which was attributed to particle aggregation. For P2SPCP NPs, the average size increased slightly from 225 nm on day 1 to 260 nm on day 7 and PDI did not change with incubation time. For P5SPCP and P7.5SPCP NPs, the average size and PDI did not change with incubation time. The results in Figures 2.6a and 2.6b indicated that P0.5SPCP NPs aggregated in culture medium whereas P2SPCP, P5SPCP and P7.5SPCP were relatively stable in culture medium with incubation. The effect of BSA grafting on the CD spectrum of PxSPCP NPs as a function of PEG MW is shown in Figure 2.6c. The absorption spectrum of BSA-P0.5SPCP NPs (red) was identical to that of free BSA whereas there was a slight change in absorption spectrum of BSA-P2SPCP NPs (gold) in the 200-125 nm region. The CD spectra of BSA-P5SPCP (dark blue) and BSA-P7.5SPCP (gray) were substantially different from that of free BSA. Therefore, the conformational stability of the grafted BSA decreased with increasing PEG MW of the NPs. Based on the CD results, P0.5SPCP and P2SPCP maintained the secondary structure of grafted BSA whereas P5SPCP and P7.5SPCP denatured the grafted protein. The effect of supplementing the culture medium with PxSPCP NPs of different PEG MW on viability of hMSCs is shown in Figure 2.6d. The viability of hMSCs decreased slightly with increasing PEG MW after

3 days of incubation in basal medium. However, viability of hMSCs was >90% for all PxSPCP NPs. As PEG2SPCP NPs had a relatively stable size distribution in culture medium (Figures 2.6a and 2.6b), only a slight effect on the secondary structure of grafted BSA (Figure 2.6c), and negligible toxicity toward hMSCs (Figure 2.6d), these NPs were selected for vascularized osteogenesis experiments with hMSCs and ECFCs in the patterned hydrogels.

2.3.4 Release Characteristics and Bioactivity of BMP2-PxSPCP NPs. The grafting efficiency of BMP2 to PxSPCP NPs decreased from 73.1±2.7% to 69.5±3.2% and 24.5±1.4% as the PEG MW was increased from 2 kDa to 5 and 7.5 kDa, respectively. This decrease was attributed to higher entrapment of the reactive succinimide groups of PxSPCP within the NPs' core with increasing PEG MW, which reduced their availability for BMP2 grafting. BMP2-PxSPCP NPs were encapsulated in LPELA hydrogel, the hydrogel was incubated in PBS, and the release of BMP2 to the incubating medium was measured with time by ELISA. Figures 2.7a to 2.7c show the release kinetic of BMP2 from the encapsulated NPs in LPELA hydrogel with PxSPCP PEG MW of 2 (Figure 2.7a), 5 (Figure 2.7b) and 7.5 kDa (Figure 2.7c), respectively. Experimental groups included BMP2-PxSPCP NPs plus plasmin encapsulated in the hydrogel (solid brown, solid gray or solid blue in Figures 2.7a to 2.7c, respectively), BMP2-PxSP NPs plus plasmin in the hydrogel (dash brown, dash gray or dash blue in Figures 2.7a to 2.7c, respectively), free BMP2 in the hydrogel (red in Figures 7a-7c), and free BMP2 plus plasmin in the hydrogel (green in Figures 2.7a-c). Approximately 80% of the loaded free BMP2 was released from the hydrogel after 21 days of incubation and the addition of plasmin to the hydrogel did not affect BMP2 release (compare red and green in Figures 2.7a-c). The incomplete (<100%)

release of free BMP2 from the hydrogel was attributed to protein adsorption to the matrix or protein denaturation during hydrogel encapsulation and gelation. ELISA measurements detected a relatively small but significant BMP2 activity with incubation time for BMP2-PxSP NPs and plasmin encapsulated in the hydrogel (see dash yellow, dash gray or dash blue in Figures 2.7a-c) but the activity decreased with increasing PEG MW of the NPs. The cumulative BMP2 activity after 21 days associated with the encapsulated BMP2-PxSP NPs with PEG MW of 2, 5 and 7.5 kDa was 30%, 20% and 19% of the total BMP2 loaded in the hydrogel, respectively. This BMP2 activity was attributed to the release of BMP2-PxSP NPs from the hydrogel which was subsequently detected by ELISA. The BMP2 grafted to PxSPCP NPs and co-encapsulated in the hydrogel with plasmin was gradually released to the medium with incubation time at a rate faster than BMP2-PxSP NPs but slower than the free BMP2. For example, the cumulative release of BMP2 from the encapsulated BMP2-P5SPCP NPs was 60% after 21 days which was higher than the encapsulated P5SP NPs at 20% and slower than the free BMP2 at 80%. The results in Figure 2.7 demonstrate that BMP2 was cleaved by plasmin from PxSPCP NPs, leading to the gradual release of the protein from the hydrogel.

2.3.5 Osteogenic Activity of BMP2 Released from PxSPCP NPs. BMP2-PxSPCP NPs (PEG MW of 2, 5 and 7.5 kDa) and hMSCs were co-encapsulated in LPELA hydrogel, incubated in osteogenic medium without DEX, and the extent of osteogenesis was measured with incubation time. The DNA contents of hMSCs with incubation time for BMP2-PxSPCP NPs with PEG MW of 2, 5 and 7.5 kDa are shown in Figures 2.8a to 2.8c, respectively; mRNA expressions of Runx2 are shown in Figures 2.8d to 2.8f; and ALP mRNA expressions are shown in Figures 2.8g to 2.8i. Experimental groups included

BMP2-P2SPCP NPs (solid brown), BMP2-P2SP NPs (dash brown), BMP2-P5SPCP NPs (solid gray), BMP2-P5SPCP NPs (dash gray), BMP2-P7.5SPCP NPs (solid blue), and BMP2-P7.5SP NPs (dash blue) co-encapsulated with hMSCs in LPELA hydrogel. Control groups were hMSCs encapsulated in LPELA hydrogel and incubated in osteogenic medium supplemented with (red) or without (purple) BMP2, and hMSCs co-encapsulated with BMP2 in the hydrogel and incubated in osteogenic medium without DEX (green). The DNA content of all groups decreased with incubation time. DNA content of those groups incubated in osteogenic medium without BMP2 or with BMP2-PxSP NPs decreased at a slower rate compared to those with BMP2 or BMP2-PxSPCP NPs, consistent with previous reports [160, 161].

The expression of Runx2 increased initially from day 4 to 7 for all experimental groups, peaked on day 7 followed by a decrease from day 7 to 14 for all BMP2-PxSPCP NPs (Figures 2.8d to 2.8f). The osteogenic activity of the experimental groups was measured by peak Runx2 expression of the encapsulated hMSCs. The osteogenic activity of the group with BMP2 added to the medium was higher than the group with BMP2 co-encapsulated with hMSCs in the hydrogel, which was attributed to denaturation of a small but significant fraction of the encapsulated BMP2 during hydrogel formation. The osteogenic activity of BMP2-PxSP NP groups (dash lines in Figures 2.8d-f) was similar to that of no BMP2 group (purple in Figures 2.8d-f), demonstrating that BMP2 grafted to non-cleavable NPs had negligible osteogenic activity. The BMP2-PxSPCP NP groups showed significantly higher osteogenic activity compared to non-cleavable BMP2-PxSP NPs, thus confirming that a significant fraction of BMP2 grafted to BMP2-PxSPCP NPs was cleaved by plasmin secreted by the encapsulated cells. Further, osteogenic activity of BMP2-P2SPCP-NP and

BMP2-P5SPCP-NP groups (solid brown in Figure 2.8d and solid gray in 8e) were similar to that of free BMP2 added to the culture medium whereas that of BM2-P7.5SPCP-NP group (solid blue in Figure 2.8f) was lower. This result was attributed to higher availability of the plasmin-cleavable peptide in P2SPCP and P5SPCP NPs for enzymatic cleavage. The peak Runx2 expression of hMSCs for BMP2-P2SPCP-NP and BMP2-P5SPCP-NP groups was 5.7 which was significantly higher than BMP2-P7.5SPCP-NP at 4.2. ALP mRNA expression of the encapsulated hMSCs peaked on day 14 for all experimental groups (Figures 2.8g to 2.8i). Similar to Runx2 expressions, the peak ALP expression of the group with BMP2 added to the medium was higher than the group with BMP2 co-encapsulated with hMSCs in the hydrogel; peak ALP expression of BMP2-PxSP NP groups (dash lines in Figures 2.8g-i) was similar to that of no BMP2 group (purple in Figures 2.8d-f); and peak ALP expression of BMP2-PxSPCP NP groups was significantly higher than the non-cleavable BMP2-PxSP NPs.The BMP2-P2SPCP-NP group (solid brown in Figure 2.8g) had the highest peak ALP expression followed by BMP2-P5SPCP (solid gray in Figure 2.8h) with BMP2-P7.5SPCP (solid blue in Figure 2.8i) as the lowest. The peak ALP expression of hMSCs for BMP2-P2SPCP-NP, BMP2-P5SPCP-NP and BMP2-P7.5SPCP-NP groups was 60, 52 and 48, respectively. As P2SPCP NPs had the most stable size distribution (Figures 2.6a-b), negligible loss of secondary structure of the grafted protein (Figure 2.6c), and highest osteogenic activity of the grafted BMP2 (Figure 2.8), these NPs were selected for co-culture experiments with hMSCs and ECFCs in the patterned hydrogels.

2.3.6 Osteogenic and Vasculogenic Differentiation of hMSCs and ECFCs in patterned hydrogels with plasmin-cleavable BMP2-P2SPCP NPs. The effect of the on-demand release of BMP2 from plasmin-cleavable NPs on osteogenesis to vasculogenesis was investigated in patterned hydrogels consisting of GelMA microchannels encapsulating hMSCs+ECFCs/VEGF-NGs in LPELA matrix encapsulating hMSCs/BMP2-P2SPCP-NPs. The results are shown in Figures 2.9 through 2.12. All experimental groups were cellular. The groups included patterned constructs with BMP2-P2SPCP-NP in LPELA matrix and VEGF-NG in GelMA channels (BMP2-P2SPCP-NP/VEGF-NG, black); un-patterned constructs with BMP2-P2SPCP-NP+VEGF-NG in a mixture of LPELA+GelMA with a composition identical to the patterned matrix (BMP2-P2SPCP-NP+VEGF-NG UnP, dash gray); patterned constructs with BMP2-P2SPCP-NP in LPELA and GelMA channels without VEGF (BMP2-P2SPCP-NP, green); patterned constructs with LPELA without BMP2 and VEGF in GelMA channels (VEGF-NG, gold); patterned constructs with BMP2 in LPELA and VEGF in GelMA (BMP2/VEGF, red); patterned constructs without BMP2 or VEGF (None, light blue); and un-patterned constructs based on a mixture of LPELA+GelMA with a composition identical to the patterned matrix without BMP2 or VEGF (None UnP, brown).

The DNA content, calcium content, ALP activity, mRNA expression of osteogenic markers Runx2, ALP, and Col I of the patterned cellular constructs are shown in Figure 2.9. The DNA content of all BMP2 or BMP2/VEGF groups (Figure 2.9a) decreased with incubation time, consistent with previous reports [160, 161] For all groups, Runx2 expression (Figure 2.9b) of the encapsulated cells peaked on day 14 whereas Col I expression (Figure 2.9d) and calcium content (Figure 2.9e) steadily increased with

incubation time. For the NP groups, ALP activity peaked on day 18 (Figures 2.9c and 2.9f) whereas it peaked on day 14 for the free BMP2/VEGF group. The groups with BMP2 and VEGF (with or without grafting to NPs/NGs) had highest peak expression of osteogenic markers Runx2 and ALP as well as highest Col I expression and calcium content on day 21. Among the groups with BMP2 and VEGF, the patterned BMP2-P2SPCP-NP/VEGF-NG group had highest expression of osteogenic markers followed by the patterned BMP2/VEGF, un-patterned BMP2-P2SPCP-NP+VEGF-NG, and patterned BMP2-P2SPCP-NP groups. For example, the Col I fold expressions of patterned BMP2-P2SPCP-NP/VEGF-NG, patterned BMP2/VEGF, un-patterned BMP2-P2SPCP-NP+VEGF-NG, and patterned BMP2-P2SPCP-NP groups were 25, 20, 22 and 15, respectively (Figure 2.9d); the calcium contents were 770, 695, 665 and 390 mg/mg DNA (Figure 2.9e); and ALP activities were 6600, 5000, 4850 and 2550 IU/mg DNA (Figure 2.9f). Interestingly, the calcium content, ALP activity, and expression of osteogenic markers for patterned BMP2-P2SPCP-NP group was significantly less than those of BMP2-P2SPCP-NP/VEGF-NG, BMP2/VEGF and un-patterned BMP2-P2SPCP-NP+VEGF-NG groups. This finding can be attributed to the lack of paracrine signaling between hMSCs and ECFCs in the absence of VEGF-NGs. The images for Alizarin red staining of the patterned BMP2-P2SPCP-NP/VEGF-NG, BMP2/VEGF and BMP2-P2SPC-NP groups are shown in Figure 2.10. The images show robust mineralization and nodule formation for these groups with the patterned BMP2-P2SPCP-NP/VEGF-NG group showing the most intense staining.

The DNA content, mRNA expression of vasculogenic markers vWF, VEGFR and VE-cadherin, and protein expression of CD31 vasculogenic marker of the patterned constructs are shown in Figure 2.11. DNA content of the groups with BMP2/VEGF or VEGF only

decreased with incubation time with differentiation of the encapsulated hMSCs and ECFCs. The expression of vasculogenic markers for the groups with BMP2/VEGF or VEGF only increased with incubation time whereas the expression for those groups without BMP2 or VEGF did not change significantly. After 10 days of incubation, the patterned BMP2-P2SPCP-NP/VEGF-NG group (black in Figure 2.11) had highest mRNA expression of vasculogenic markers vWF, VEGFR, VE-cadherin and CD31 as well as highest CD31 protein expression followed by the patterned BMP2/VEGF (red in Figure 2.11), un-patterned BMP2-P2SPCP-NP+VEGF-NG (gray in Figure 2.11) and patterned VEGF-NG (gold in Figure 2.11) groups. For example, the normalized CD31 mRNA expressions (Figure 2.11e) of the patterned BMP2-P2SPCP-NP/VEGF-NG, patterned BMP2/VEGF, un-patterned BMP2-P2SPCP-NP+VEGF-NG and patterned VEGF-NG groups were 100, 68, 60 and 28, respectively, and the normalized CD31 protein expressions of those groups were 1.0, 0.96, 0.9 and 0.75. Similar to the osteogenic markers in Figure 2.9, the expression of vasculogenic markers for the patterned VEGF-NG group was significantly less than the patterned BMP2-P2SPCP-NP/VEGF-NG, patterned BMP2/VEG and un-patterned BMP2-P2SPCP-NP+VEGF-NG groups. The fluorescent images for CD31 immunostaining of the patterned BMP2-P2SPCP-NP/VEGF-NG, BMP2/VEGF, and VEGF-NG groups are shown in Figure 2.12. The images show robust vascularization for the patterned BMP2-P2SPCP-NP/VEGF-NG as well as BMP2/VEGF groups.

2.4. Discussion

Peptide-based nanomaterials, due to their versatility, are very attractive as a cell-responsive morphogen delivery system in tissue engineering [162] In this work, we

designed a peptide-PEG macromer composed of a phenylalanine sequence for self-assembly and a plasmin-cleavable sequence for BMP2 release in response to plasmin secretion by MSCs and ECFCs. The hydrophilic PEG block of the hybrid macromer provided stability in physiological medium while the hydrophobic phenylalanine sequence induced self-assembly into core-shell NPs with the peptides in the core and the PEGs in the hydrated corona [163, 164] The measured zeta potential of P0.5SPCP NPs (−11.2 mv) was lower than the reported value for the triblock poly(ethylene glycol)-b-poly(L-glutamic acid)-b-poly(L-phenylalanine) (PEG-b-PGlu-b-PPhe) nanogels at -20 mv [142] The measured zeta potentials of PxSPCP NPs (x=2, 5, and 7.5 kDa) were higher than the reported values for PEG-b-PGlu-b-PPhe nanogels and the amphiphilic Arg−His3−Phe4 oligo-peptide RH3F4 (−2.5 mv) [142, 165] These results was attributed to the existence of negatively-charged carboxyl groups in the corona of PxSPCP NPs [165]

The CD spectrum of BSA-PxSPCP NPs in Figure 2.6c showed progressively larger deviation from that of ungrafted BSA with increasing PEG MW. The CD spectrum of BSA-PEG0.5SPCP NPs with PEG MW of 500 Da was identical to that of ungrafted BSA whereas the spectrum of BSA-PEG2SPCP NPs with PEG MW of 2 kDa was slightly different in the 200-215 nm range. On the other hand, the spectra of BSA-PEG5SPCP and BSA-PEG7.5SPCP NPs with 5 and 7.5 kDa PEG MW deviated significantly from that of ungrafted BSA. This deviation was attributed to greater segregation of the peptide and PEG blocks into the core and corona of the NPs, respectively, with increasing PEG MW. As the succinimide group used for BSA grafting is hydrophobic, the grafted BSA would increase be associated with the hydrophobic core with increasing PEG MW, leading to greater loss of BSA secondary structure and denaturation of the protein. The increase in the

hydrodynamic size of PEG0.5SPCP NPs in aqueous solution (Figure 2.6a and 2.6b) with incubation time was attributed to the imbalance of hydrophobicity and hydrophilicity of the PEG-peptide macromer which led to aggregation of the NPs in aqueous medium. The release kinetic of BMP2 from BMP2-PxSPCP NPs decreased with increasing PEG MW (Figures 2.7a-c). This decrease was attributed to the increased segregation of the peptide and PEG blocks of PxSPCP macromer into the core and corona of the NPs, respectively, leading to greater entrapment of the plasmin-cleavable peptide in the core of the NPs, and decreased availability of plasmin to the peptide. Further, the longer PEG chains on the NPs' corona increased the entropically-driven compression energy required for diffusion of plasmin in the corona layer, which in turn reduced the release of BMP2 from the NPs [166, 167].

The hMSC/ECFC co-culture results in patterned constructs (Figures 2.9-12) demonstrate that the on-demand release of BMP2 from plasmin-cleavable PxSPCP NPs enhanced osteogenesis and vasculogenesis compared to the direct addition of BMP2. The enhancement can be attributed to the release of BMP2 from PxSPCP NPs in response to enzymes secreted by the encapsulated hMSCs and ECFCs, particularly uPA, tPA, plasminogen, MMP2 and MT-MMP enzymes. The measured enzyme secretions of MSCs and ECFCs in Figures 2.3 and 2.4 are consistent with the results from previous reports [134, 168, 169] Further, co-cultures of MSCs and ECFCs are known to stimulate capillary morphogenesis by secreting MMPs and plasminogen [170] The enhancement in osteogenesis/vasculogenesis observed in Figures 2.9-12 with on-demand release of BMP2 can be attributed to a) release of VEGF from VEGF-NGs in the first 5 days of culture to differentiate ECFCs to the endothelial lineage, b) secretion of proteolytic factors like

MMPs, plasminogen, tPA, and bFGF by the endothelial cells, c) diffusion of the proteolytic factors from the microchannels to the matrix, d) cleavage of the plasmin-cleavable peptide in BMP2-PxSPCP NPs by the diffused proteolytic factors leading to the release of BMP2, e) osteogenic differentiation of hMSCs by the released BMP2, and f) secretion of proteolytic and vasculogenic factors by the differentiated hMSCs. These events led to the coupling of growth factor release by the differentiated hMSCs and ECFCs which enhanced osteogenesis and vasculogenesis.

The results of this work show that hMSCs and ECFCs encapsulated in a patterned composite hydrogel release proteolytic factors like MMPs, plasminogen and tPA as well as others and that the released factors are able to cleave plasmin-degradable peptides embedded in PxSPCP NPs to release morphogens like BMP2 on-demand. The results further show that the on-demand release of BMP2 leads to a coupling of paracrine signaling between the differentiating hMSCs and ECFCs. The on-demand release of BMP2 from the NPs in response to secretions of MSCs/ECFCs not only enhances osteogenesis and vasculogenesis but it has the potential to reduce many undesired side-effects of BMP2 therapy in bone regeneration [171]

2.5 Conclusion

Bifunctional, hybrid PEG-peptide PxSPCP NPs with a triphenylalanine (FFF) self-assembly peptide and a lysine-phenylalanine-threonine-lysine (KFTK) plasmin-cleavable peptide are developed in this work for the on-demand release of BMP2 in response to proteolytic factors secreted by the differentiating hMSCs and ECFCs encapsulated in a patterned hydrogel construct. The hMSCs and BMP2-PxSPCP NPs were encapsulated in the matrix whereas hMSCs+ECFCs and VEGF-NGs were encapsulated in the

microchannels of the patterned construct. The PxSPCP NPs had a core-corona morphology with the self-assembling peptides in the core and PEGs in the corona. The stability of NPs in aqueous solution and the BMP2 stability against denaturation was a strong function of PEG MW. The P2SPCP NPs with PEG MW of 2 kDa showed the most stable particle size distribution and protein secondary structure with incubation. The BMP2 grafted to P2SPCP NPs and co-encapsulated in SPELA hydrogel with plasmin was gradually released to the medium with incubation time at a rate faster than the non-cleavable BMP2-PxSP NPs but slower than the free BMP2. Further, the released BMP2 from the NPs by the action of plasmin induced differentiation of hMSCs encapsulated in the LPELA hydrogel. The on-demand release of BMP2 from P2SPCP NPs in the patterned constructs in response to proteolytic factors like MMPs, plasminogen and tPA as well as others secreted by the encapsulated cells led to highest extent of osteogenesis and vasculogenesis and coupling of paracrine signaling between the differentiating hMSCs and ECFCs. The on-demand, cell-triggered release of BMP2 is a promising strategy for promoting vascularized osteogenesis and reducing many undesired side-effects of BMP2 therapy in regeneration of skeletal tissues.

Table 2.1. The forward and reverse sequences for PCR primers

Gene	Sequence
Plasminogen	F : 5"-TTTGTCTCTGGAGTGAAAATGC-3" R: 5"-AGACTGTATGTTTGGGAATGGG-3"
PAI	F : 5"-TCATGGGCCAAGTGATGGAAC-3" R: 5"-CATGCACACTGTTTCTGGGGA-3"
tPA	F : 5"-GGAAGTACAGCTCAGAGTTCTGCAGCACCCCTGC-3" R: 5"-GATGCGAAACTGAGGCTGGCTGTACTGTCTC-3"
uPA	F : 5"-CACGCAAGGGGAGATGAA-3" R: 5"-ACAGCATTTTGGTGGTGACTT-3"
uPAR	F : 5"-TGGAGATAGAGCCCCAGATG-3" R: 5"-TTATCACAGGCAGCCCTAGG-3"
MT1-MMP	F : 5"-CCATTGGGCATCCAGAAGAGAGC-3" R: 5"-GGATACCCAATGCCCATTGGCCA-3"
MMP-2	F : 5"-GGCCCTGTCACTCCTGAGAT-3" R: 5"-GGCATCCAGGTTATCGGGGA-3"

Table 2.2 Average size, distribution, zeta potential, and grafting efficiency of PxSPCP NPs

	PEG-peptide			
	P0.5SPCP	P2SPCP	P5SPCP	P7.5SPCP
PEG M.Wt (kDa)	0.5	2	5	7.5
Size (nm)	145	225	265	325
PDI	0.131	0.153	0.161	0.162
Zeta potential (mV)	-11.2	18.00	25.9	26.3
Grafting efficiency%	81.3	73.1	69.5	24.5

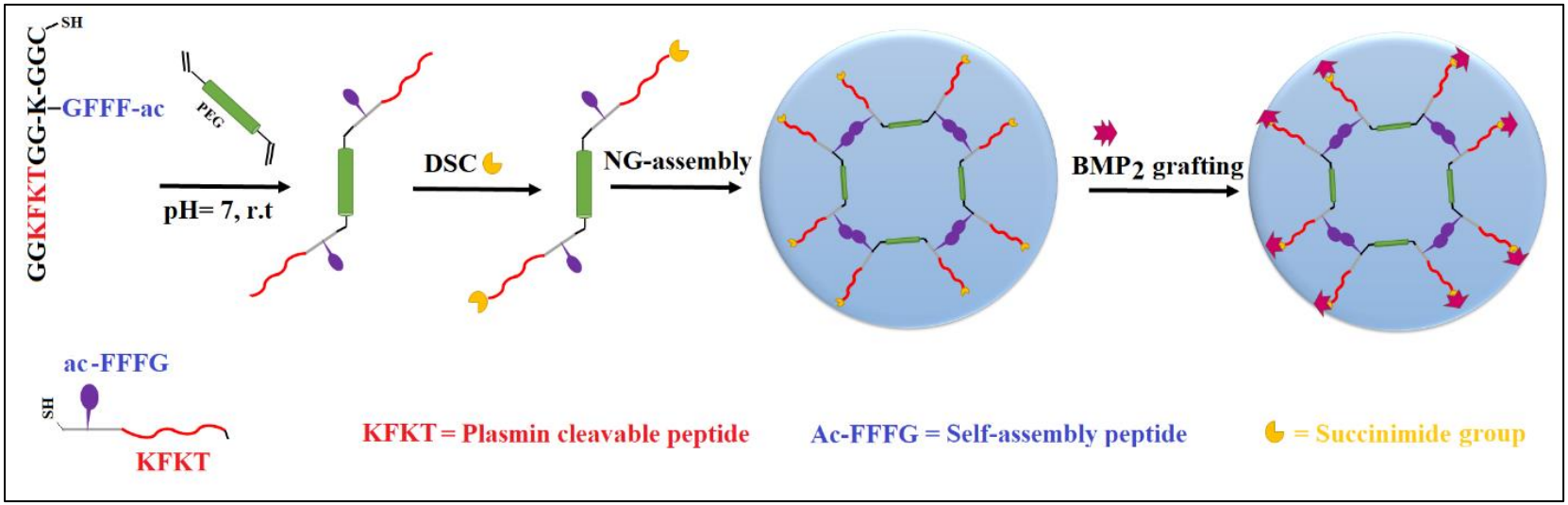

Figure 2.1. Schematic diagram for the synthesis of plasmin-cleavable, self-assembled, BMP2-grafted PxSPCP NP.

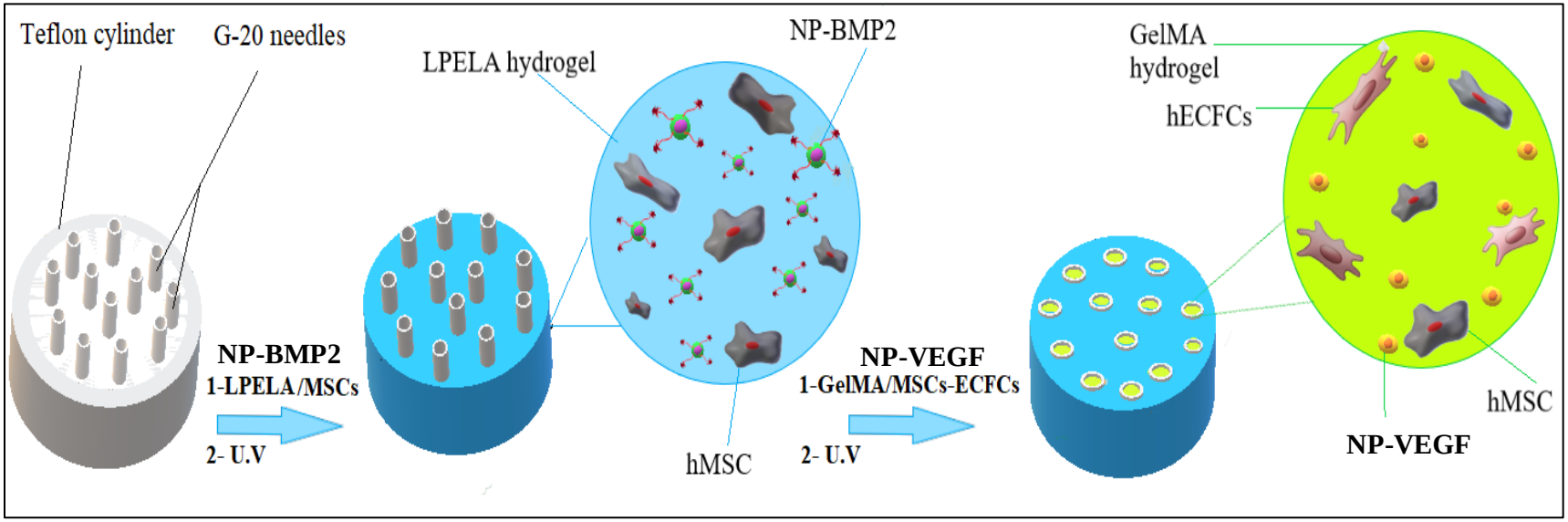

Figure 2.2. Schematic diagram for generating the patterned, cellular constructs. The LPELA hydrogel precursor solution loaded with hMSCs and BMP2-PxSPCP NPs was injected inside a Teflon cylinder fitted with needles. After LPELA gelation, needles were removed and the GelMA precursor solution loaded with ECFCs+hMSCs and VEGF-NGs was injected in the microchannels and crosslinked. The constructs were cultured in appropriate medium with time and analyzed with respect to the expression of markers for osteogenesis and vasculogenesis.

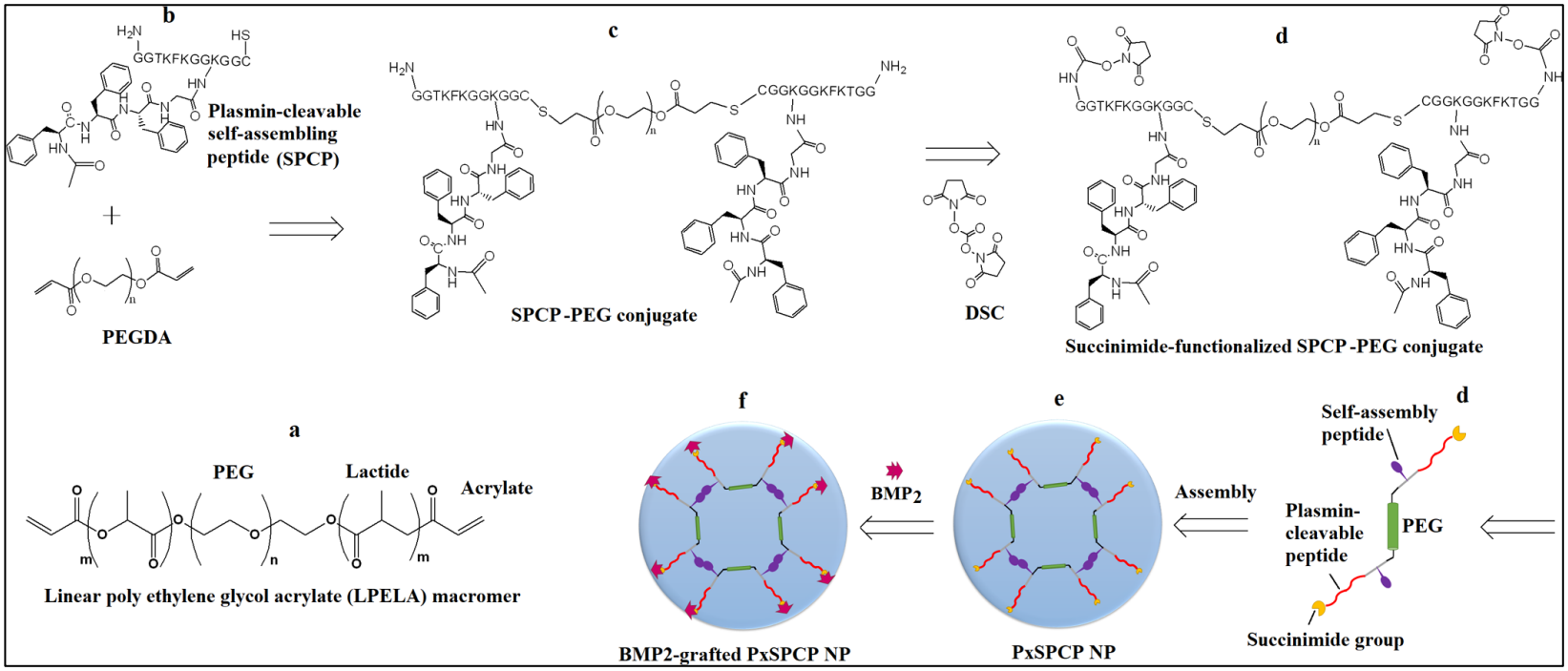

Figure 2.3 Schemes showing chemical structures of linear polyethylene glycol (LPELA) macromer (a), polyethylene glycol diacrylate (PEGDA, b), plasmin-cleavable, self-assembling peptide (SPCP, b), SPCP-PEG conjugate (c), and succinimide-functionalized SPCP-PEG conjugate (PxSPCP, d). Schematic diagram showing the self-assembly of PxSPCP to form NPs (e) and grafting of BMP2 to PxSPCP NPs (f)

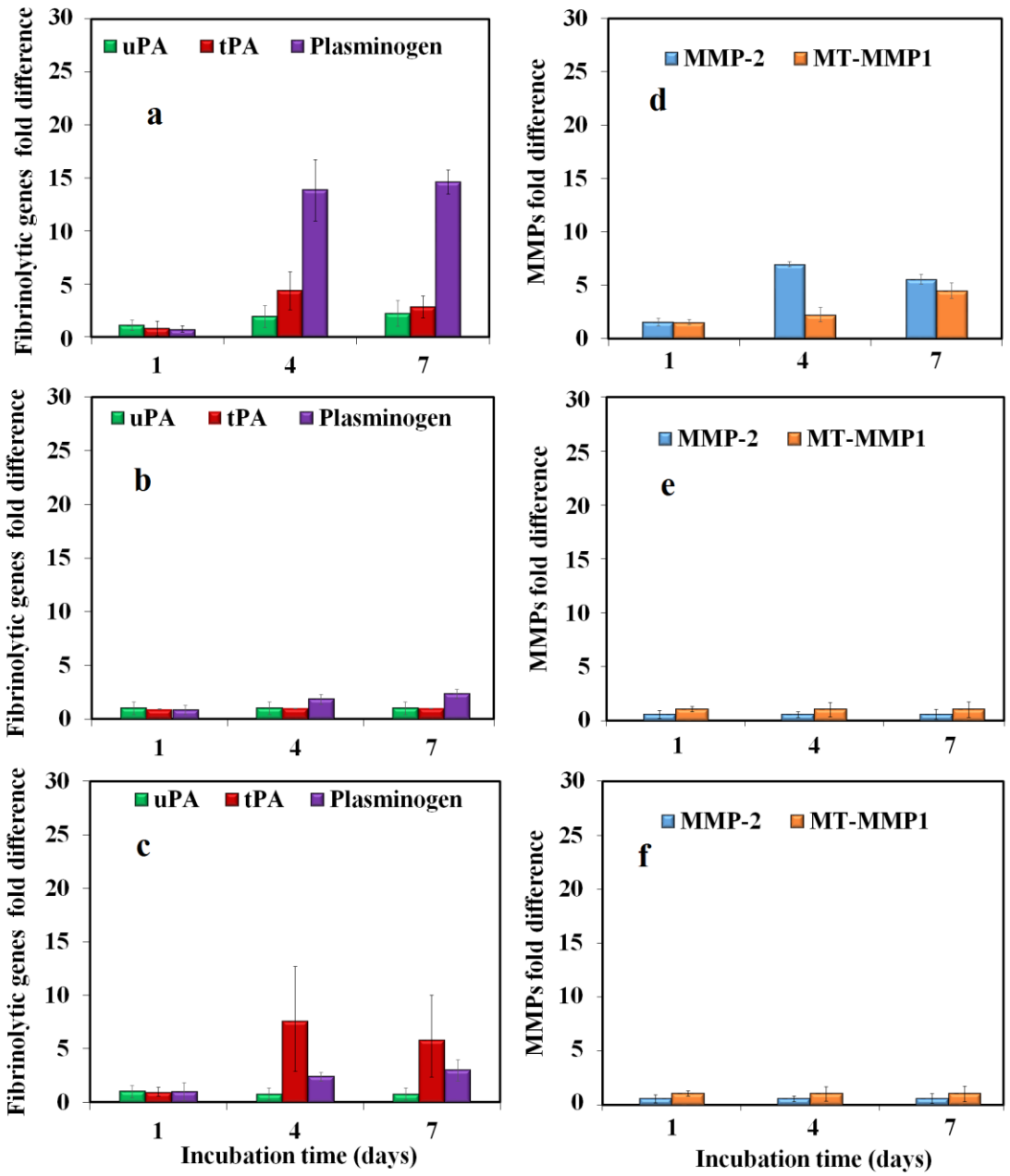

Figure 2.4 Messenger RNA expressions of fibrinolytic genes (uPA, tPA and plasminogen) and MMPs (MMP-2 and MT-MMP1) of the unpatterend and patterned construvts for (a and d)- MSCs in osteogenic media (b,e)- ECFCs in vasculogenic media and (c,f)- MSCs/ECFCs in vasculogenic media in pattern matrices, respectively.

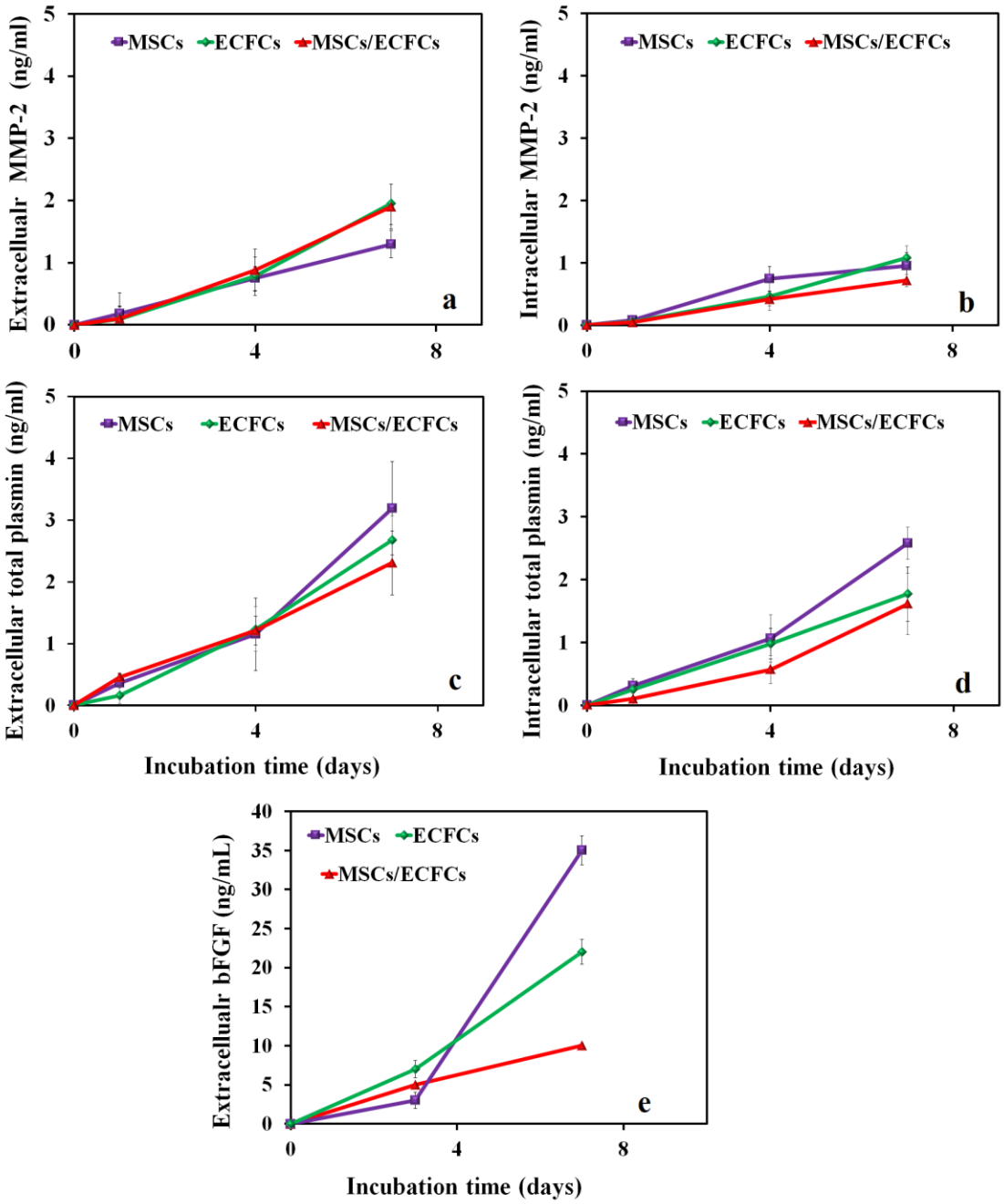

Figure 2.5 Extra- and intracellular protein expressions of total plasmin and MMP-2 as well as extracellular bFGF of the unpatterned and patterned constructs (a-e). Groups included unpatterend MSCs in osteogenic media (purple)- Unpatternd ECFCs in vasculogenic media (green), and patterned MSCs/ECFCs in vasculogenic media (red), respectively.

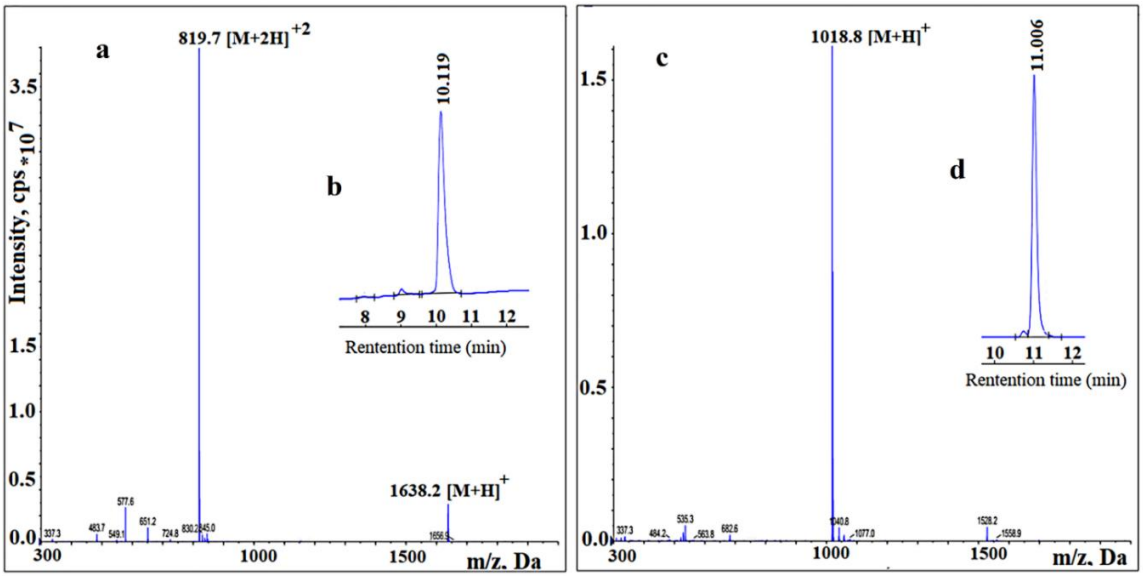

Figure 2.6 Mass spectra and the RP-HPLC chromatogram of G2KTFKGG-K(Ac-FFFG)G2C (SPCP, a-b) and G2-K(Ac-FFFG)G2C (SP, c-d).

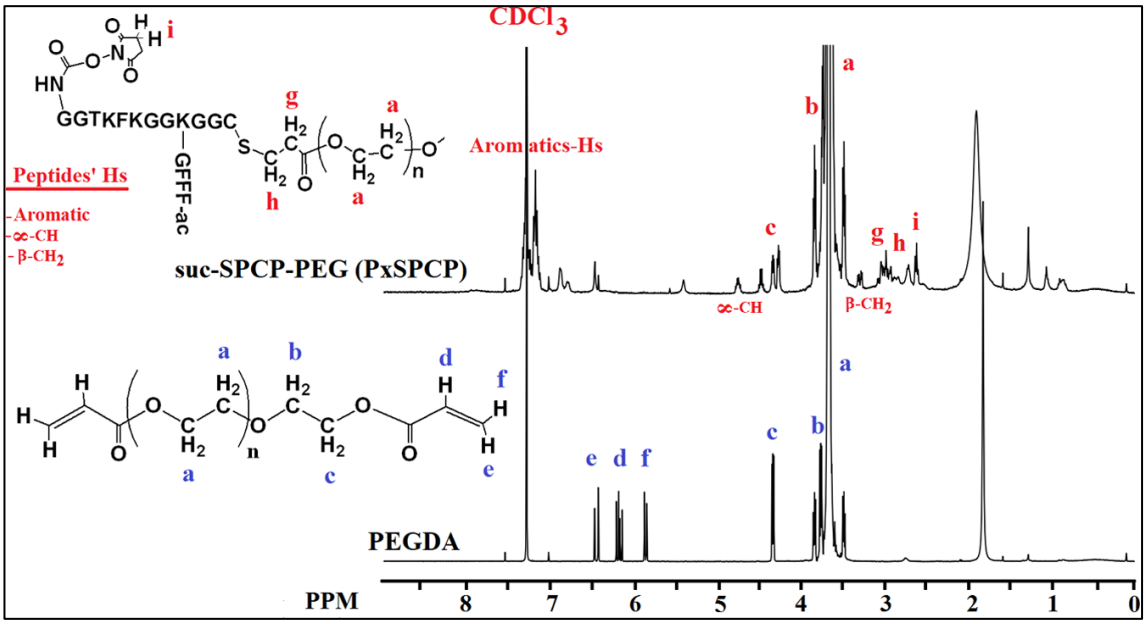

Figure 2.7 ^{1}H-NMR spectra of polyethylene glycol diacrylate (PEGDA) and succinimide-terminated suc-SPCP-PEG conjugate showing the assignment of all peaks and their corresponding chemical structures in the macromers.

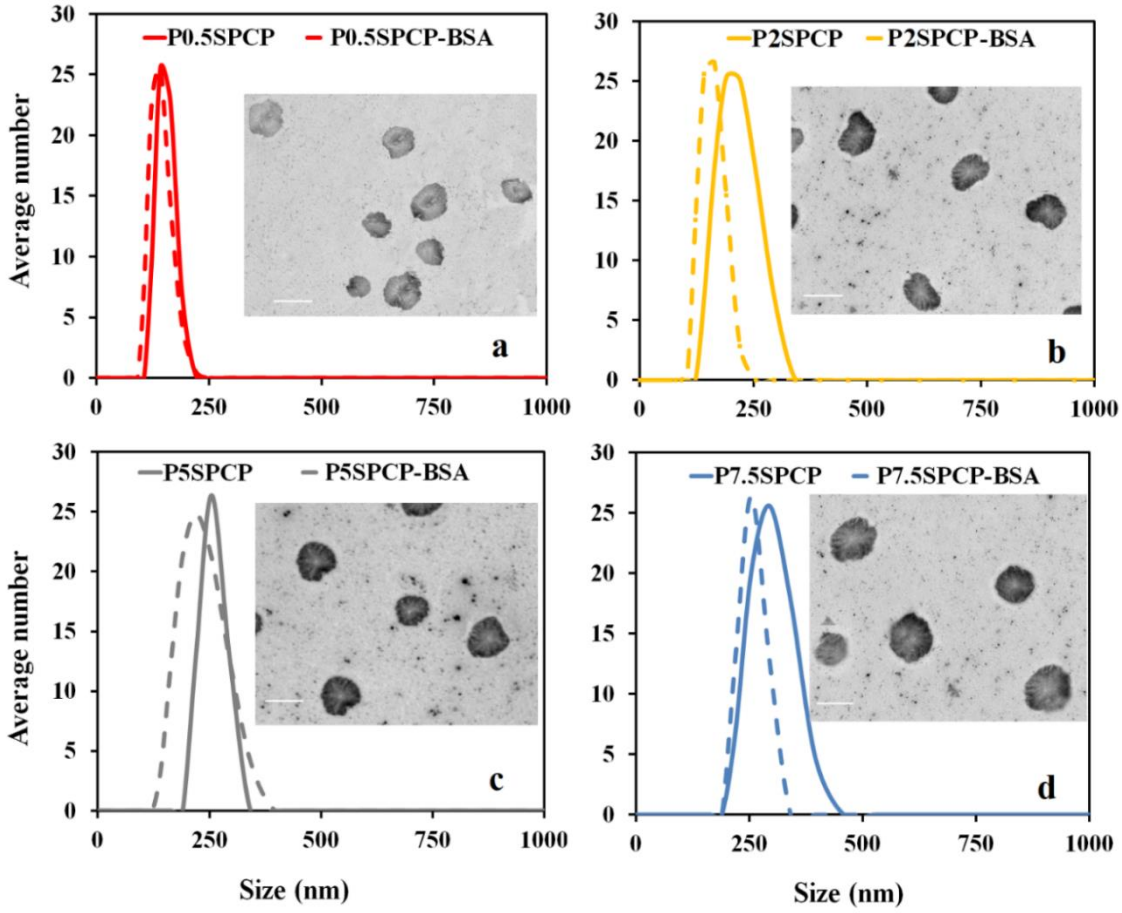

Figure 2.8 Dynamic light scattering analysis (DLS) of the effect of PEG MW on PxSPCP NPs size distribution. PxSPCP NPs (solid lines) and BSA grafted PxSPCP NPs (dashed lines). The abbreviations PxSPCP represent NPs with x = 0.5, 2, 5, and 7.5 kDa PEG MW, SP and CP represent NPs with self-assemble and cleavable peptides, respectively. Morphology of the dried NPs is shown in the inset SEM images in (a–d). Scale bar represents 200 nm.

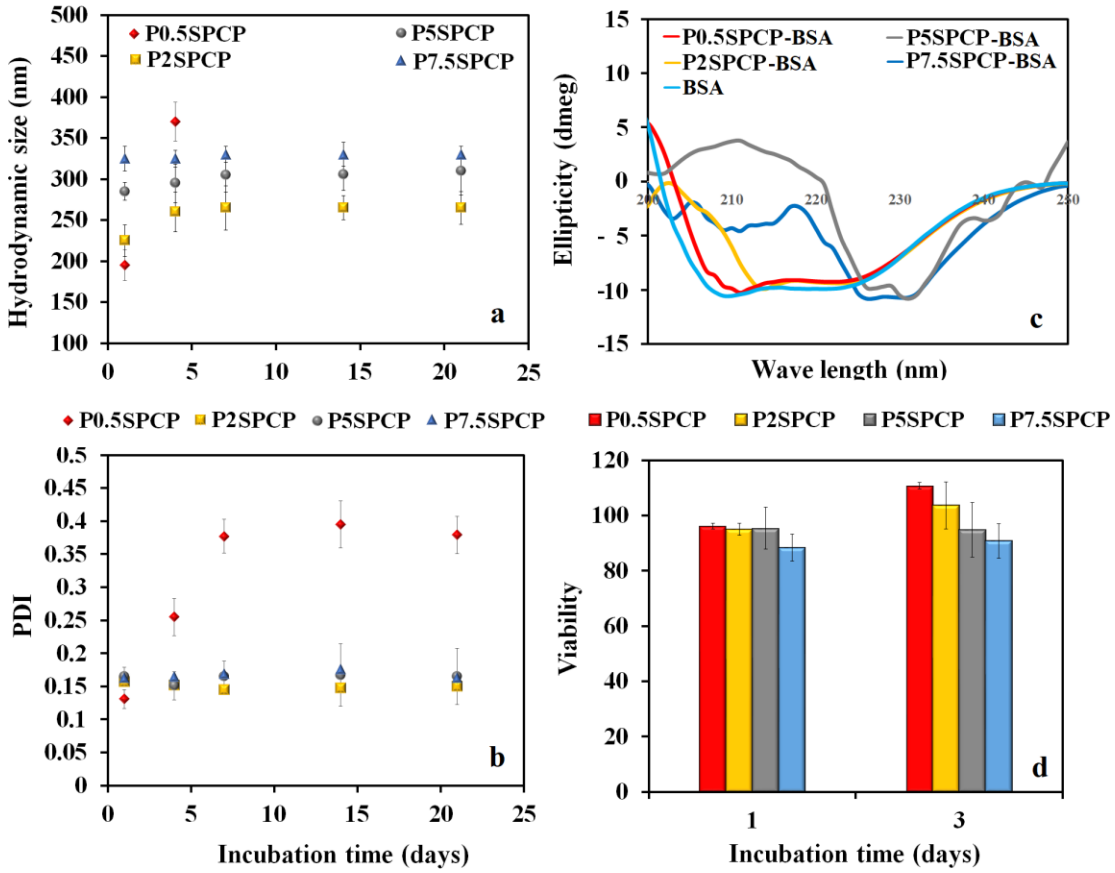

Figure 2.9 Average particle size and polydispersity index (PDI) of PxSPCP nanoparticles in stability tracking from Dynamic light scattering analysis (a and b). Circular dichroism (CD) spectra of free BSA and BSA grafted PxSPCP NPs (c). Viability of PxSPCP on hMSCs using Celltiter-96 (MTS) assay (d). Error bars correspond to means ± 1 SD for n=3.

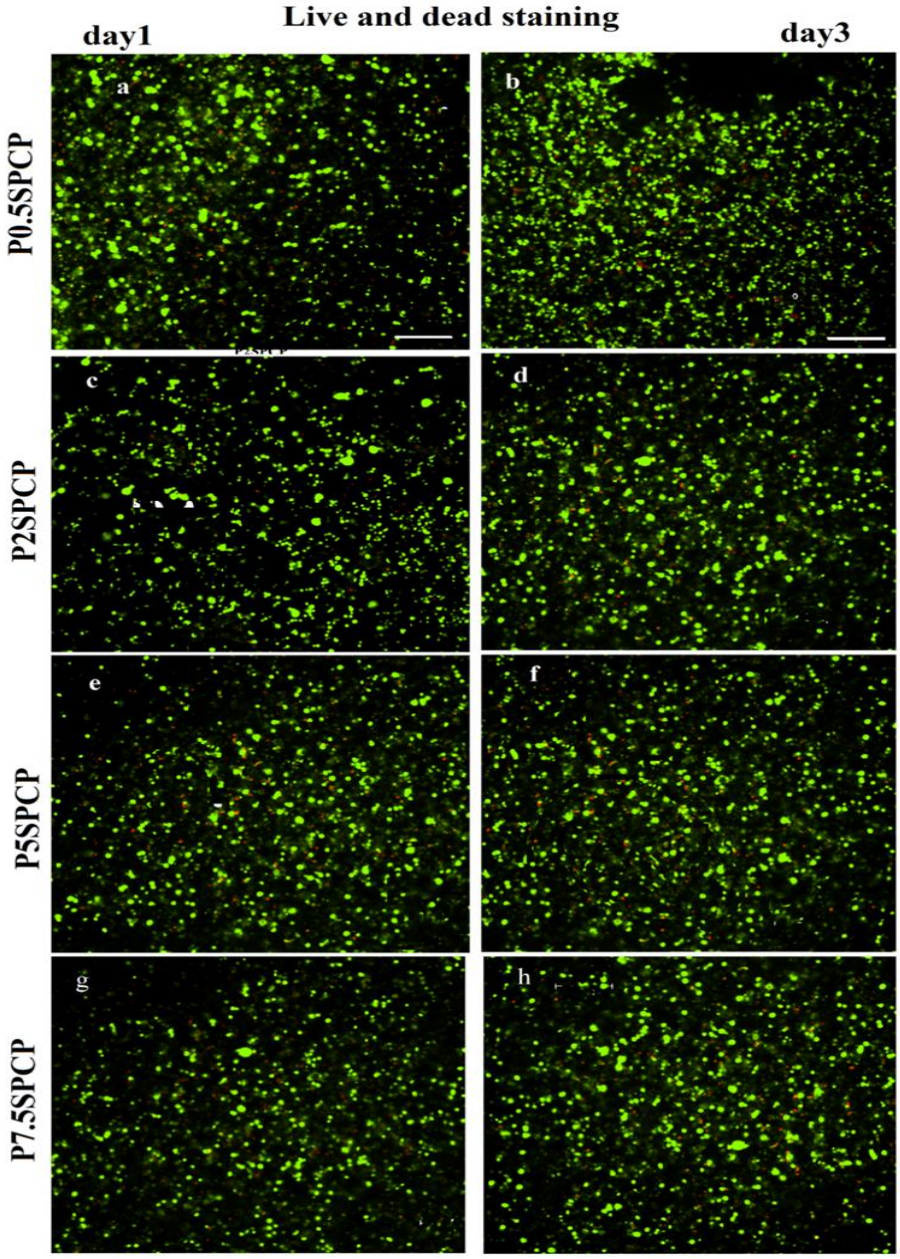

Figure 2.10 Fluorescence images of live (green) and dead (red) staining of hMSCs encapsulated in LPELA hydrogel along with PxSPCP (x=3, 5, and 7.5 kDa) after 1 and 3 days of incubation (a-h). Scale bar of 100 um.

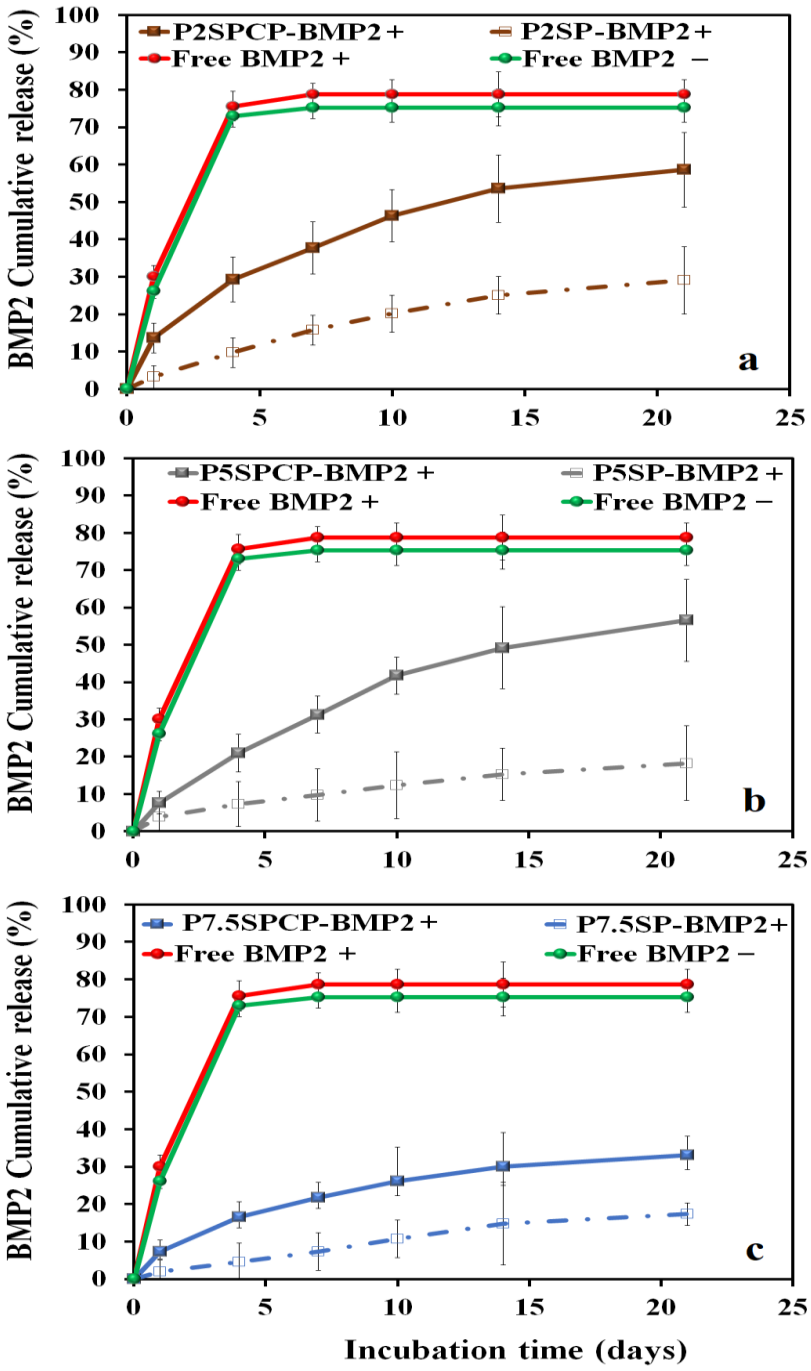

Figure 2.11: The release kinetics of BMP2 grafted to P2SPCP, P2SP, P5SPCP, P5SP, P7.5SPCP and P7.5SP NPs, respectively, encapsulated in LPELA hydrogel, in response to exogenous plasmin (+). The figure also shows the release kinetics of free BMP2 (-, solid green) and free BMP2 with plasmin (+, solid red), respectively. The cumulative release of BMP2 was measured by Enzyme-Linked Immunosorbent Assay (a-c) Error bars correspond to means ± 1 SD for n=3.

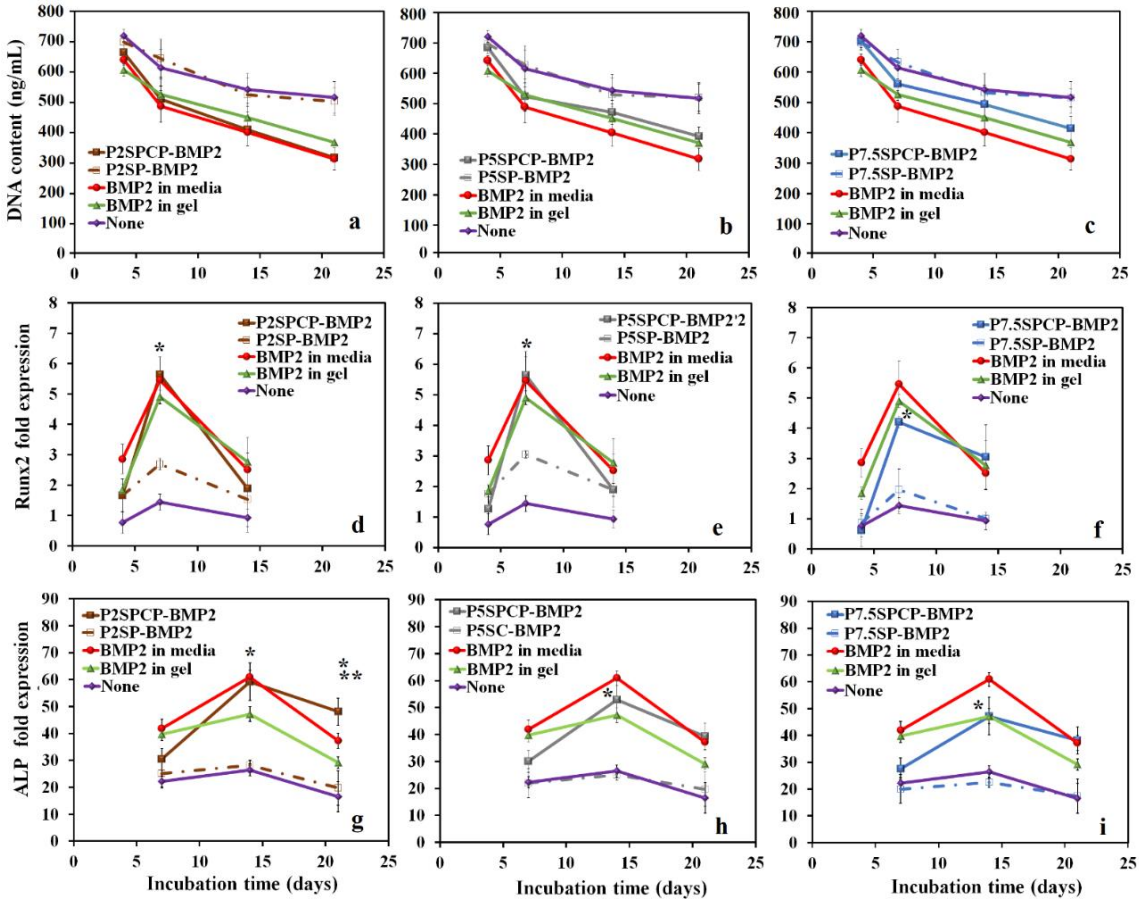

Figure 2.12: The Osteogenic activity of plasmin-cleavable BMP2 on hMSCs encapsulated in LPELA hydrogel. DNA content (a-c), and mRNA expression of osteogenic markers Runx2 (d-f) and ALP (g-i) for hMSCs encapsulated in LPELA. Groups included constructs without BMP2 (solid purple), with free BMP2 in media (solid red), with encapsulated BMP2 (solid green), with PxSPCP-BMP2 (solid brown for x=2; solid gray for x=5; and solid blue for x=7.5 kDa); and with PxSP-BMP2 (dashed brown for x=2; dashed gray for x=5; and dashed blue for x=7.5 kDa). Constructs were incubated in osteogenic medium for 21 days (without BMP2, or DEX).

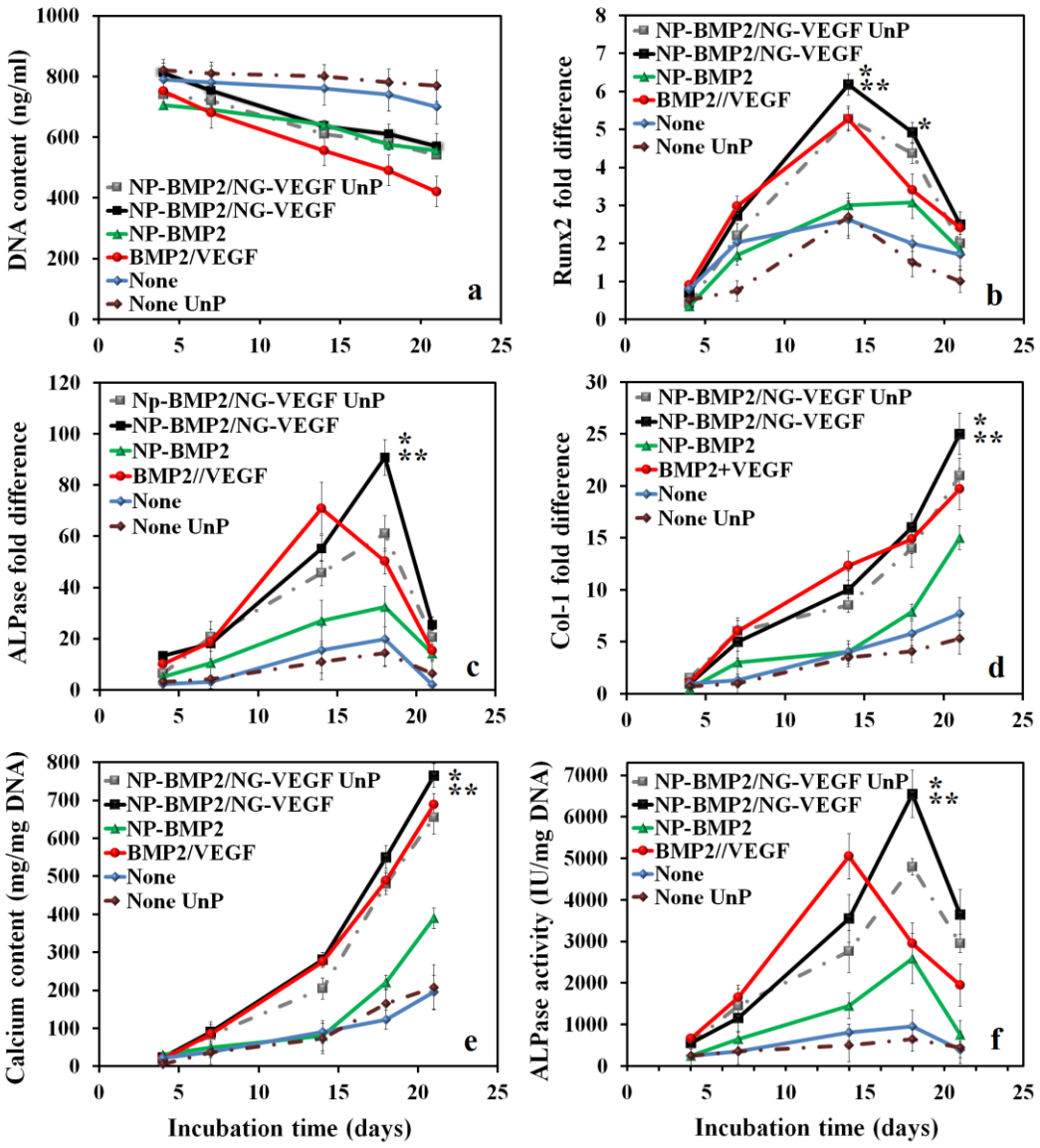

Figure 2.13: DNA content (a), mRNA expression of osteogenic markers Runx2 (b), ALPase (c), Col I (d) and calcium content (e), ALPase activity (f) for hMSCs and ECFCs encapsulated in the patterned and constructs. Groups included patterned constructs without VEGF/BMP2 (solid blue), with VEGF/BMP2 (solid red), with NP-BMP2 (solid green), and with NG-VEGF/NP-BMP2 (solid black); unpatterned osteogenic constructs with NG-VEGF/NP-BMP2 (dashed gray) and without VEGF/BMP2 (dashed light blue). Constructs were incubated in vasculogenic medium for 7 days, vasculogenic/osteogenic medium for 3 days, and osteogenic medium for 11 days (without VEGF, BMP2, or DEX). "An asterisk" represents a statistically significant difference in the ordinate between the test and None groups for the same time point. "An asterisk" represents a statistically significant difference between the test and None groups for the same time point; "Two asterisks" represents a significant difference between the test group and patterned construct with VEGF/BMP2. Error bars correspond to means ± 1 SD for n=3.

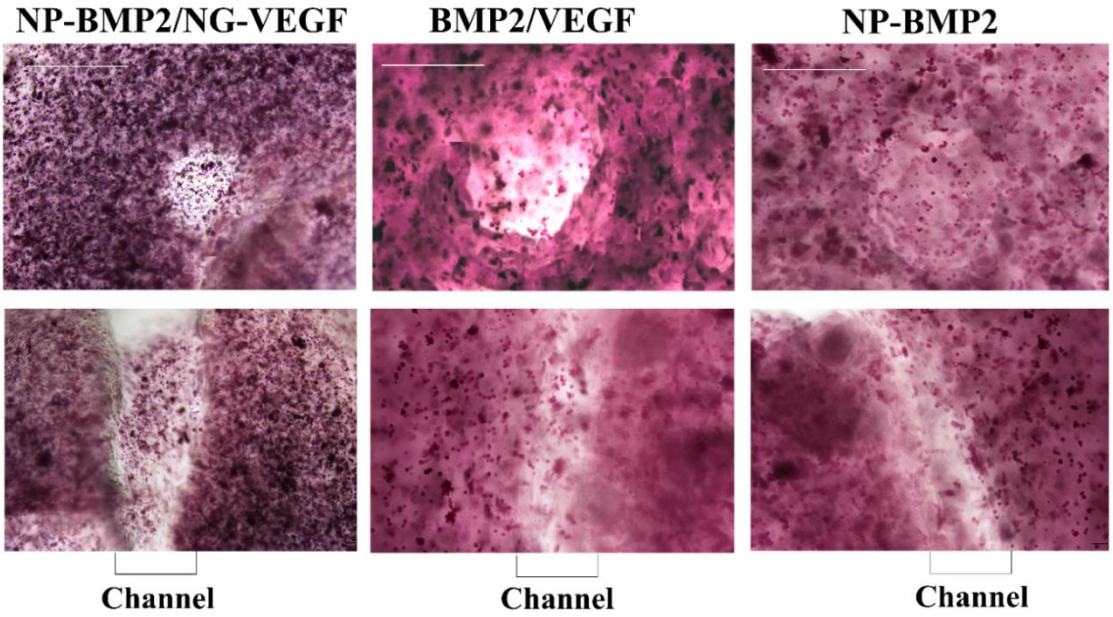

Figure 2.14 Alizarin red stained images of the constructs of a patterned microchannel with NP/NG-grafted BMP2/VEGF, directly added BMP2/VEGF and patterned NP-grafted BMP2 only, after 21 days of incubation. The top images show Alizarin red staining the top of the channel while the bottom images show Alizarin red staining along the length of a microchannel. Scale bar is 500 um.

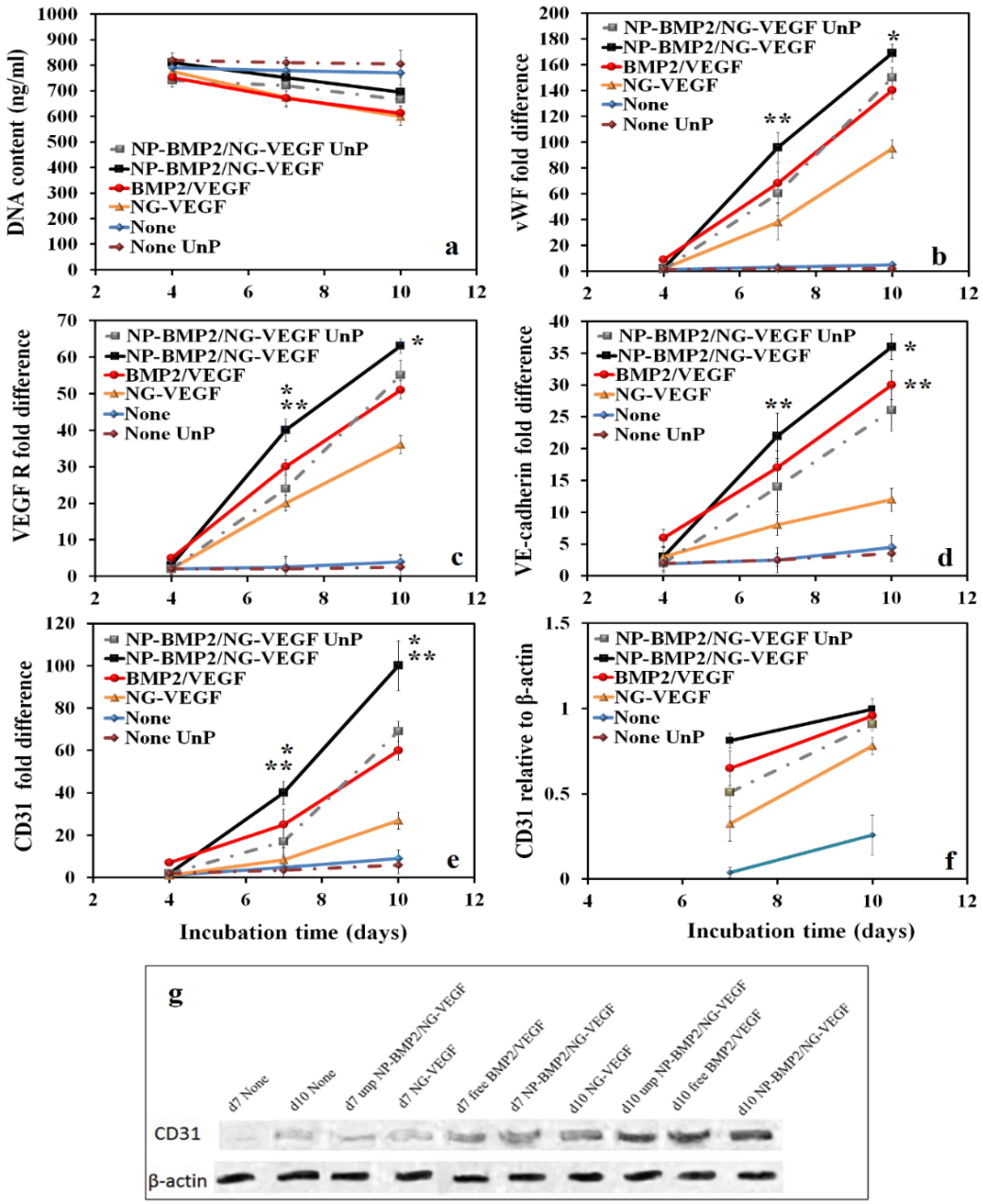

Figure 2.15 DNA content (a), mRNA expression of vasculogenic markers vWF (b), VEGFR (c), VE-cadherin (d), CD31 (e), and CD31 protein expression (f) and representative western blot bands (g) for hMSCs and ECFCs encapsulated in the patterned and unpatterned constructs. Groups included patterned constructs without VEGF/BMP2 (blue), with VEGF/BMP2 (red), NG-VEGF (golden) and with NG-VEGF/NP-BMP2 (black); unpatterned vasculogenic constructs with NG-VEGF/NP-BMP2 (gray) and without VEGF/BMP2 (light blue). “An asterisk” represents a statistically significant difference in the ordinate between the test and None groups for the same time point.

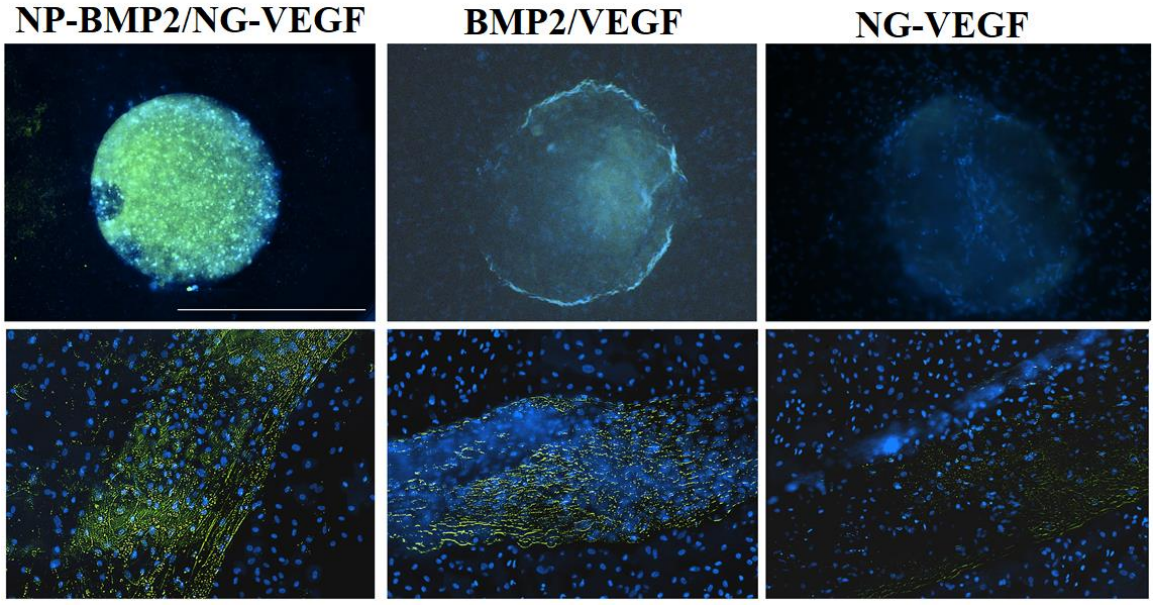

Figure 2.16 Fluorescence images of CD31 expression stained (green) of the microchannel patterned constructs with NG-VEGF/NP-BMP2, VEGF/BMP2, and patterned NG-VEGF after 7 days of incubation. The top images show CD31 staining the top of the channel while the bottom images show CD31 staining along the length of a microchannel. Scale bar is 500 um.

CHAPTER 3: SYNTHESIS AND CHARACTERIZATION OF PHOTO-CROSS LINKABLE SERICIN HYDROGELS FOR STEM CELLS ENCAPSULATION

3.1 Introduction

Natural hydrogels have been widely used as a 3D matrix for delivery and immobilization of stem cells in soft tissue regeneration owing to its resemblance to natural extracellular matrix (ECM) as they provide biocompatibility, biodegradability, and natural cell binding sites [172]. *In-situ*-forming hydrogels have been known as promising biomaterials in tissue repairing applications because their pre-gel solutions can be injected into the damaged site through minimally invasive surgical procedures and fill irregular shape defects before gelation [173]. Among various starting biomaterials, sericin and fibroin, the silk main proteins, have become the topic of research in tissue engineering with various forms of cell delivery systems, such as films, scaffolds and hydrogels due to its excellent biocompatibility, biodegradability and valuable bioactivities [174, 175]. Silk industry is the major source of sericin that produces as a by-product around 50K tons annually. However, such sericin was degraded (sericin^{degraded}) because of the harshness extraction method used in the degumming process. The sericin^{degraded} was hard to crosslinked in the form of hydrogels to be used in tissue engineering applications [176]. Instead, sericin^{degraded} was used to form cross-linkable, composite hydrogels with other polymers by biotoxic crosslinkers leading to losing some of the sericin's natural bioactivities [176]. Sericin is a family of "gluelike" proteins produced in nature by the silkworm as a 20-30 % of total cocoon weight [177]. It is highly hydrophilic with a

molecular weight that ranges from 20 to 400 kDa and consists of 32% of serine and 18 amino acids, including essentials [178]. Structurally, silk sericin is a globular protein consisting of random coil and β-sheets [178, 179]. Because of its biocompatibility, biodegradability and bioactivities, sericin has been increasingly used to synthesize various types of cell delivery systems, such as scaffolds films, and hydrogels in anticipating of repairing tissues [174, 175]. Silk sericin is shown to accelerate several mammalian cell lines proliferation and attachment [180] such as keratinocytes, fibroblasts, epithelial cells and osteoblasts[181]. Further, sericin was used for bone tissue engineering regarding its ability to promote nucleation of bone-like hydroxyapatite [175]. Sericin hydrogels have been developed that could be formed under physiological conditions, and the structure of sericin can be chemically modified through its hydroxyl, amino, and carboxyl groups to control the properties of the resulting biomaterials. A 3D sericin gel has been synthesized that it is an injectable material, promotes cell adhesion and long-term survival, and possesses multiple physical and chemical properties that provide a sustained drug release ability, which can be tailored and customized to different tissue repair applications, serving as a multifunctional platform for cell therapy [182].

In this study, sericin was extracted from silk cocoon and modified with isocyanatoethyl methacrylate to form urethane methacrylated sericin (SerAte), Figure 3.1. Ultraviolet light was used to cross-link the *in situ* SerAte hydrogels by the free radical polymerization reaction. The physical properties of the SerAte hydrogels were characterized. Cells attachment and proliferation were observed when the hMSCs were cultured in the SerAte hydrogels. The final goal of this study is to develop the *in situ* SerAte hydrogels for encapsulation and delivery of stem cells in tissue regeneration.

3.2 Materials and Methods

Materials. Silk Cocoons was obtained from the Yarn Tree USA Company (Greenville, Sc). Diethyl ether, citric acid, lithium chloride, and isocyanatoethyl methacrylate (IEM) were purchased from VWR (Bristol, CT). Streptomycin, L-proline, ascorbic acid, sodium pyruvate, and β-glycerol phosphate were purchased from Sigma-Aldrich (St. Louis, MO). Dexamethasone (DEX) were purchased from Lonza (Hopkinton, MA). Phosphate-buffer saline (PBS) and Dulbecco's Modified Eagle's Medium (DMEM) were purchased from GIBCO BRL (Grand Island, NY). Trypsin and fetal bovine serum (FBS) were received from Invitrogen (Carlsbad, CA) and Atlas Biologicals (Fort Collins, CO), respectively. Collagenase type 3 was purchased from Worthington (Lakewood, NJ). TRITC-conjugated Phalloidin and 4,6-diamidino-2-phenylindole (DAPI) were purchased from EMD Millipore (Billerica, MA). The Live and Dead calcein-AM (cAM) and ethidium homodimer-1 (EthD) cell viability/cytotoxicity kit was purchased from Molecular Probes (Life Technologies, Grand Island, NY). The dialysis tubes with molecular weight (MW) cutoff of 3.5 kDa was purchased from Spectrum Laboratories (Rancho Dominquez, CA). Bovine serum albumin (BSA) was received from Jackson ImmunoResearch (West Grove, PA). Trichrome collagen staining

3.2.1 Extraction of Sericin from Cocoons. Silk cocoons were cleaned by soaking in ether followed by washing with soap water. The cleaned cocoons were dried and chopped into small pieces. Nine grams of the chopped cocoons were boiled for 30 mins in 160 mL of 1.25% citric acid to prepare the aqueous sericin solution. Then, the solution was filtered (paper filtration) and centrifuged at 4.4 rpm to remove insoluble fibers. The clear filtrate was dialyzed immediately against deionized water for three days with a 3.5 kDa molecular

weight cutoff dialysis tube at the ambient condition with a change of deionized water every 6 h. Finally, the dialyzed cocoon solution was lyophilized to dryness and stored at -20 ^{o}C.

3.2.2 Modification of sericin and SerAte Hydrogel formation. SerAte was synthesized following the literature protocol [183]. Briefly, 1.0 g of extracted sericin, after vacuum-drying in oven at 50 °C for 24 h, was dissolved at 2 wt % in anhydrous LiCl/DMSO solution at 60 °C for 45 min under nitrogen atmosphere, and isocyanatoethyl methacrylate (IEM) of different folds molar excess (relative to the serine), as listed in Table 3.1, was added dropwise to the solution, and the reaction continued for 24 h. The product was dialyzed against deionized water for at least 48 h, followed by centrifugation to remove the precipitate, which was then flash frozen in liquid nitrogen, and lyophilized, resulting in a powder that was analyzed by the degree of modification by ^{1}H NMR. Introducing of urethane methacryloly groups to the hydroxyl groups of sericin was to produce photo-crosslinkable sericin methacryloyl (SerAte). When exposed to UV light, the sericin methacryloyl (SerAte) solution was rapidly crosslinked in situ forming a sericin hydrogel through photo-polymerization of methacryloyl groups. Urethane methacrylated SerAte is expected to be the more hydrophilic end-group and decreased degradation time due to possible hydrogen bonding between the urethane group and molecules of water as well as increase the porosity and pore sizes.

3.2.3 Circular Dichroism. Circular Dichroism (CD) spectra were recorded using a JASCO J815 spectropolarimeter (JASCO, Essex, UK) at room temperature. The sample was prepared by dissolving the freeze-dried sericin and SerAte in deionized water at a concentration of 0.1 mg/mL. Infrared (IR) spectrum of the sericin and SerAte samples as a

powder was measured in a range of 650-4000 cm^{-1} using a Perkin Elmer 100 spectrometer with an attenuated total reflection diamond cell attachment.

3.2.4 SDS Polyacrylamide Gel Electrophoresis. SDS-PAGE analysis was used to determine the molecular weight of sericin before and after modification. Extracted sericin and SerAte powders were dissolved in 2x sample buffer (BioRad, Hercules, CA) with 5% 2-mercaptoethanol. The proteins were separated using a vertical slab gel electrophoretic system with a 4-20% stacking gel. Electrophoresis was performed at 100 V and 15 mA for 80 min. The proteins were stained with Biosafe Coomassie brilliant blue R-250 for 1h and de-stained using DIH_2O, according to supplier's instructions.

3.2.5 Thermogravimetric Analysis. Thermogravimetric analysis (TGA) of the sericin and SerAte was performed using a universal V4.4A thermogravimetric analyzer (TA Instruments, New Castle, DE). Five mg of the samples in Al_2O_3 crucibles were heated from 30°C to 700°C at a rate of 10°C/min and sample weight was recorded with time.

3.2.6 Gelation and Rheological measurements. To study the gelation and mechanical properties, the SerAte macromers have crosslinked in aqueous solution by UV free-radical polymerization with Irgacure 2959 (CIBA, Tarrytown, NY) photoinitiator as described [184]. Briefly, the SerAte macromer was dissolved in the initiator solution vortexed and loaded on the Peltier plate of the rheometer (TA Instruments AR-2000, New Castle, DE) to measure the gelation time. A 20 mm plate acrylic geometry was used at a gap distance of 500 µm. A sinusoidal shear strain with the frequency of 1 Hz and 1% strain was applied on the sample while the sample was irradiated with a BLAK-RAY 100-W mercury long-wavelength (365 nm) UV lamp (Model B100-AP; UVP, Upland, CA). The storage (*G'*) and loss moduli (*G"*) of the samples were recorded with irradiation time. The time at which

the storage (*G'*) equals loss modulus (*G''*) was recorded as the gelation time. To measure the compressive modulus of the SerAte hydrogels, the precursor solutions were transferred to a mold (polytetrafluoroethylene PTFE, 5 cm x 3cm x 750 nm) and the mold was covered with transparent glass. Next, the samples were irradiated with UV for 3 min to complete the crosslinking reaction. Samples with disk-shaped were cut from the hydrogel using puncture, loaded on the Peltier plate and subjected to a uniaxial compressive force at a displacement rate of 7.5 um/s. The slope of the linear matches to the stress-strain curve for 10% strain was taken as the compressive modulus, as described before [184].

3.2.7 Swelling Ratio and Stability Analysis. The swelling property of each hydrogel was determined by the final weight divided by the initial weight of the disk-shaped hydrogels. The initial weights of hydrogels were recorded (Wi). Hydrogels were immersed in 2 mL of PBS at room temperature, and then the weights after immersion over time were recorded (Wt). Surrounding water was drained and blotted out with Whatman filter paper from hydrogels before weighing. The swelling ratios were calculated from Wt/Wi. For the stability test, the disk-shaped hydrogels were incubated with 2mL of PBS at room temperature. The hydrogel mass reduction at each time point was monitored. The hydrogels were collected, washed with DI water, and dried in vacuum for 2h at 40 C^{o} before the dry weight was measured. The dry weight at the starting point was measured as (Wd). The dry weight measured at different time points was symbolized (Wt). Normalized hydrogel dry weight was calculated as Wt/ Wd.

3.2.8 Scanning Electron Microscopy. The microstructure of the sericin hydrogels was imaged using a VEGA3 SBU variable pressure scanning electron microscope (SEM; Tescan, Kohoutovice, Czech Republic) at 8 keV accelerating voltage. The freeze-dried

samples were immersed in liquid nitrogen and cut with a surgical blade to expose a freshly cut surface. The surface was coated with gold using a Denton Desk II sputter coater (Moorestown, NJ) at 20 mA for 75 s and imaged with SEM.

3.2.9 Potential biocompatibility and human MSCs adhesion on the SerAte hydrogel. Human MSCs (Lonza, Allendale, NJ) were cultured in an α-MEM medium supplemented with 16 % FBS, 3mM glutamine, 100 units/mL penicillin and 100 µg/mL streptomycin (basal medium). After reaching 70% confluency, the hMSC cells were detached with 0.1% trypsin- 0.03% EDTA and sub-cultured at a ratio of 1:3 for <7 passages, according to supplier's instructions. Cell adhesion experiments were done with different hydrogels of comparable compressive moduli. Twenty four well culture plates were coated with a thin layer of 15, 17 and 20 wt% SerAte II, and crosslinked with UV to form the hydrogels. Next, hMSCs were seeded on the surface of the gels at a density of $5x10^3$ cells/cm^2 and cultured in basal medium for cell attachment. For immunofluorescent staining, wells were washed twice in PBS and fixed with 4% paraformaldehyde (Sigma Aldrich) at 4°C for 30 min. Next, samples were permeabilized with 0.1% Triton X-100 and 100 mM glycine in PBS for 15 min and blocked with 4 % BSA and 0.5 mM glycine in PBS for 30 min. Next, blocked samples were incubated with TRITC-conjugated phalloidin in blocking buffer for 15 min at ambient conditions. After washing three times with PBS, the cell-seeded hydrogel samples were counter-stained with DAPI to image the cell nuclei. The stained samples were imaged with an inverted fluorescent microscope (Nikon Eclipse Ti ε, Nikon, Melville, NY).

To evaluate the biocompatibility potential of SerAte-II to hMSCs, assessment of cellular viability was carried out using the DNA content. Human mesenchymal stem cells

(hMSCs) were encapsulated in the SerAte II hydrogel in a basal medium at a density of 1×10^6 cells/mL. At time points (1, and 3 days), cell-laden hydrogels were washed with serum-free DMEM followed by washing with PBS. Next, the samples were lysed with 10 mM Tris supplemented with 0.2% triton in PBS and then lysed samples were used for measurement of DNA content using Quant-it PicoGreen as we previously described [184]. Cell-free hydrogel well plates were used as controls.

3.2.10 Cell viability assay. For the cell viability assay, the hydrogels were prepared and cultured as described to culture the cells. Live/dead staining was conducted to evaluate the cell viability of hMSCs encapsulated in the hydrogels by using Cell stain Double Staining Kit (Dojindo Laboratories, Tokyo, Japan). At days 1 and 3 of culture, the cell-laden disk-shape hydrogels were collected, washed with PBS, and incubated with serum-free medium containing calcein-AM (2 μM) and propidium iodide (4 μM) for 15 minutes. Next, the live and dead cells were imaged with an inverted fluorescent microscope (Nikon Eclipse Ti ε, Nikon, Melville, NY).

3.3 Results

3.3.1 Extraction of sericin and synthesis of sericin urethane methacryloyl (SerAte). Sericin was extracted from silk cocoons using the acid, citric acid method (See "Methods" for details), which is shown to extract sericin protein (properties by citric acid). We introduced methacryloyl groups onto the reactive hydroxyl groups of sericin to obtain three sericin derivatives (SerAte-I, SerAte-II and SerAte-III) with different levels of methacryloyl modification by varying feed ratios of IEM to sericin, as in Table 3.1. The ^{1}HNMR spectra of the extracted sericin and SeraAte are shown in Figure 3.2a. The spectra showed that the modification of sericin by isocyanato ethyl methacryloyl groups are successful onto sericin as the new chemical shift "a" (δ 1.9 ppm) was corresponding to the

methyl protons and the chemical shift “b” (δ 5.4 ppm and 5.7 ppm) was resulting from the double bond protons. The modification degrees were calculated to be 24%, 31% and 40% by comparing the area of the methacrylate vinyl proton peaks to the area of the protons associated with the serine and glycine groups, 3.6–4.0 (Ser CH_2 and Gly CH_2), in the sericin backbone [181].

3.3.2 Effect of methacryalion on the secondary structure of SerAte. Circular Dichroism (CD) spectra of the extracted sericin in PBS are shown in figure 3.3. The figure shows the spectral comparison between extracted sericin and the SerAte with different modifications in aqueous solution at rt. The CD curve of sericin displays two shallow, negative bands centered at 217 and 230 nm. These results indicate that the conformation of sericin is a coil containing a small amount of the β-form. The presence of the β-form in sericin could be due to high serine content [185].

No major differences or spectral shifts were observed between the spectra of the sericin (dashed line) and SerAte (solid line). Thus, we concluded that the secondary structure of sericin remained intact upon the modification and was not affected during the process.

3.3.3 Mechanical properties, biodegradability and biocompatibility

3.3.3.1 Gelation kinetics of SerAte. The effect of UV irradiation time on storage (G’) and loss (G”) moduli of a 24, 30, 40 wt% SerAte precursor solutions are shown in Figure 3.3 a-c. The gelation time of the SerAte precursor solution (the time at which G’= G”) was 80, 120 and, 190 s, respectively. The SerAte-I-15 solution did not form a hydrogel upon UV irradiation (data not shown). However, the wt% of SerAte-II and SerAte-III solutions formed a gel (G’≥ G”) in aqueous solution with the presence of photoinitiator with UV irradiation. Gelation time decreased steadily from 190±25 s to 90±30 s as the modification % increased from 24% to 40%. Based on the results in figure 3.3, the 30 % modification

of sericin was selected for methacrylation of the extracted sericin in subsequent degradation and cell culture experiments.

3.3.3.2 The microstructure of SerAte Hydrogels. Scanning EM images of hydrogels with 24, 30, and 40 wt% SerAte after freeze-drying is shown in Figure 3.4a-d. The crosslinked SerAte hydrogels showed stable, interconnected, highly porous morphology with <5 μm thick walls. At least 20 pores were selected from each SEM image of the freeze-dried hydrogel samples to determine the mean and standard deviation of the pore sizes. The pore size of the SerAte hydrogels decreased from 54±16 μm to 28±14 μm and 21±10 μm as the concentration of SerAte-II in the precursor solution increased from 15 wt% to 17.5 % and 20 %, respectively. Compared to other hydrogels, x and y gels had significantly bigger pore sizes. This may be the fact that x and y gels could adsorb more water. After lyophilization, the space water occupied resulted in the formation of pores [186].

3.3.3.3 Compressive Modulus and Swelling Ratios of SerAte Hydrogels. Figures 3.2d-f show the effect of SerAte concentration in the precursor solution on swelling ratio in aqueous solution, sol fraction, and compressive modulus of the hydrogels crosslinked with high-intensity Omni Cure UV system. The compressive modulus of the hydrogels increased from 1.8±0.3 to 7.7±0.4 kPa with increasing SerAte concentration from 10 to 25 wt% (Figure 3.3b), respectively, whereas the swelling ratio in PBS decreased from 390±40% to 150±25% and sol fraction decreased from 12±3% to 7±2%.

3.3.3.4 Thermal Stability of SerAte. The thermogravimetric analysis graph of the extracted sericin (round dots) and SerAte after methacrylation (solid line) are shown in Figure 3.3c. Thermal degradation of the extracted sericin and SerAte commenced at 230°C and ended at 400°C resulting in a 64 % mass loss. There was not a significant difference

between the thermographs of the extracted sericin and SerAte. Analysis of the TGA results indicated that SerAte was thermally more stable than sericin because there was a statistically significant difference ($p<0.05$) between mass losses of SerAte and sericin with increasing temperature. Sericin and SerAte hydrogels underwent three stages of thermal degradation including dehydration, depolymerization, and decomposition (Figure 3.3c). The first stage was from room temperature to around 110 °C, where the mass loss revealed the removal of adsorbed water molecules in sericin and SerAte hydrogels. The second major decomposition was attributed to the degradation of sericin and SerAte occurred in the temperature range of 120–410 °C. At this stage, the mass loss of sericin hydrogel was faster than that of serAte, indicating that SerAte could improve the thermal stability of the sericin and delay the thermal degradation process. At the last stage, the mass loss occurred from 420 °C to 600 °C, which was associated with the breakdown of sericin and SerAte [186].

The lyophilized SerAtes were highly porous (Figure 3.5). The pore sizes, porosity, equilibrium weight swelling ratios, and degradation rates (in PBS at 37^{o}C) of these hydrogels were negatively correlated with methacrylation degrees (Table and Figure.), while SerAtes' stiffness was positively correlated with methacrylation degrees (compressive moduli were 4 kPa for SerAte-I, 15 kPa for SerAte-II, and 36 kPa for SerAte-III). These correlations were likely attributed to different crosslinking densities resulting from different levels of methacrylation across these hydrogels, which provides a practical way of adjusting these physical and chemical properties to meet diverse therapeutic requirements."

3.3.4 Cell Adhesion and Proliferation. The ability of sericin to promote cell attachment is one of the key biological properties that are focused on this research. Human MSCs are well known to adhere and proliferate on TCP, and therefore TCP was used as a control in comparison to the SerAte-II. Figures 5a-d show the attachment of hMSCs on 2D SerAte-II hydrogel at day1 and day3. At the initial attachment period day1, the number of cells attached to the TCP and SerAte hydrogel was the same.

3.4 Discussion

Silk-sericin has been increasingly used in tissue engineering with various forms of cell delivery systems, such as films, scaffolds and hydrogels due to its excellent biocompatibility, biodegradability and valuable bioactivities [174, 175]. Silk industry is the major source of sericin that produces as a by-product of around 50K tons annually. However, such sericin was degraded (sericin^{degraded}) because of the harshness extraction method used in the degumming process. The sericin^{degraded} was hard to crosslinked in the form of hydrogels to be used in tissue engineering applications [176]. Instead, sericin^{degraded} was used to form cross-linkable, composite hydrogels with other polymers by biotoxic crosslinkers leading to losing some of the sericin's natural bioactivities [176]. To maintain sericin's natural properties and forming hydrogels, an aqueous solution of 1.25% of citric acid was used to extract sericin from the cocoon. The yield percent of sericin based on the weight of the feather was 35%. Citric acid is used to hydrolytically degum sericin from fibroin under acidic conditions [187]. Urea treatment step was not included since extraction with urea has a significant impact on sericin conformation [182]. The extracted sericin obtained through the citric acid extraction method has two clearly different bands in SDS-PAGE at the molecular weights (MW), approximately 85 kDa, and 100 kDa. These bands

were closely consistent with the previously reported value of approximately 60 kDa, 100 kDa, and 130 kDa [174]. In contrast, SerAte-II has a less intense band at the molecular weight 85 kDa, a wide range of molecular weights above 85 kDa and below 250 kDa that is probably related to the multiple modifications of sericin by IEM [188]. As an alternative hydrogel, a new chemical functionalization approach to an acid extracted sericin hydrogel for tissue engineering by a photo-crosslinking method. By introducing ethyl methacryloyl groups to sericin, sericin ethyl methacryloyl (SerAte) have successfully synthesized as a hydrogel precursor for photo-crosslinking. Sericin modification with IEM and its gelation method had an advantage over other sericin scaffolds. The network density and porous structures of SerAtes were tuned simply by altering SerAtes methacrylation degrees that controlled degradation rates and drug release kinetics.

The microstructure of SerAte hydrogels with different modifications showed 20−100 μm range of internal pore size with high porosity and pore interconnectivity. Having high degrees of porosity and pore interconnectivity had a critical role in cells and substance penetration, homogenous cell distribution, promote cell-cell interactions, nutrients and metabolites transfer, and tissue growth. For instance, matrices with large pore sizes between 115 to 335 μm were suitable for the formation of cartilaginous tissue. while, matrices with small pore sizes were appropriate for chondrocyte phenotypes [189, 190]. The swelling ratio is another essential factor for the development of hydrogels in therapeutic applications. Many studies have revealed that increased hydrogels' porosity and interconnectivity can improve the rate of swelling of the hydrogels because of increasing the contact area between the hydrogels and media [173, 191]. Further, the enlarge in porosity and interconnectivity could lead to a decrease in the solid content of the

hydrogels, and result in a lower storage modulus [192]. In our result, the swelling ratio of SerAte-I, II and II hydrogels were absorbing water from 1.5 up to 2.25-fold their initial weight, showing that the hydrogels exhibited hydrophilic properties similar to tissue environment and the capability to uptake cell culture medium. From the stability test, no weight loss was observed from both hydrogels during 21 days, indicating that they could support the entire cell culture experiments and were suitable for tissue engineering applications.

These results of cell adhesion confirmed that SerAte hydrogel does facilitate cell attachment, even though there were no cell adhesion sequences such as RGD and YIGSR present in the protein. At day3, there were significantly more cells attached to the SerAte as compared to TCP. Previous studies that were focusing on B. Mori sericin reported that it supports fibroblasts adhesion and proliferation. It has been reported that the serine-rich repetitive sequences found in sericin are responsible for the cell attachment activity [193]. Next, the grafting of sericin with methacrylate groups did not result in a significant decrease in cell proliferation activity, and sericin-MA coatings from both species showed a higher number of attached cells compared to the TCP control (Figure 3.5). Although it was hypothesized that the functionalization process might denature or degrade the sericin peptides, hence poses a negative effect on the bioactivity, it was not reflected in this [181].

3.5 Conclusion

A photo-polymerizable urethane methacrylate sericin (SerAte) was prepared from sericin extracted from silk cocoon and used as a hydrogel for mesenchymal stem cells immobilization. Human MSCs seeded on SerAte hydrogel had elongated spindle-shape morphology compared to tissue culture plate TCP. Human MSCs seeded on SerAte

hydrogels showed a similar rate of proliferation as those seeded on TCP. Further, the mechanical properties, the network density and porous structures of SerAtes were tunable simply by controlling Sericin's methacrylation degrees covering the range of the mechanical properties of various native tissues. Based on these results, this urethane methacrylated sericin extracted from the cocoon is highly effective biopolymer, biomimetic scaffold for encapsulation and delivery of stem cells to regenerate 3D artificial tissue.

The short outcomes of collagen-based hydrogels in tissue engineering applications are poor mechanical stability and poor durability prior to the secretion of natural ECM proteins by the cells to resist matrix degradation [176, 184]. Gelatin and gelatin derivatives show good solubility only in hot solutions, which might impact the procedure of gelation and cell encapsulation [176]. Stable silk sericin biomaterials, such as films, sponges, and hydrogels, are prepared by cross-linking, ethanol precipitation, or blending with other polymers [175]. For instance, Films (2D) and scaffolds (3D) have been obtained by blending SS with gelatin or glycogen and cross-linking with glutaraldehyde. Both matrices were biocompatible, and SS promoted the attachment and proliferation of feline fibroblasts in the 3D scaffolds but became toxic at concentrations of 5 and 7.5 wt%.

Table 3.1 Percent degree of urethane methacrylation of Sericin when reacting with various molar ratio of IEM

	Abbreviation	Modification %
1	SerAte-I	24
2	SerAte-II	31
3	SerAte-III	40

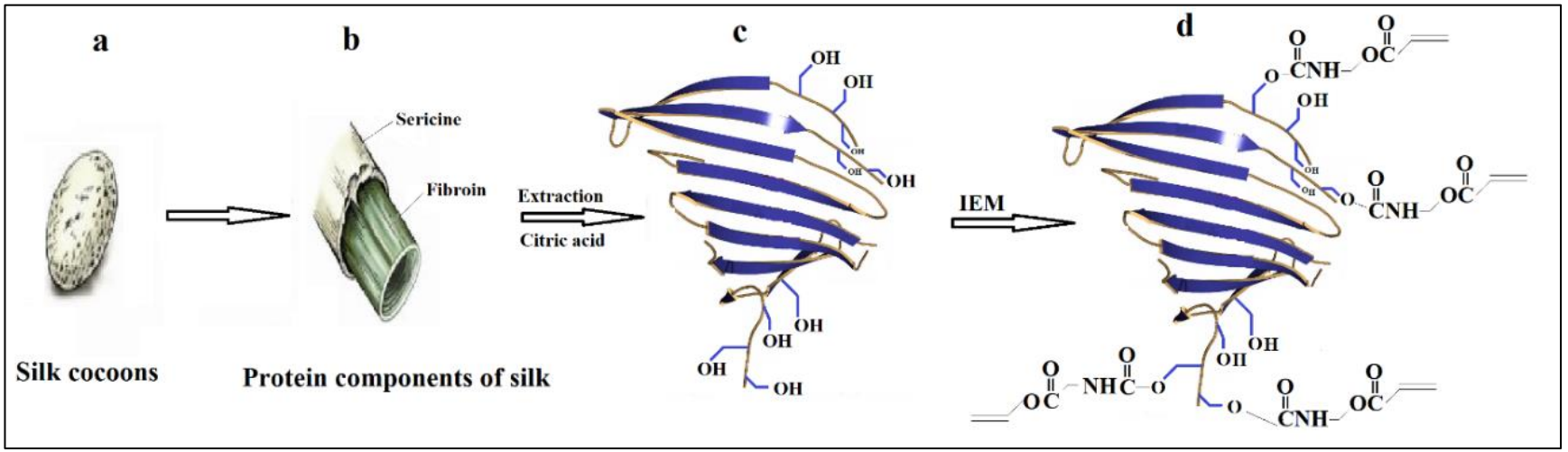

Figure 3.1: Schematic diagram of sericin extraction and modification. (a,b) sericin was extracted from silk cocoons into an aqueous solution containing citric acid. (c) The hydroxyl group of serine residues in sericin was converted to urethane methacrylate(d).

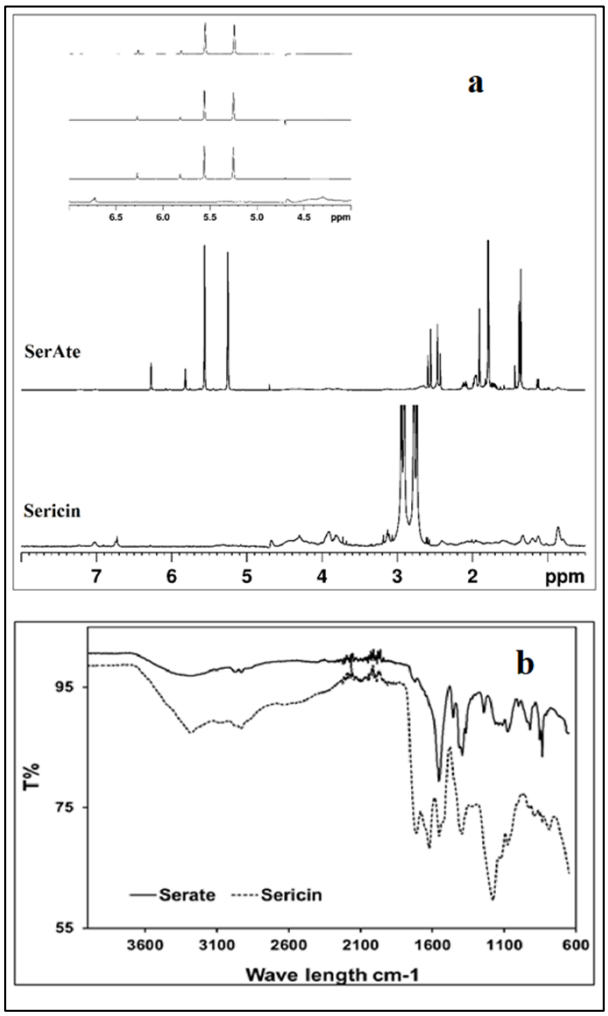

Figure 3.2. (a) ^{1}H NMR spectra of Sericin and SerAte with 24%, 31%, and 40% degree of modification. (b) Spectra of sericin and SerAte in the range of 500-4000 cm^{-1}.

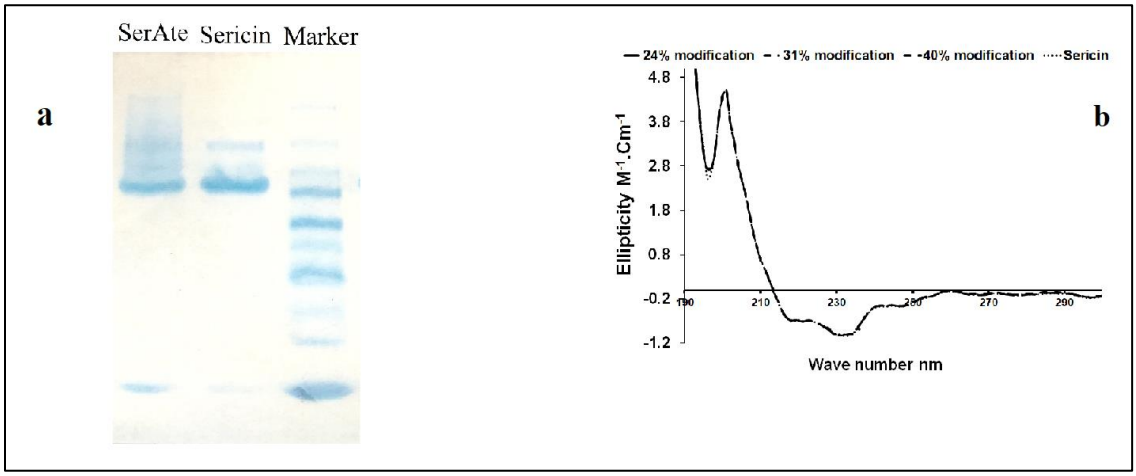

Figure 3.3 (a) SDS-PAGE from left to right for SerAte, Sericin, and standard protein MW markers. (b) CD spectra of 0.1 mg/mL Sericin and SerAte in PBS with 24%, 31%, and 40% degree of modification.

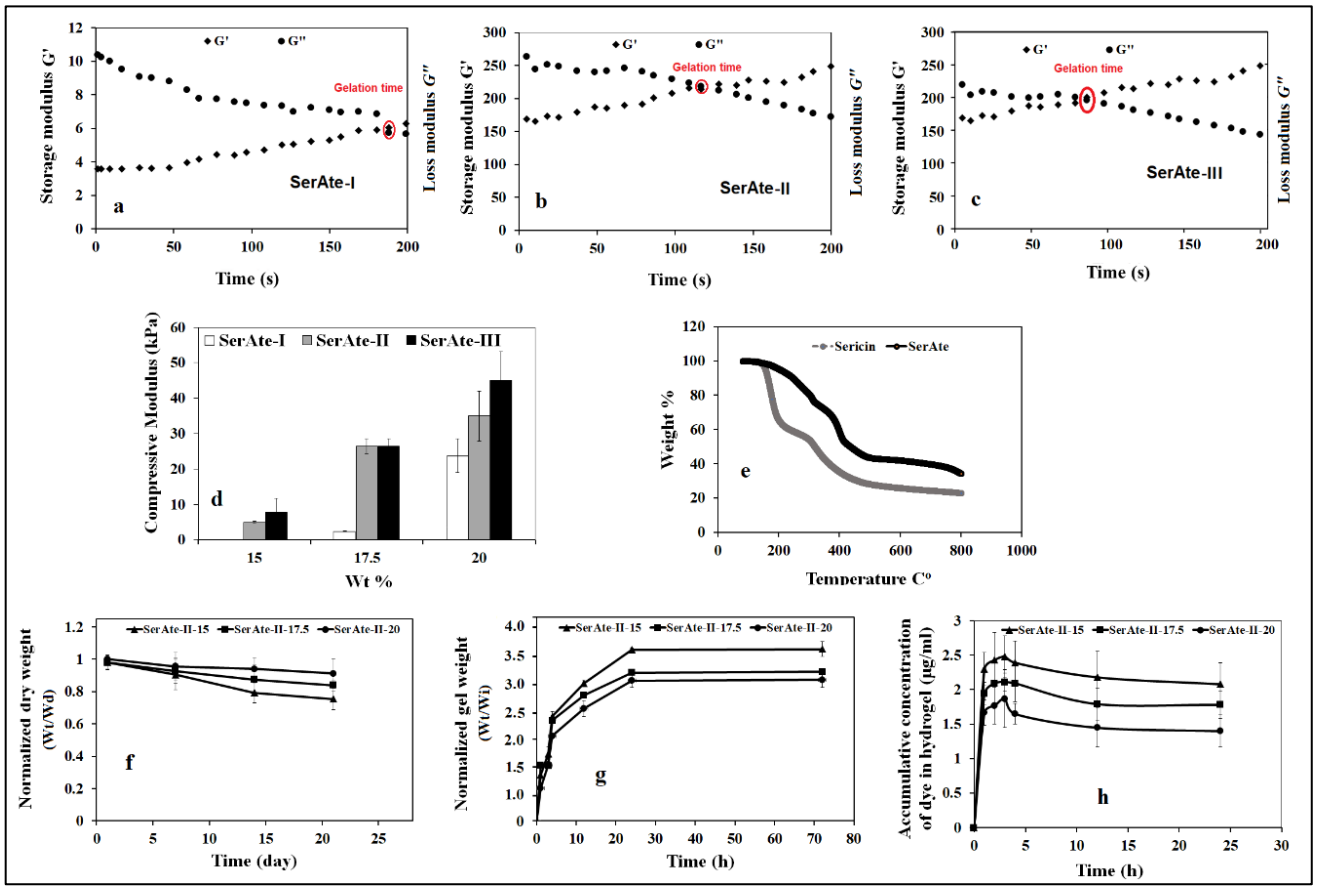

Figure 3.4 (a-c) Effect of UV exposure time on storage (G') and loss (G") moduli of 20 wt% SerAte precursor solution (G'=G'' at gelation time) with photoinitiator. (d) Effect of SerAte concentration on the hydrogel compressive modulus. (e) TGA thermograms of the extracted sericin (black curve) and modified sericin (SerAte, gray curve) (f) The stability of the hydrogels. The weight loss was observed over time. Swelling ratios of the hydrogels after gelation and immersion into PBS. The weight change due to water absorption was monitored over time. (g) Permeability of the hydrogels in term of molecular retention using dye retention study. (h) The values expressed are means ± SD, n = 3

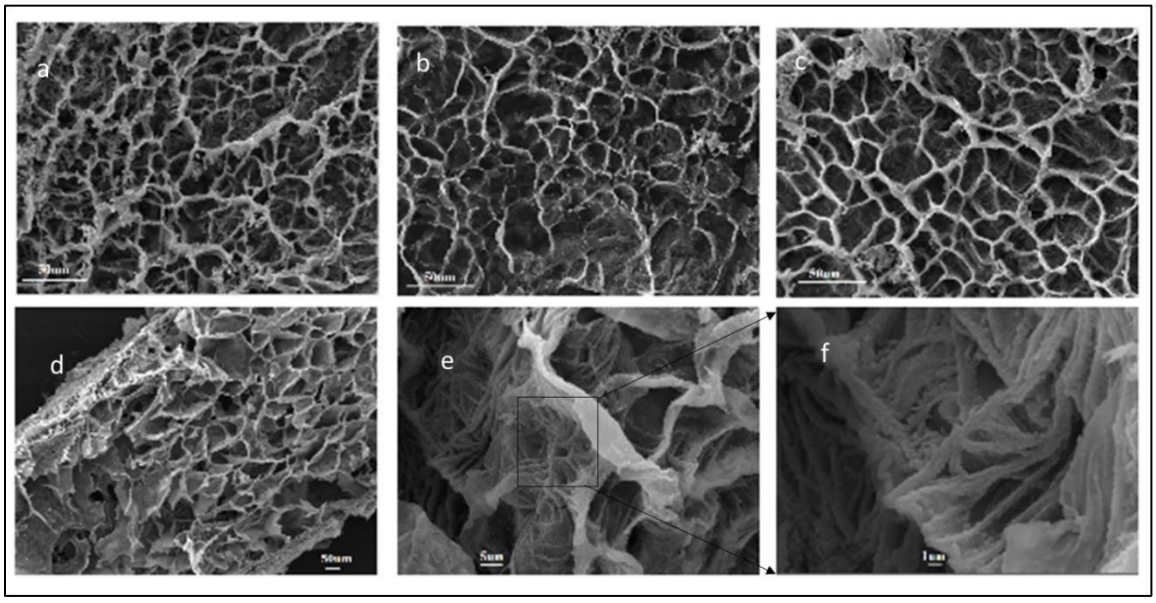

Figure 3.5. SEM images of freeze-dried SerAte precursor solution after UV crosslinking with SerAte II concentrations of 15 (a), 17.5 (b) and (c) 20 wt% (scale bar in a-d is 50 µm). (d) presents si(e &f) show the fibrous structure of SerAte (scale bar is 5um and 1um).

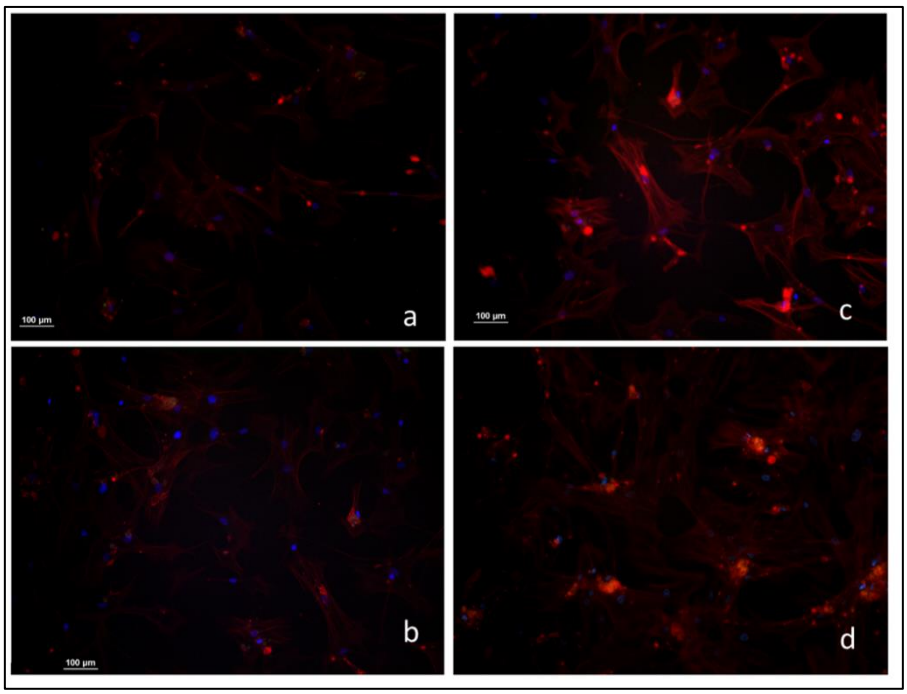

Figure 3.6. DAPI (blue) and phalloidin (red) stained images of hMSCs seeded on TCP (a), as a control, and SerAte II with 15, 17.5, and 20 wt% (b-d) hydrogels after 3 incubation in basal medium, respectively (scale bar in a-d is 100 µm).

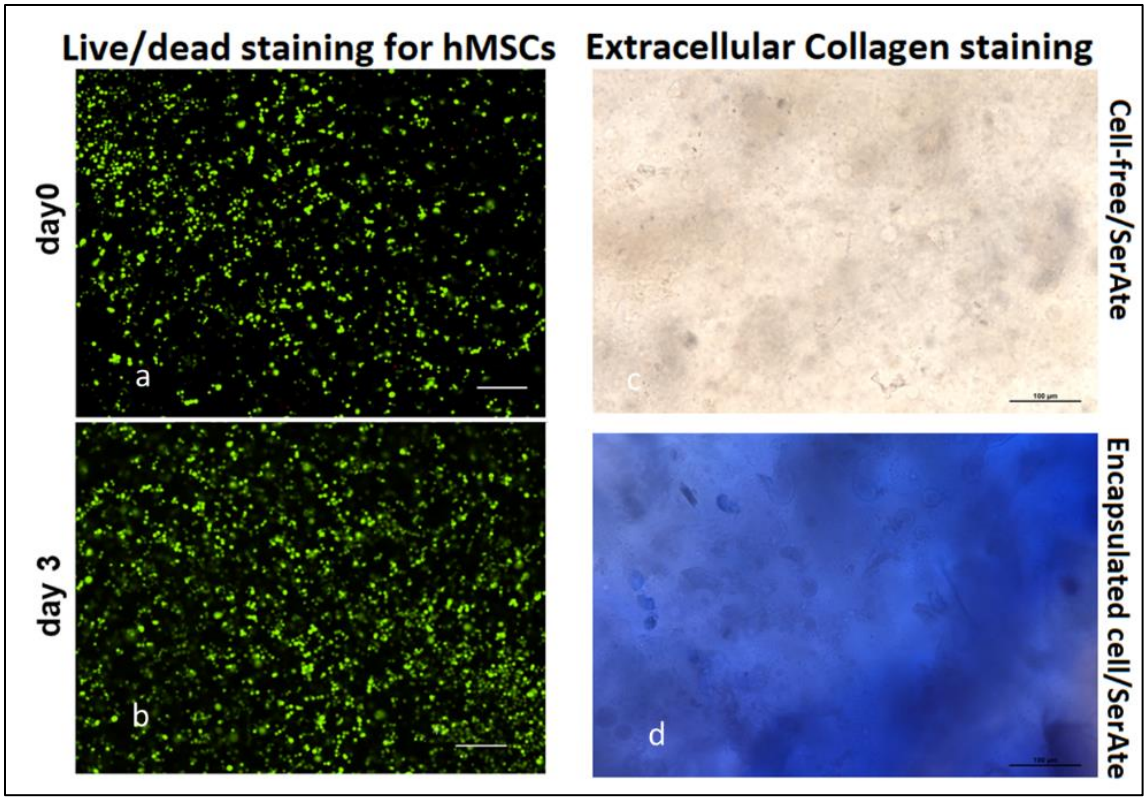

Figure 3.7 (a and b) Live (green) and dead (red) stained images of hMSCs encapsulated in 20 wt % SerAte II hydrogels after zero- and 3-days incubation. (c and d) Trichrome staining for the detection of extracellular collagen for encapsulated hMSCs in SerAte II.

CHAPTER 4: SUMMARY OF FINDINGS AND FUTURE STUDIES

The results of the research presented in this dissertation show that the on-demand release of rhBMP2 from plasmin cleavable NPs in the patterned constructs in response to proteolytic factors like plasmin, MMPs, and tPA as well as others secreted by the encapsulated cells led to highest extent of osteogenesis and vasculogenesis and coupling of paracrine signaling between the differentiating hMSCs and ECFCs. This was accomplished by three main studies.

The first study investigated that hMSCs and ECFCs encapsulated in a patterned composite hydrogel release proteolytic factors like MMPs, plasminogen and tPA as well as others and that the released factors are able to cleave plasmin-degradable peptides embedded in NPs to release morphogens like rhBMP2 on-demand. The mRNA expressions of uPA, tPA, and plasminogen in the fibrinolytic cascade for the LPELA encapsulated MSCs, GelMA encapsulated ECFCs, and GelMA encapsulated MSCs + ECFCs with incubation time. The encapsulated hMSCs expressed significant levels of uPA, tPA, plasminogen, MMP2 and MT-MMP1 in osteogenic medium. The encapsulated ECFCs did not express significant levels of proteases of the fibrinolytic cascade and the expressions did not change with differentiation in a vasculogenic medium. The encapsulated hMSCs + ECFCs expressed significant levels of tPA and plasminogen with differentiation in vasculogenic medium. At the protein level for all cells, the extra- and intra-cellular expressions of plasmin and MMP2 for the encapsulated hMSCs, ECFCs, and hMSCs+ECFCs increased with cell differentiation.

Based on the results in first study, where the encapsulated hMSCs showed higher expression of proteases with differentiation in osteogenic medium as compared to ECFCs or hMSCs+ECFCs in vasculogenic medium. The next study investigated the design of a peptide-PEG macromer composed of a phenylalanine sequence for self-assembly and a plasmin-cleavable sequence for BMP2 release in response to plasmin secretion by MSCs and ECFCs. The PxSPCP NPs had a core-corona morphology with the self-assembling peptides in the core and PEGs in the corona. The stability of NPs in aqueous solution and the BMP2 stability against denaturation was a strong function of PEG MW. The P2SPCP NPs with PEG MW of 2 kDa showed the most stable particle size distribution and protein secondary structure with incubation.

The last study investigated the release characteristics, the bioactivity of the released BMP2, and osteogenic and vasculogenic differentiation of hMSCs and ECFCs in patterned hydrogels with plasmin-cleavable BMP2-P2SPCP NPs. The BMP2 grafted to P2SPCP NPs and co-encapsulated in LPELA hydrogel with plasmin was gradually released to the medium with incubation time at a rate faster than the non-cleavable BMP2-PxSP NPs but slower than the free BMP2. Further, the released BMP2 from the NPs by the action of plasmin induced differentiation of hMSCs encapsulated in the LPELA hydrogel. Human MSCs and BMP2-PxSPCP NPs were encapsulated in the matrix whereas hMSCs+ECFCs and VEGF-NGs were encapsulated in the microchannels of the patterned construct. Our results showed that the hMSC/ECFC co-culture results in patterned constructs demonstrate that the on-demand release of BMP2 from plasmin-cleavable PxSPCP NPs enhanced osteogenesis and vasculogenesis compared to the direct addition of BMP2.

REFERENCES

1. Ami R. Amini, C.T.L., and Syam P. Nukavarapu, *Bone Tissue Engineering: Recent Advances and Challenges.* Crit Rev Biomed Eng., 2012. **40**(5): p. 363–408.
2. Kishor K. Sivaraj, R.H.A., *Blood vessel formation and function in bone.* Development, 2016. **143**: p. 2706-2715.
3. Kinaci A, N.V., Ring DC., *Trends in bone graft use in the United States.* Orthopedics, 2014. **37**(9): p. e783-8.
4. Barati, D., et al., *Spatiotemporal release of BMP-2 and VEGF enhances osteogenic and vasculogenic differentiation of human mesenchymal stem cells and endothelial colony-forming cells co-encapsulated in a patterned hydrogel.* Journal of Controlled Release, 2016. **223**: p. 126-136.
5. Aleksejs Zavorins, M.P., Girts Salms, Andrejs Skagers, Inese Cakstina, Janis Locs, *Reaction of Subcutaneous Connective Tissue of Experimental Animals on Bone Marrow Mesenchymal Stromal Cell Coated Hydroxyapatite.* ACTA CHIRURGICA LATVIENSIS, 2012. **12**: p. 45-50.
6. Phillips, F., I. Lieberman, and D. Polly, *Minimally Invasive Spine Surgery: Surgical Techniques and Disease Management*. 2014: Springer New York.
7. Albrektsson T1, J.C., *Osteoinduction, osteoconduction and osseointegration.* Eur Spine J., 2001. **10**(2): p. S96-101.
8. Agarwal R, W.K., Umscheid CA, Welch WC, *Osteoinductive bone graft substitutes for lumbar fusion: a systematic review.* J Neurosurg Spine, 2009. **11**(6): p. 729-40.
9. Gupta A, K.N., Sharif K, Main BJ, Albers CE, El-Amin Iii SF, *Bone graft substitutes for spine fusion: A brief review.* World J Orthop, 2015. **6**(6): p. 449-56.
10. Kaufmann, M.L., Philip Matern, Katie Morrison-Graham, Devon Quick, Jon Runyeon Art edited and created by Leeah Whittier, *Anatomy & Physiology*. 2019: Open Oregon State, Oregon State University.
11. Arnett, M.M.a.T.R., *The Key Role of the Blood Supply to Bone.* Bone Res., 2013. **3**(1): p. 203–215.
12. Erlebacher, A., Filvaroff, E. H., Gitelman, S. E. and Derynck, R. , *Toward a molecular understanding of skeletal development.* Cell, 1996. **80**: p. 371-378.
13. Stefanie Inglis, D.C., David I. Wilson, Janos M. KanczlerEmail author and Richard O. C. Oreffo, *Human endothelial and foetal femur-derived stem cell co-cultures modulate osteogenesis and angiogenesis.* Stem Cell Research & Therapy, 2016. **7**: p. 13.
14. Brandi ML, C.-O.P., *Perspective - vascular biology and the skeleton.* J Bone Miner Res., 2006. **21**(2).

15. Zou, D., et al., *Blood vessel formation in the tissue-engineered bone with the constitutively active form of HIF-1alpha mediated BMSCs.* Biomaterials, 2012. **33**(7): p. 2097-108.
16. Jacobsen, K.A., et al., *Bone formation during distraction osteogenesis is dependent on both VEGFR1 and VEGFR2 signaling.* J Bone Miner Res, 2008. **23**(5): p. 596-609.
17. Jabalee J, F.-O.T., *Vascular endothelial growth factor signaling affects both angiogenesis and osteogenesis during the development of scleral ossicles.* Dev Biol., 2015. **406**(1): p. 52-62.
18. Duan X1, M.Y., Liu Y1, Nicolae C1, Olsen BR1, Berendsen AD2., *Vegfa regulates perichondrial vascularity and osteoblast differentiation in bone development.* Development., 2015. **142**(11): p. 1984-91.
19. Kopp, H.G., et al., *Functional heterogeneity of the bone marrow vascular niche.* Ann N Y Acad Sci, 2009. **1176**(7): p. 47-54.
20. Gerber, H.P.a.F., N. , *Angiogenesis and bone growth. Trends Cardiovasc. Med. 10, 223-228.* Trends Cardiovasc. Med., 2000. **10**(10): p. 223-228.
21. Dai, J.a.R., A. B. M. , *VEGF: an essential mediator of both angiogenesis and endochondral ossification.* J. Dent. Res., 2007. **86**(86): p. 937-950.
22. Kusumbe, A.P., Ramasamy, S. K. and Adams, R. H., *Coupling of angiogenesis and osteogenesis by a specific vessel subtype in bone. Nature 507, 323-328.* Nature, 2014. **507**(507): p. 323-328.
23. Ramasamy, S.K., Kusumbe, A. P., Wang, L. and Adams, R. H, *Endothelial Notch activity promotes angiogenesis and osteogenesis in bone.* Nature, 2014. **507**(507): p. 376-380.
24. Maes, C., et al., *Increased skeletal VEGF enhances beta-catenin activity and results in excessively ossified bones.* EMBO J, 2010. **29**(2): p. 424-41.
25. Lowery, J.W., et al., *The role of BMP2 signaling in the skeleton.* Crit Rev Eukaryot Gene Expr, 2011. **21**(2): p. 177-85.
26. Deckers MM, v.B.R., van der Horst G, Hoogendam J, van Der Bent C, Papapoulos SE, Löwik CW., *Bone morphogenetic proteins stimulate angiogenesis through osteoblast-derived vascular endothelial growth factor A.* Endocrinology, 2002. **143**(4): p. 1545-53.
27. Lee, S.-H., *Matrices and scaffolds for delivery of bioactive molecules in bone and cartilage tissue engineering.* Advanced Drug Delivery Reviews, 2007: p. 339–359.
28. Kangwon Lee, E.A.S., and David J. Mooney, *Growth factor delivery-based tissue engineering: general approaches and a review of recent developments.* J R Soc Interface, 2011: p. 153–170.
29. Jaya Maitra, V.K.S., *Cross-linking in Hydrogels - A Review.* American Journal of Polymer Science, 2014. **2014, 4(2): 25-31**(2): p. 25-31.
30. Makhdom AM, H.R., *The role of growth factors on acceleration of bone regeneration during distraction osteogenesis.* Tissue Engineering Part B: Reviews. **19**(5): p. 442-53.
31. Malizos KN, P.L., *The healing potential of the periosteum: molecular aspects.* Injury, 2005. **36**(3): p. S13-9.

32. Villars F, B.L., Bareille R, Amedee J, *Effect of human endothelial cells on human bone marrow stromal cell phenotype: role of VEGF?* Journal of cellular biochemistry., 2000. **79**(4): p. 672-85.
33. Bompais, H., et al., *Human endothelial cells derived from circulating progenitors display specific functional properties compared with mature vessel wall endothelial cells.* Blood, 2004. **103**(7): p. 2577-84.
34. Lee K, S.E., Mooney DJ *Growth factor delivery-based tissue engineering: general approaches and a review of recent developments.* . J R Soc Interface, 2011. **8**: p. 153-170.
35. Vo TN, K.F., Mikos AG, *Strategies for controlled delivery of growth factors and cells for bone regeneration.* Adv Drug Deliv Rev, 2012. **64**: p. 1292-1309.
36. Santo VE, G.M., Mano JF, Reis RL, *Controlled release strategies for bone, cartilage, and osteochondral engineering--Part II: challenges on the evolution from single to multiple bioactive factor delivery.* . Tissue Eng Part B Rev 2013. **19**: p. 327-352.
37. Ramoshebi LN, M.T., Teare J, Renton L, Patton J, Ripamonti U, *Tissue engineering: TGF-beta superfamily members and delivery systems in bone regeneration.* Expert Rev Mol Med, 2002: p. 1-11.
38. Celeste AJ, I.J., Taylor RC, Hewick RM, Rosen V, Wang EA, Wozney JM, *Identification of transforming growth factor beta family members present in bone-inductive protein purified from bovine bone.* Proc Natl Acad Sci U S A, 1990: p. 9843-7.
39. Fischer J, K.A., Wolfart S, Pautke C, Warnke PH, Plank C, Smeets R, *Future of local bone regeneration - Protein versus gene therapy.* J Craniomaxillofac Surg, 2011. **39**: p. 54-64.
40. Aryal, R., et al., *Bone Morphogenetic Protein-2 and Vascular Endothelial Growth Factor in Bone Tissue Regeneration: New Insight and Perspectives.* Orthopaedic Surgery, 2014. **6**(3): p. 171-178.
41. Kanczler JM, O.R., *Osteogenesis and angiogenesis: the potential for engineering bone.* Eur Cell Mater, 2008. **15**: p. 100-14.
42. Tiffany N. Vo, F.K.K., 1 and Antonios G. Mikos, *Strategies for Controlled Delivery of Growth Factors and Cells for Bone Regeneration.* Adv Drug Deliv Rev., 2013. **64**: p. 1292–1309.
43. Kaigler D, W.Z., Horger K, Mooney DJ, Krebsbach PH, *VEGF scaffolds enhance angiogenesis and bone regeneration in irradiated osseous defects.* J Bone Miner Res, 2006. **21**: p. 735-44.
44. Huang YC, K.D., Rice KG, Krebsbach PH, Mooney DJ, *Combined angiogenic and osteogenic factor delivery enhances bone marrow stromal cell-driven bone regeneration.* J Bone Miner Res., 2005. **20**: p. 846-57.
45. Cui Q., D.A., and Irvine JN Jr., *Combined angiogenic and osteogenic factor delivery for bone regenerative engineering.* Curr Pharm Des, 2013: p. 3374-83.
46. Wenjie Zhang, C.Z., Yiqun Wu, Dongxia Ye, Shaoyi Wang, Duohong Zou, Xiuli Zhang, David L. Kaplan, and Xinquan Jiang, *VEGF and BMP-2 Promote Bone Regeneration by Facilitating Bone Marrow Stemcell Homing and Differentiation.* European Cells and Materials, 2014. **27**: p. 1-12.

47. Takahashi, Y., M. Yamamoto, and Y. Tabata, *Enhanced osteoinduction by controlled release of bone morphogenetic protein-2 from biodegradable sponge composed of gelatin and Î²-tricalcium phosphate.* Biomaterials, 2005. **26**(23): p. 4856-4865.
48. H. Uludag, D.D.A., R. Palmer, G. Timony, J. Wozney, *Characterization of rhBMP-2 pharmacokinetics implanted with biomaterial carriers in rat ectopic model.* J. Biomed. Mater. Res., 1999. **46**: p. 193–202.
49. R.P. Félix Lanao, S.C.G.L., J.G.C. Wolke, J.A. Jansen, *In vitro degradation rate of apatitic calcium phosphate cement with incorporated PLGA microspheres.* Acta Biomater, 2011. **7**: p. 3459–3468.
50. E.W.H. Bodde, O.C.B., F.G.M. Russel, A.G. Mikos, P.H.M. Spauwen, J.A.Jansen, *The kinetic and biological activity of different loaded rhBMP-2 calcium phosphate cement implants in rats,*. J. Biomed. Mater. Res. A 2008. **87**: p. 780–791.
51. Zhang, S., et al., *Polyethylenimine-coated albumin nanoparticles for BMP-2 delivery.* Biotechnol Prog, 2008. **24**(4): p. 945-56.
52. Mano JF, S.G., Azevedo HS, Malafaya PB, Sousa RA, Silva SS, Boesel LF, Oliveira JM, Santos TC, Marques AP, Neves NM, *Natural origin biodegradable systems in tissue engineering and regenerative medicine: present status and some moving trends.* Journal of the Royal Society Interface, 2007. **4**(17): p. 999-1030.
53. Ulijn R. V., B.N., Jayawarna V., Thornton P. D., Todd S. J., Mart R. J., Smith A. M., Gough J. E., *Bioresponsive hydrogels.* Mater.Today, 2007. **10**: p. 40-4810.
54. Nguyen HG, M.K., Wang Q, *Upregulation of osteogenesis of mesenchymal stem cells with virus-based thin films.* Nanotheranostics, 2018. **2**(1).
55. Bashur CA, D.L., Goldstein AS, *Effect of fiber diameter and orientation on fibroblast morphology and proliferation on electrospun poly(D,L-lactic-co-glycolic acid) meshes.* Biomaterials, 2006. **27**(33): p. 5681-8.
56. Burg, K.J.L., S. Porter, and J.F. Kellam, *Biomaterial developments for bone tissue engineering.* Biomaterials, 2000. **23**(2): p. 2347-2359.
57. FrÃhlich, M., et al., *Tissue engineered bone grafts: biological requirements, tissue culture and clinical relevance.* Current stem cell research & therapy, 2008. **3**(4): p. 254.
58. Bose, S., M. Roy, and A. Bandyopadhyay, *Recent advances in bone tissue engineering scaffolds.* Trends in Biotechnology, 2012. **30**(10): p. 546-554.
59. Vats, A., et al., *Embryonic stem cells and tissue engineering: delivering stem cells to the clinic.* Journal of the Royal Society of Medicine, 2005. **98**(8): p. 346-350.
60. Jabbari, E., *Hydrogels for Cell Delivery.* Gels, 2018. **4**(3): p. 58.
61. Danial Barati, S.K., Seyed Ramin Pajoum Shariati, Seyedsina Moeinzadeh, Roger H. Sawyer, and Esmaiel Jabbari, *Synthesis and Characterization of Photocrosslinkable Keratin Hydrogels for Stem Cell Encapsulation* Biomacromolecules, 2016.
62. Akhtar MF, H.M., Ranjha NM. Methods of synthesis of hydrogels, *Methods of synthesis of hydrogels… A review.* Saudi Pharmaceutical Journal, 2016. **24**(5): p. 554-9.
63. Langer, A.K.a.R., *Microengineered hydrogels for tissue engineering.* Biomaterials, 2007. **28**(34).

64. Mihaila SM, R.R., Marques AP, Gomes ME, *Hydrogels in Bone Tissue Engineering: A Multi-Parametric Approach*, in *Applications of Hydrogels in Regenerative Medicine*, InGELS, Editor. 2016. p. 165-197.
65. Kohane DS, L.R., *Polymeric biomaterials in tissue engineering. Pediatric research.* Pediatric research, 2008. **63**(5).
66. Moeinzadeh, S., et al., *Gelation characteristics and osteogenic differentiation of stromal cells in inert hydrolytically degradable micellar polyethylene glycol hydrogels.* Biomacromolecules, 2012. **13**(7): p. 2073-2086.
67. Vats, A., et al., *Stem cells: sources and applications.* Clin Otolaryngol Allied Sci, 2002. **27**(4): p. 227-32.
68. R.L, N.A., *Topics in Tissue Engineering.* 2005. **2**.
69. GK., N., *From lab bench to market: critical issues in tissue engineering.* Ann N Y Acad Sci, 2002. **961**: p. 372-385.
70. Knight MA, E.G., *Tissue engineering: progress and challenges.* Plast Reconstr Surg, 2004. **114**: p. 26E-37E.
71. Shohreh Mashayekhan, M.H.a.A.F., *Stem Cells in Tissue Engineering.* Pluripotent Stem Cells, 2013.
72. T Langhans M, Y.S., S Tuan R, *Stem cells in skeletal tissue engineering: technologies and models.* Current stem cell research & therapy. **11**(6): p. 453-74.
73. Yousefi, A.M., et al., *Prospect of Stem Cells in Bone Tissue Engineering: A Review.* Stem Cells Int, 2016. **2016**: p. 6180487.
74. Hutton D. L., G.W.L., *Stem cell-based approaches to engineering vascularized bone.* Current Opinion in Chemical Engineering, 2014. **3:** p. 75-82.
75. Tang, M., et al., *Human embryonic stem cell encapsulation in alginate microbeads in macroporous calcium phosphate cement for bone tissue engineering.* Acta Biomater, 2012. **8**(9): p. 3436-45.
76. Coutu D. L., F.M., Galipeau J, *Mesenchymal stem cells and tissue repair.* InRegenerative Therapy Using Blood-Derived Stem Cells, 2012: p. 35-51.
77. S., N., *Concise review: Umbilical cord derived mesenchymal stem cell bank.* Progress in Stem Cell, 2017. **4**(3-4): p. 228-33.
78. Si, J.W., X.D. Wang, and S.G. Shen, *Perinatal stem cells: A promising cell resource for tissue engineering of craniofacial bone.* World J Stem Cells, 2015. **7**(1): p. 149-59.
79. Shi Y, I.H., Wu JC, Yamanaka S, *Induced pluripotent stem cell technology: a decade of progress.* Nature reviews Drug discovery, 2017. **6**(2): p. 115.
80. Robert Passier, C.M., *Origin and use of embryonic and adult stem cells in differentiation and tissue repair.* Cardiovascular Research, 2003. **58**(2): p. 324–335.
81. Dolatshahi-Pirouz, A., et al., *Micro- and nanoengineering approaches to control stem cell-biomaterial interactions.* J Funct Biomater, 2011. **2**(3): p. 88-106.
82. Ferraro F, C.C., Scadden D, *Adult stem cels and their niches*. In The Cell Biology of Stem Cells. 2010: Springer, Boston, MA. 155-168.
83. Yoo, K.R.S.a.S.Y., *Phage-Based Artificial Niche: The Recent Progress and Future Opportunities in Stem Cell Therapy.* Stem Cells International, 2019.

84. M., S.P.A.P.S.A.S.M.B.C.N.P., *Characterization of the optimal culture conditions for clinical scale production of human mesenchymal stem cells.* Stem Cells, 2006. **2**: p. 462-71.
85. D.R., P.M.F.M.A.M.B.S.C.J.R.K.D.R.M.J.D.M.M.A.S.D.W.C.S.M., *Multilineage potential of adult human mesenchymal stem cells.* Science, 1999. **284**(5411): p. 143-7.
86. V.M., W.S.G.T.P.S.J.Y.R.G.M.J.M.C.A.I.G., *Mesenchymal cell-based repair of large, full-thickness defects of articular cartilage.* J Bone Joint Surg Am, 1994. **76**(4): p. 76(4):579-92.
87. S, B.S.P.K.A.A.S.M.H.W.C.J.N.K., *Bone regeneration by implantation of purified, culture-expanded human mesenchymal stem cells.* J Orthop Res, 1998. **16**(2): p. 155-62.
88. Koob, S., et al., *Bone formation and neovascularization mediated by mesenchymal stem cells and endothelial cells in critical-sized calvarial defects.* Tissue Eng Part A, 2011. **17**(3-4): p. 311-21.
89. Pirosa A, G.R., Alexander PG, Tuan RS, *Engineering in-vitro stem cell-based vascularized bone models for drug screening and predictive toxicology.* Stem cell research & therapy, 2018. **9**(1): p. 112.
90. Shieh SJ, V.J.S.-o.-t.-a.t.e.f.t.e.t.o.b., *State-of-the-art tissue engineering: from tissue engineering to organ building.* Surgery, 2005. **137**(1): p. 1-7.
91. Wu X, R.-A.E., Guleserian KJ, Perry TE, Masuda Y, Sutherland FW, Schoen FJ, Mayer Jr JE, Bischoff J, *Tissue-engineered microvessels on three-dimensional biodegradable scaffolds using human endothelial progenitor cells.* American Journal of Physiology-Heart and Circulatory Physiology, 2004. **287**(2): p. H480-7.
92. Baldwin, J., et al., *In vitro pre-vascularisation of tissue-engineered constructs A co-culture perspective.* Vasc Cell, 2014. **6**(1): p. 13.
93. Bramfeldt, H., et al., *Scaffold vascularization: a challenge for three-dimensional tissue engineering.* Curr Med Chem, 2010. **17**(33): p. 3944-67.
94. Paschalaki KE, R.A., *Recent advances in Endothelial Colony Forming Cells toward their use in clinical translation.* Frontiers in medicine, 2018. **5**: p. 295.
95. Colunga, T. and S. Dalton, *Building Blood Vessels with Vascular Progenitor Cells.* Trends Mol Med, 2018. **24**(7): p. 630-641.
96. Zhang S, Z.M., Ye Z, Zhou Y, Tan WS, *Fabrication of viable and functional pre-vascularized modular bone tissues by coculturing MSCs and HUVECs on microcarriers in spinner flasks.* Biotechnology journal, 2017. **12**(8): p. 1700008.
97. Hur J, Y.C., Kim HS, Choi JH, Kang HJ, Hwang KK, Oh BH, Lee MM, Park YB, *Characterization of Two Types of Endothelial Progenitor Cells and Their Different Contributions to Neovasculogenesis.* Arteriosclerosis, thrombosis, and vascular biology, 2004. **24**(2): p. 288-93.
98. Stefanadis, A.B.D.T.C.A.N.P.C., *The Role of Endothelial Progenitor Cells in Vascular Repair after Arterial Injury and Atherosclerotic Plaque Development.* Stem Cells International, 2009. **2019**.
99. Cho, S.W., et al., *Improvement of postnatal neovascularization by human embryonic stem cell derived endothelial-like cell transplantation in a mouse model of hindlimb ischemia.* Circulation, 2007. **116**(21): p. 2409-19.

100. Sergio Caballero, N.S., Aqeela Afzal, Kyung-Hee Chang, Sergio Li Calzi, Dennis L. Guberski, Timothy S. Kern and Maria B. Grant, *Ischemic Vascular Damage Can Be Repaired by Healthy, but Not Diabetic, Endothelial Progenitor Cells.* Diabetes, 2007. **56**(4): p. 960-967.
101. Melchiorri AJ, B.L., Kimerer LK, Hibino N, Fisher JP, *In Vitro Endothelialization of Biodegradable Vascular Grafts Via Endothelial Progenitor Cell Seeding and Maturation in a Tubular Perfusion System Bioreactor.* Tissue engineering Part C, Methods, 2016. **22**: p. 663-70.
102. Tongers J, R.J., Losordo DW, *Role of endothelial progenitor cells during ischemia-induced vasculogenesis and collateral formation.* Microvasc Res, 2010. **79**(3): p. 200-6.
103. H. Chopra, M.K.H., D. L. Kwong, C. F. Zhang, and E. H. N., *Insights into Endothelial Progenitor Cells: Origin, Classification, Potentials, and Prospects.* Stem Cells Int., 2018(9847015).
104. Ruei-Zeng Lina, R.M.-L., Dan Lib, Shou-Ching Jaminetb, Arin K. Greenec, and Juan M. Melero-Martin, *Human endothelial colony-forming cells serve as trophic mediators for mesenchymal stem cell engraftment via paracrine signaling.* National Academy of Sciences, 2014. **111**(28): p. 10137-4.
105. Medina RJ, B.C., Sabatier F, Dignat-George F, Melero-Martin JM, et al, *Endothelial progenitors: a consensus statement on nomenclature. Stem Cells Transl Med. (2017) 6:1316–20. doi: 10.1002/sctm.16-0360.* Stem Cells Transl Med., 2017. **6**: p. 1316–20.
106. Lin Y, W.D., Solovey A, Hebbel RP, *Origins of circulating endothelial cells and endothelial outgrowth from blood. J Clin Invest 105(1):71–77.* J Clin Invest, 2000. **105**(1): p. 71-77.
107. Kaushal S, e.a., *Functional small-diameter neovessels created using endothelial progenitor cells expanded ex vivo.* Nat Med, 2001. **7**(9): p. 1035-1040.
108. Melero-Martin, J.M., et al., *Engineering robust and functional vascular networks in vivo with human adult and cord blood-derived progenitor cells.* Circ Res, 2008. **103**(2): p. 194-202.
109. Sarker M., C.X.B., Schreyer D.J., *Experimental approaches to vascularisation within tissue engineering constructs.* J Biomater Sci Polym 2015. **26**: p. 683.
110. Dimitar Tasev, P.K., and Victor W.M. van Hinsbergh, *Therapeutic potential of human-derived endothelial colony-forming cells in animal models.* Tissue Engineering Part B: Reviews, 2016. **22**(5): p. 371-82.
111. Lin R.-Z., M.-L.R., Zhou B., Pu W.T., and Melero-Martin J.M., *Equal modulation of endothelial cell function by four distinct tissue-specific mesenchymal stem cells.* Angiogenesis, 2012. **15**.
112. Traktuev, D.O., et al., *Robust functional vascular network formation in vivo by cooperation of adipose progenitor and endothelial cells.* Circ Res, 2009. **104**(12): p. 1410-20.
113. Novosel EC, K.C., Kluger PJ., *Vascularization is the key challenge in tissue engineering.* Adv Drug Deliv Rev., 2011. **63**(4-5): p. 300-11.
114. Stock, U.A. and J.P. Vacanti, *Tissue engineering: current state and prospects.* Annu Rev Med, 2001. **52**: p. 443-51.

115. Jonitz, A., et al., *Oxygen consumption, acidification and migration capacity of human primary osteoblasts within a three-dimensional tantalum scaffold.* Journal of Materials Science: Materials in Medicine, 2011. **22**(9): p. 2089-2095.
116. Goerke SM, P.J., Hager S, Strassburg S, Torio-Padron N, Stark GB, Finkenzeller G, *Human endothelial progenitor cells induce extracellular signal-regulated kinase-dependent differentiation of mesenchymal stem cells into smooth muscle cells upon cocultivation.* Tissue Eng Part A, 2012. **18**(23): p.:2395-405.
117. Amini, A.R., C.T. Laurencin, and S.P. Nukavarapu, *Bone tissue engineering: recent advances and challenges.* Crit Rev Biomed Eng, 2012. **40**(5): p. 363-408.
118. Schmitt, P.J., et al., *Long-Segment Fusion for Adult Spinal Deformity Correction Using Low-Dose Recombinant Human Bone Morphogenetic Protein-2: A Retrospective Review of Fusion Rates.* Neurosurgery, 2016. **79**(2): p. 212-21.
119. Zhang, W.J., et al., *Vegf and Bmp-2 Promote Bone Regeneration by Facilitating Bone Marrow Stem Cell Homing and Differentiation.* European Cells & Materials, 2014. **27**: p. 1-12.
120. Kempen, D.H.R., et al., *Effect of local sequential VEGF and BMP-2 delivery on ectopic and orthotopic bone regeneration.* Biomaterials, 2009. **30**(14): p. 2816-2825.
121. Mercado, A.E. and E. Jabbari, *Effect of encapsulation or grafting on release kinetics of recombinant human bone morphogenetic protein-2 from self-assembled poly (lactide-co-glycolide ethylene oxide fumarate) nanoparticles.* Microscopy research and technique, 2010. **73**(9): p. 824-833.
122. Mercado, A.E., et al., *Effect of grafting BMP2-derived peptide to nanoparticles on osteogenic and vasculogenic expression of stromal cells.* J Tissue Eng Regen Med, 2014. **8**(1): p. 15-28.
123. Monteiro, N., et al., *Nanoparticle-based bioactive agent release systems for bone and cartilage tissue engineering.* Regenerative Therapy, 2015. **1**: p. 109-118.
124. Kazemzadeh-Narbat, M., et al., *Engineering Photocrosslinkable Bicomponent Hydrogel Constructs for Creating 3D Vascularized Bone.* Advanced Healthcare Materials, 2017. **6**(10).
125. Zisch, A.H. and M. Ehrbar, *Cell-demanded release of growth factors*, in *Comprehensive biomaterials. Biocompatibility, surface engineering, and delivery of drugs, genes and other molecules*. 2011, Elsevier. p. 463-473.
126. He, X. and E. Jabbari, *Material properties and cytocompatibility of injectable MMP degradable poly (lactide ethylene oxide fumarate) hydrogel as a carrier for marrow stromal cells.* Biomacromolecules, 2007. **8**(3): p. 780-792.
127. Carragee, E.J., E.L. Hurwitz, and B.K. Weiner, *A critical review of recombinant human bone morphogenetic protein-2 trials in spinal surgery: emerging safety concerns and lessons learned.* Spine J, 2011. **11**(6): p. 471-91.
128. van Rijt, S. and P. Habibovic, *Enhancing regenerative approaches with nanoparticles.* Journal of the Royal Society Interface, 2017. **14**(129): p. 20170093.
129. Mura, S., J. Nicolas, and P. Couvreur, *Stimuli-responsive nanocarriers for drug delivery.* Nature materials, 2013. **12**(11): p. 991.
130. Balaji, S., S.G. Keswani, and T.M. Crombleholme, *The role of mesenchymal stem cells in the regenerative wound healing phenotype.* Advances in wound care, 2012. **1**(4): p. 159-165.

131. Lee, D.E., N. Ayoub, and D.K. Agrawal, *Mesenchymal stem cells and cutaneous wound healing: novel methods to increase cell delivery and therapeutic efficacy.* Stem cell research & therapy, 2016. **7**(1): p. 37.
132. Kachgal, S. and A.J. Putnam, *Mesenchymal stem cells from adipose and bone marrow promote angiogenesis via distinct cytokine and protease expression mechanisms.* Angiogenesis, 2011. **14**(1): p. 47-59.
133. Singer, A.J. and R.A. Clark, *Cutaneous wound healing.* New England journal of medicine, 1999. **341**(10): p. 738-746.
134. Neuss, S., et al., *Secretion of fibrinolytic enzymes facilitates human mesenchymal stem cell invasion into fibrin clots.* Cells Tissues Organs, 2010. **191**(1): p. 36-46.
135. Walker, N.G., *The role of mesenchymal stem cells from adult human bone marrow in in vitro wound models*, in *Department of Materials Science and Engineering*. 2013, University of Sheffield: UK. p. 211.
136. Huang, C., et al., *The role of substrate topography on the cellular uptake of nanoparticles.* Journal of Biomedical Materials Research Part B: Applied Biomaterials, 2016. **104**(3): p. 488-495.
137. Backes, B.J., et al., *Synthesis of positional-scanning libraries of fluorogenic peptide substrates to define the extended substrate specificity of plasmin and thrombin.* Nature biotechnology, 2000. **18**(2): p. 187.
138. Mandal, D., A.N. Shirazi, and K. Parang, *Self-assembly of peptides to nanostructures.* Organic & biomolecular chemistry, 2014. **12**(22): p. 3544-3561.
139. Matson, J.B. and S.I. Stupp, *Self-assembling peptide scaffolds for regenerative medicine.* Chemical communications, 2012. **48**(1): p. 26-33.
140. Panda, J.J. and V.S. Chauhan, *Short peptide based self-assembled nanostructures: implications in drug delivery and tissue engineering.* Polymer Chemistry, 2014. **5**(15): p. 4418-4436.
141. Reches, M. and E. Gazit, *Formation of closed-cage nanostructures by self-assembly of aromatic dipeptides.* Nanoletters, 2004. **4**(4): p. 581-585.
142. Song, S.J., et al., *Amphiphilic Peptide Nanorods Based on Oligo-Phenylalanine as a Biocompatible Drug Carrier.* Bioconjugate chemistry, 2017. **28**(9): p. 2266-2276.
143. Guo, C., et al., *Triphenylalanine peptides self-assemble into nanospheres and nanorods that are different from the nanovesicles and nanotubes formed by diphenylalanine peptides.* Nanoscale, 2014. **6**(5): p. 2800-2811.
144. Adler-Abramovich, L., et al., *Thermal and Chemical Stability of Diphenylalanine Peptide Nanotubes: Implications for Nanotechnological Applications.* Langmuir, 2006. **22**(3): p. 1313-1320.
145. Castelletto, V., et al., *Self-assembly of PEGylated peptide conjugates containing a modified amyloid Î²-peptide fragment.* Langmuir, 2010. **26**(12): p. 9986-9996.
146. Tzokova, N., et al., *The Effect of PEO Length on the Self-Assembly of Poly (ethylene oxide)âˆ’ Tetrapeptide Conjugates Prepared by â€œClickâ€• Chemistry.* Langmuir, 2009. **25**(18): p. 11082-11089.
147. Harris, J.L., et al., *Rapid and general profiling of protease specificity by using combinatorial fluorogenic substrate libraries.* Proceedings of the National Academy of Sciences, 2000. **97**(14): p. 7754-7759.

148. Moeinzadeh, S. and E. Jabbari, *Mesoscale simulation of the effect of a lactide segment on the nanostructure of star poly(ethylene glycol-co-lactide)-acrylate macromonomers in aqueous solution.* J Phys Chem B, 2012. **116**(5): p. 1536-43.
149. Moeinzadeh, S., et al., *Nanostructure formation and transition from surface to bulk degradation in polyethylene glycol gels chain-extended with short hydroxy acid segments.* Biomacromolecules, 2013. **14**(8): p. 2917-28.
150. He, X., J. Ma, and E. Jabbari, *Effect of grafting RGD and BMP-2 protein-derived peptides to a hydrogel substrate on osteogenic differentiation of marrow stromal cells.* Langmuir, 2008. **24**(21): p. 12508-12516.
151. Barati, D., et al., *Time Dependence of Material Properties of Polyethylene Glycol Hydrogels Chain Extended with Short Hydroxy Acid Segments.* Polymer (Guildf), 2014. **55**(16): p. 3894-3904.
152. He, X., X. Yang, and E. Jabbari, *Combined effect of osteopontin and BMP-2 derived peptides grafted to an adhesive hydrogel on osteogenic and vasculogenic differentiation of marrow stromal cells.* Langmuir, 2012. **28**(12): p. 5387-97.
153. Yang, X., et al., *Three-dimensional-engineered matrix to study cancer stem cells and tumorsphere formation: effect of matrix modulus.* Tissue Eng Part A, 2013. **19**(5-6): p. 669-84.
154. Barati, D., et al., *Synthesis and Characterization of Photo-Cross-Linkable Keratin Hydrogels for Stem Cell Encapsulation.* Biomacromolecules, 2017. **18**(2): p. 398-412.
155. Henderson, J.A., X. He, and E. Jabbari, *Concurrent differentiation of marrow stromal cells to osteogenic and vasculogenic lineages.* Macromol Biosci, 2008. **8**(6): p. 499-507.
156. Pfaffl, M.W., *A new mathematical model for relative quantification in real-time RT-PCR.* Nucleic Acids Res, 2001. **29**(9): p. e45.
157. Moeinzadeh, S., et al., *Experimental and computational investigation of the effect of hydrophobicity on aggregation and osteoinductive potential of BMP-2-derived peptide in a hydrogel matrix.* Tissue Eng Part A, 2015. **21**(1-2): p. 134-46.
158. Moeinzadeh, S., S.R. Pajoum Shariati, and E. Jabbari, *Comparative effect of physicomechanical and biomolecular cues on zone-specific chondrogenic differentiation of mesenchymal stem cells.* Biomaterials, 2016. **92**: p. 57-70.
159. Barati, D., et al., *Effect of organic acids on calcium phosphate nucleation and osteogenic differentiation of human mesenchymal stem cells on peptide functionalized nanofibers.* Langmuir, 2015. **31**(18): p. 5130-40.
160. Oliveira, J.M., et al., *The osteogenic differentiation of rat bone marrow stromal cells cultured with dexamethasone-loaded carboxymethylchitosan/poly(amidoamine) dendrimer nanoparticles.* Biomaterials, 2009. **30**(5): p. 804-13.
161. Burdick, J.A. and K.S. Anseth, *Photoencapsulation of osteoblasts in injectable RGD-modified PEG hydrogels for bone tissue engineering.* Biomaterials, 2002. **23**(22): p. 4315-4323.
162. Pan, P., et al., *Self-assembled supramolecular systems for bone engineering applications.* Current Opinion in Colloid & Interface Science, 2018.
163. Mahato, R.I., *Biomaterials for delivery and targeting of proteins and nucleic acids*. 2004: CRC Press.

164. Lee, J.H., J. Kopecek, and J.D. Andrade, *Proteinâ€• resistant surfaces prepared by PEOâ€ containing block copolymer surfactants.* Journal of biomedical materials research, 1989. **23**(3): p. 351-368.
165. Desale, S.S., et al., *Biodegradable hybrid polymer micelles for combination drug therapy in ovarian cancer.* Journal of Controlled Release, 2013. **171**(3): p. 339-348.
166. Suk, J.S., et al., *PEGylation as a strategy for improving nanoparticle-based drug and gene delivery.* Advanced drug delivery reviews, 2016. **99**: p. 28-51.
167. Damodaran, V.B. and C. Fee, *Protein PEGylation: An overview of chemistry and process considerations.* European Pharmaceutical Review, 2010. **15**(1): p. 18-26.
168. Ries, C., et al., *MMP-2, MT1-MMP, and TIMP-2 are essential for the invasive capacity of human mesenchymal stem cells: differential regulation by inflammatory cytokines.* Blood, 2007. **109**(9): p. 4055-4063.
169. Ghajar, C.M., et al., *Mesenchymal stem cells enhance angiogenesis in mechanically viable prevascularized tissues via early matrix metalloproteinase upregulation.* Tissue engineering, 2006. **12**(10): p. 2875-2888.
170. Ghajar, C.M., et al., *Mesenchymal cells stimulate capillary morphogenesis via distinct proteolytic mechanisms.* Experimental cell research, 2010. **316**(5): p. 813-825.
171. James, A.W., et al., *A Review of the Clinical Side Effects of Bone Morphogenetic Protein-2.* Tissue Eng Part B Rev, 2016. **22**(4): p. 284-97.
172. Junmin Zhu, R.E.M., *Design properties of hydrogel tissue-engineering scaffolds.* Expert Rev Med Devices, 2011: p. 607–626.
173. Panita Maturavongsadit, J.A.L., Kamolrat Metavarayuth, Xia Zhao, Limin Chen, Yuan Lin, and Qian Wang, *Promotion of In Vitro Chondrogenesis of Mesenchymal Stem Cells Using In Situ Hyaluronic Hydrogel Functionalized with Rod-Like Viral Nanoparticles* Biomacromolecules, 2016: p. 1930−1938.
174. Asakura, H.T.a.A.K., *Native Structure and Degradation Pattern of Silk Sericin Studied by 13C NMR Spectroscopy.* Macromolecules 2005.
175. Regina Inês Kunz, R.M.C.B., Lucinéia de Fátima Chasko Ribeiro, and Maria Raquel Marçal Natali, *Regina Inês Kunz, Rose Meire Costa Brancalhão, Lucinéia de Fátima Chasko Ribeiro, and MariSilkworm Sericin: Properties and Biomedical Applications.* BioMed Research International, 2016: p. 19.
176. Pawar, M.N.P.a.A.P., *Silk sericin and its applications: A review.* Journal of Scientific & Industrial Research, 2004: p. 323-329.
177. Z. Wang, Y.Z., J. Zhang, L. Huang, J. Liu, Y. Li, G. Zhang, S.C. Kundu, L., *Exploring natural silk protein sericin for regenerative medicine: an injectable, photoluminescent, cell-adhesive 3D hydrogel.* Sci. Rep, 2014: p. 6074.
178. L. Lamboni, M.G., G. Yang, Q. Wan, *Silk sericin: A versatile material for tissue engineering and drug delivery.* Biotechnol. Adv, 2015: p. 1855-1867.
179. Pornanong Aramwit, S.K., Titpawan Nakpheng, and Teerapol Srichana., *The Effect of Sericin from Various Extraction Methods on Cell Viability and Collagen Production.* Int J Mol Sci., 2010;: p. 2200–2211.
180. Kunz, R.I.e.a., *Silkworm Sericin: Properties and Biomedical Applications.* BioMed research international, 2016: p. 8175701.

181. Hidetoshi Teramoto, K.-i.N., and Chiyuki Takabayashi., *Chemical Modification of Silk Sericin in Lithium Chloride/ Dimethyl Sulfoxide Solvent with 4-Cyanophenyl Isocyanate.* Biomacromolecules 2004: p. 1392-1398.
182. Danial Barati, S.K., Seyed Ramin Pajoum Shariati, Seyedsina Moeinzadeh, Roger H. Sawyer, and Esmaiel Jabbari, *Synthesis and Characterization of Photocrosslinkable Keratin Hydrogels for Stem Cell Encapsulation* Biomacromoleculus, 2016: p. 1-44.
183. Khoon S. Lim, J.K., April Reeves, Laura A. Poole-Warren, Subhas C. Kundu, Penny J. Martens, *The Influence of Silkworm Species on Cellular Interactions with Novel PVA/Silk Sericin Hydrogels.* Macromol. Biosci. , 2012: p. 322–332.
184. Fujia Chen, D.P., Fritz Vollrath, *Silk cocoon (Bombyx mori): Multi-layer structure and mechanical properties.* Acta Biomaterialia, 2012: p. 2620-2627.
185. Meirong Yang, Y.W., Gang Tao, Rui Cai, Peng Wang, Liying Liu, Lisha Ai, Hua Zuo, Ping Zhao, Ahmad Umar, Chuanbin Mao and Huawei He, *Fabrication of Sericin/Agrose Gel Loaded Lysozyme and Its Potential in Wound Dressing Application.* Nanomaterials 2018: p. 235.

APPENDIX A: PERMISSION TO REPRINT CHAPTER THREE

Plasmin-Cleavable Nanoparticles for On-Demand Release of Morphogens in Vascularized Osteogenesis

Author: Safaa Kader, Mehri Monavarian, Danial Barati, et al

Publication: Biomacromolecules

Publisher: American Chemical Society

Date: Aug 1, 2019

PERMISSION/LICENSE IS GRANTED FOR YOUR ORDER AT NO CHARGE

This type of permission/license, instead of the standard Terms & Conditions, is sent to you because no fee is being charged for your order. Please note the following:

- Permission is granted for your request in both print and electronic formats, and translations.
- If figures and/or tables were requested, they may be adapted or used in part.
- Please print this page for your records and send a copy of it to your publisher/graduate school.
- Appropriate credit for the requested material should be given as follows: "Reprinted (adapted) with permission from (COMPLETE REFERENCE CITATION). Copyright (YEAR) American Chemical Society." Insert appropriate information in place of the capitalized words.
- One-time permission is granted only for the use specified in your request. No additional uses are granted (such as derivative works or other editions). For any other uses, please submit a new request.

BACK CLOSE WINDOW